Interacting Mechanisms Driving Synchrony in Neural Networks with Inhibitory Interneurons

by

Scott Rich

A dissertation submitted in partial fulfillment
of the requirements for the degree of
Doctor of Philosophy
(Applied and Interdisciplinary Mathematics)
in the University of Michigan
2018

Doctoral Committee:

Associate Professor Victoria Booth, Co-Chair
Professor Michal Zochowski, Co-Chair
Assistant Professor Sara Aton
Professor Daniel Forger

Scott Rich

sbrich@umich.edu

ORCID iD: 0000-0001-7982-742X

To Nicole, who has filled my life with good times.

"That's one thing Earthlings might learn to do, if they tried hard enough: Ignore the awful times and concentrate on the good ones."— Kurt Vonnegut, Slaughterhouse-Five

ACKNOWLEDGEMENTS

This dissertation represents six years of hard work of which I am extremely proud. Thank you to the University of Michigan and the Applied and Interdisciplinary Mathematics program for making this work possible, and also fulfilling my lifelong dream of being able to call myself an alumnus of this great school. However, achieving my PhD is only the second most important thing to occur during my graduate studies.

Instead, the most important part of my six year odyssey in grad school occurred in (of all places for a die-hard Wolverine like myself) Columbus, Ohio. My graduate studies led me to a graduate summer school program there that ended up being the most formative two weeks of my adult life, not because of what I learned (but don't worry Danny Forger, I still learned a lot), but because of who I met. Were it not for that program, and the winding road that took me there, I would have never met the most important person in my life, my wife Nicole.

Nicole, without you I'm not sure if I would have made it to this point, and I certainly would not be anywhere near as happy as I am today. Your voice was the fuel that moved me forward on this journey. I can't wait to face all of the future's challenges and adventures with the best partner and friend anyone could ask for.

I was fortunate enough to develop an amazing group of friends in Ann Arbor that helped to support me along this journey as well. Luckily, one of these people I brought up to the cold Midwest with me from my days down in the South at Duke. John, thanks for being a consumate friend, for always having my back, and for doing

an amazing job convincing me that you were interested in whatever breakthrough in my research I was boring you with during halftime of that day's Duke game.

Audra and Gabe, thanks for being the best office mates anyone could ask for (and Mike, our unofficial fourth office resident). Graham, Caitlin, Brittany, and Jackie, thank you for welcoming me into the world of neuroscience (and tolerating my ignorant questions in class) and being my family in the Big House student section (and encouraging my use of the cow bell). Finally, a special thanks to Penny and Rezzy for filling the hole that my apartment's "no dogs" policy left in my heart.

I would be remiss not to acknowledge my family for providing the foundation of my thirst for knowledge that led me to this accomplishment. Mom and Dad, thank you for always encouraging me to follow that path I truly wanted, not the path that I felt I was "supposed to". Marlee, living in the same city as you was an experience that I'll always remember, especially considering that your globetrotting ways may mean we're never living less than a thousand miles apart again.

Finally, I must thank Victoria Booth and Michal Zochowski for being absolutely fantastic advisors. I can honestly say that I truly *enjoyed* my graduate experience, which is no small feat, thanks largely to your stewardship. Victoria, your work is what drew me to U of M, and I consider myself infinitely lucky that you agreed to talk about your research with me when I was a lowly first year. Those conversations were what confirmed to me that I wanted to be a computational neuroscientist. As a special thank you, I tried my best not to include "what's more" in the nearly two hundred pages of this dissertation. Michal, your constantly demanding the best of me brought out the best in me. For someone who is so stingy with praise, I still always felt your confidence and support, and never worked harder than I did to hear you simply say "this looks interesting" in our weekly meetings. I will look back

fondly our research meetings for the rest of my career, despite the tendency for those meetings to often require neighboring offices to shut their doors due to our tendency to get loud, and, all joking aside, will be fortunate if I ever have meetings that are that productive, engaging, and enlightening again.

TABLE OF CONTENTS

LIST OF FIGURES

Figure

ABSTRACT

Computational neuroscience contributes to our understanding of the brain by applying techniques from fields including mathematics, physics, and computer science to neuroscientific problems that are not amenable to purely biologic study. One area in which this interdisciplinary research is particularly valuable is the proposal and analysis of mechanisms underlying neural network behaviors. Neural synchrony, especially when driven by inhibitory interneurons, is a behavior of particular importance considering this behavior play a role in neural oscillations underlying important brain functions such as memory formation and attention. Typically, these oscillations arise from synchronous firing of a neural population, and thus the study of neural oscillations and neural synchrony are deeply intertwined. Such network behaviors are particularly amenable to computational analysis given the variety of mathematical techniques that are of use in this field.

Inhibitory interneurons are thought to drive synchrony in ways described by two computational mechanisms: Interneuron Network Gamma (ING), which describes how an inhibitory network synchronizes itself; and Pyramidal Interneuron Network Gamma (PING), which describes how a population of interneurons inter-connected with a population of excitatory pyramidal cells (an E-I network) synchronizes both populations. As first articulated using simplified interneuron models, these mechanisms find network properties are the primary impetus for synchrony. However, as neurobiologists uncover interneurons exhibiting a vast array of cellular and intra-connectivity properties, our understanding of how interneurons drive oscillations must account for this diversity. This necessitates an investigation of how changing

interneuron properties might disrupt the predictions of ING and PING, and whether other mechanisms might interact with or disrupt these network-driven mechanisms.

In my dissertation, I broach this topic utilizing the Type I and Type II neuron classifications, which refer to properties derived from the mathematics of coupled oscillators. Classic ING and PING literature typically utilize Type I neurons which always respond to an excitatory perturbation with an advance of the subsequent action potential. However, many interneurons exhibit Type II properties, which respond to some excitatory perturbations with a delay in the subsequent action potential. Interneuronal diversity is also reflected in the strength and density of the synaptic connections between these neurons, which is also explored in this work.

My research reveals a variety of ways in which interneuronal diversity alters synchronous oscillations in networks containing inhibitory interneurons and the mechanisms likely driving these dynamics. For example, oscillations in networks of Type II interneurons violate ING predictions and can be explained mechanistically primarily utilizing cellular properties. Additionally, varying the type of both excitatory and inhibitory cells in E-I networks reveals that synchronous excitatory activity arises with different network connectivities for different neuron types, sometimes driven by cellular properties rather than PING. Furthermore, E-I networks respond differently to varied strengths of inhibitory intra-connectivity depending upon interneuron type, sometimes in ways not fully accounted for by PING theory.

Taken together, this research reveals that network-driven and cellularly-driven mechanisms promoting oscillatory activity in networks containing inhibitory interneurons interact, and oftentimes compete, in order to dictate the overall network dynamics. These dynamics are more complex than those predicted by the classic ING and PING mechanisms alone. The diverse dynamical properties imparted to oscillating

neural networks by changing inhibitory interneuron properties provides some insight into the biological need for such variability.

CHAPTER I

Introduction

1.1 Neurons: the basis of biological and computational neuroscience

For centuries, human beings' understanding of their own capacity for thought and reason was limited to Rene Descartes famously straightforward platitude, "I think, therefore I am". Generations of existential and epistemological philosophers to follow would flounder trying to expand upon this simple principle and explain the more complicated facets of human consciousness such as emotion and knowledge. While metaphysical approaches to these questions led only to endless debate with no possibility of resolution, the scientific method provided concrete advances in humanity's understanding of its own cognitive faculties. Through this research into the brain, which makes up modern neuroscience, scientists have turned Decartes' hackneyed phrase around: neuroscientific advances have helped humans understand who we are through a better understanding of how we think.

Incredibly, the vastly complicated structure that is the brain is made up of a single fundamental unit: the neuron. First recognized via the late 19th century work of Santiago Ramon y Cajal [35], the neuron is a specialized cell that is electrically excitable and can respond to both chemical and electrical signalling. Perhaps not coincidentally, most neurons function similarly to bits in modern computers, switch-

ing between binary "on" and "off" states via the cell's membrane potential. Via the interaction of billions of neurons switching between these binary states, all of human consciousness, thought, and emotion is brought into existence.

1.1.1 Action potentials

All cells are secured from the external world via a phospholipid bilayer that makes up the cellular membrane. This membrane is itself an incredibly robust biological structure capable of preventing extracellular materials from entering the interior of the cell, and vice-versa. In this bilayer, the external barrier is made up of hydrophilic phosphate groups, while the interior of the barrier is made up of hydrophobic fatty acids. The fact that the membrane contains both hydrophilic and hydrophobic elements ensures that both polar compounds and non-polar compounds cannot easily traverse this structure. This also leads cells to develop an electrical potential across their membrane due to the differential accumulation of charged ionic species inside and outside of the cell brought about by more intricate properties of the phospholipid bilayer [6].

However, if this membrane was entirely impermeable, the existence of multicellular organisms would be nigh impossible. Avoiding this dilemma, evolutionary processes led to the development of tools with which the cell can communicate with other cells and gain information about the extracellular environment. This is achieved via proteins that embed themselves in the cellular membrane, allowing for inter-cellular communication via the bonding of specialized signalling molecules to the protein. Additionally, these proteins can facilitate the transport of particular biological structures into or out of the cell via a so-called "channel" through the membrane created by the protein. Such channels often only open in specific circumstances and preferentially allow passage to specific compounds. The most common

of these ion channels present on neurons are those that selectively allow the passage of sodium (Na^+) or potassium (K^+) ions, while channels also exist for chlorine (Cl^-) and calcium (Ca^{2+}) ions [6].

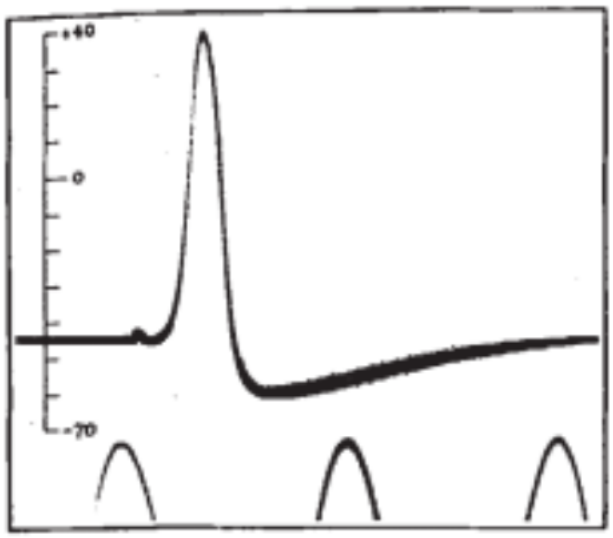

Figure 1.1: One of the earliest recordings of a neuronal actional potential performed by Hodgkin and Huxley [56].

At rest, neurons typically achieve a membrane potential of between -60 and -80 mV, primarily driven by the distribution of Na^+ and K^+ ions across the membrane. This potential may become more positive (depolarize) or more negative (hyperpolarize) driven by a variety of factors, most commonly signalling from other neurons (the fashion by which this communication occurs will be discussed in more detail in Section 1.2). If such signalling causes the neuron's voltage to rise past a voltage threshold (the value of which is a crucial source of heterogeneity between the variety of types of neurons), Na^+ ion channels will open and begin allowing postiviely charged ions into the interior of the cell, driven by the concentration and voltage gradient across the membrane. Such activity further increases the neuron's voltage, and the resulting feedback loop leads to an abrupt spike in the voltage. As the membrane potential rises, K^+ ion channels open and allow postively charged ions

out of the neuron, driven by the new voltage gradient created by the voltage spike. The high membrane potential also causes Na+ ion channels to close, which results in an even quicker drop in the membrane voltage. The neuron will then settle back to its resting membrane potential following a period of hyperpolarization in which the neuron is unable to respond to external stimuli. This process of a quick spike in membrane voltage followed by a return to the resting potential is called the action potential [6, 56], and is illustrated by an example experimental recording in Fig 1.1. Fig 1.2 shows a cartoon diagram of the action potential in which each of the stages of this dynamic, and the behaviors of the Na^+ (bottom) and K^+ (top-right) channels at each stage, are highlighted.

The action potential as described above constitutes the "on" state of the neuron that can be thought of as analogous to the binary switch that makes up the fundamental bit of computer systems. This electrical activity is the primary characteristic that differentiates neurons from other cells, and is brought about via the action of the unique ion channels present in the cellular membranes of neurons as opposed to other cells. We will discuss in Section 1.2 how this "on" state is communicated to other neurons, allowing for the large-scale computations achieved by networks of neurons.

1.1.2 The historical development of computatonal neural models

The action potential has a very distinct profile when the membrane voltage is plotted as a function of time. Modeling this activity mathematically quickly became an important question for neuroscientists, given that such a model might reveal some of the intricacies underlying the generation of the action potential. In fact, this question could be considered the beginning of the field of computational neuroscience.

In the mid-20th century, scientists and mathematicians lacked the power of mod-

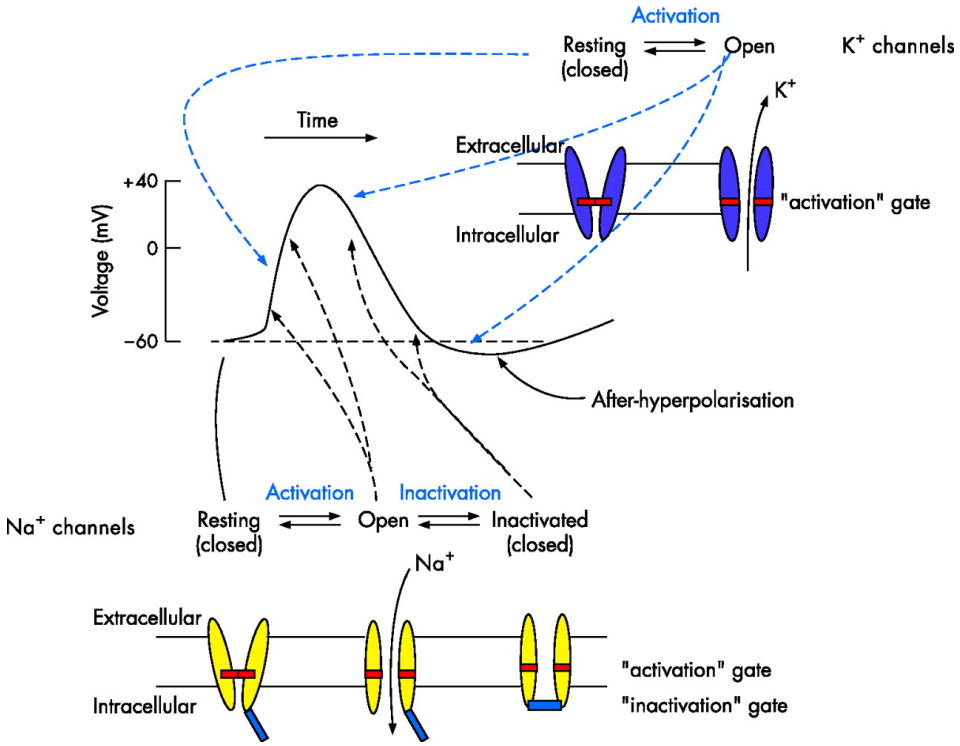

Figure 1.2: A diagramatic representation of the action potential and the corresponding activity of Na^+ and K^+ ions at the different dynamical stages. The Na^+ channel (bottom), which allows the flow of positively charged ions into the cell, opens during the initial uptick in membrane voltage and closes once the membrane voltage reaches its peak, positive value. Meanwhile, the K^+ channel (top-right), which allows the flow of positively charged ions out of the cell, is closed during the initial rise in membrane voltage and opens once the peak, positive value of this voltage is achieved [6].

ern computers that may have been able to utilize brute-force methods to simply fit a function to the shape of an action potential. This deficit turned out to be a stroke of luck, as it forced neuroscientists to develop a model making direct use of the biology underlying the action potential, which proved to be much more useful in understanding the dynamics of the neuron. Alan Lloyd Hodgkin and Andrew Fielding Huxley were the first to develop such a model in 1952.

The genius of Hodgkin and Huxley lied in their use of analogy to electrical circuits: by thinking of the cell membrane as a capacitor and the ion channels as conductors, the pair brought the tools of physics and electromagnetism to bear on the problem of the biological neuron. Hodgkin and Huxley sought to understand the activity of

Na^+ and K^+ separately by looking at each ion channel individually. Utilizing voltage clamp experiments, in which the membrane voltage is artificially controlled and any currents that arise from changing this voltage are measured, the pair were able to use nonlinear differential equations to model the currents resulting from the flow of particular ions through their corresponding ion channels. Ohm's Law can relate this current to a change in voltage across the membrane. This insight led to the creation of the Hodgkin-Huxley equations, which are stated in full in Section 1.5.1 [57].

The Hodgkin-Huxley equations were the first conductance-based model of the neuron, meaning that each term and variable is directly related to a biophysical conductance caused by a particular ion's flow across the cellular membrane. Utilizing Hodgkin and Huxley's technique, conductance-based models of any type of neuron can be developed; indeed, dozens of neurons are now modeled in the "Hodgkin-Huxley formalism", although the original Hodgkin-Huxley equations came about based upon experiments on the squid giant axon. The direct correlation between this mathematical model and the biophysics of the neuron is best illustrated by the insights into the makeup of the ion channels brought about by this work. In articulating a differential equation to the activity of Na^+ ions, Hodgkin and Huxley found the best fit came about with two variables governing whether the channel was active or not, with one of these variables raised to the third power. Years later, more advanced biological techniques revealed that the Na^+ ion channel was indeed made up of four subunits, three alike and one different, exactly as predicted by the Hodgkin-Huxley equations. This also holds true for the K^+ channel, which the Hodgkin-Huxley equations predicted consisted of four identical subunits and was confirmed by later research [57].

While the Hodgkin-Huxley equations remain of paramount use today (and in-

deed, the work included in this dissertation makes use exclusively of conductance-based models of neurons), mathematicians both before and after Hodgkin and Huxley sought to model the action potential in a computationally simpler fashion. Perhaps the simplest of these alternative models, actually predating Hodgkin and Huxley, is the integrate-and-fire model, which involves a single differential equation with an artificial threshold and reset dictating the onset of an action potential [1]. The integrate-and-fire model is a very rough approximation of the action potential, however, and as such many mathematicians have altered this model to better match a variety of neural behaviors. A model put forth by Eugene Izhikevich, which makes use of two coupled differential equations with threshold and reset conditions, is ubiquitous throughout computational neuroscience and commonly used as a "middle ground" between the biophysical accuracy of conductance-based models and the computational simplicity of the integrate-and-fire model [58]. All three of these model types are used in the computational literature, and the choice of model is dependent upon the aims of the study and the computational resources available.

1.1.3 Classifying neuron excitability profiles

Mathematical principles are useful beyond simply articulating models of the action potential and the dynamics of neurons. Indeed, they are also used in order to quantify the properties of neurons that are responsible for their diverse behaviors. Many of these properties are encapsulated by the neuron's current-frequency relation (I-F Curve) and Phase Response Curve (PRC). The I-F Curve is a straightforward function representing the relationship between a tonic current applied to a neuron and the corresponding frequency of repetitive action potential firings. The PRC, however, is a slightly more complicated measure.

The PRC came about originally from the mathematical study of coupled oscilla-

tors, but for a neuron this is an experimentally obtainable measure that characterizes membrane excitability properties. To measure the PRC experimentally on a neuron, or computationally on a neuron model, one first ensures the neuron is firing reptitively, and then perturbs the neuron via a brief and small current pulse at various phases in the oscillatory firing cycle. After this perturbation, the timing of the next action potential is measured, and is compared to what the timing of this action potential would have been sans perturbation. If the neuron fired earlier than expected it is said that the perturbation caused "phase advance", while if the neuron fired later than expected the perturbation caused "phase delay". A plot of these changes in phase as a function of the timing of the perturbation yields the PRC. A diagramatic representation of this process can be seen in Fig 1.3.

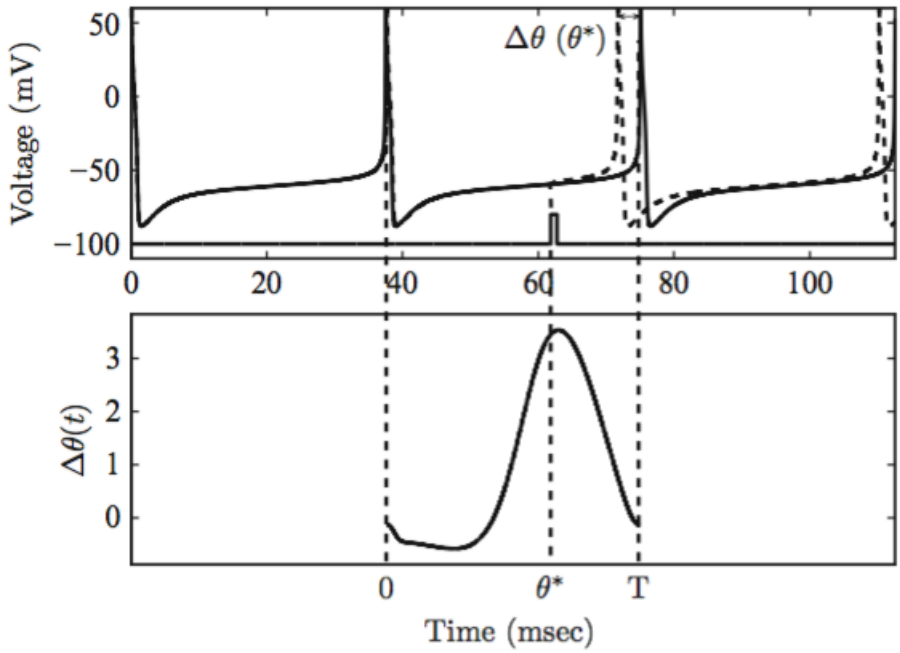

Figure 1.3: An illustrative example of how the PRC is calculated. Top: a small, excitatory perturbation in the current driving a repetitively firing neuron delivered at approximately 60 ms leads to an earlier than expected firing of the subsequent action potential (the dashed line compared to the solid line). Bottom: the resulting PRC, which plots the change in phase against the timing of the perturbation, with the phase advance corresponding to the example in the top panel highlighted [95].

The correspondence between certain properties of the I-F Curve and PRC led to the articulation of the Type I and Type II classifications of neuron excitability. These classifications arose historically both from the concepts of excitability type [55] and the mathematical analysis of the type of bifurcation that leads to periodic firing in mathematical neuron models. While recent work has shown that the relationship between the PRC, the I-F curve and the bifurcation type are not definite [41], usually saddle node on an invariant cycle (SNIC) bifurcations are associated with Type I properties and subcritical Hopf bifurcations are associated with Type II properties [98, 38]. Additionally, the presence of an M-type adaptation current (discussed in Section 1.1.4) has been shown to change Type I neurons into Type II neurons through a corresponding change in the bifurcation type, as discussed in detail in Section 1.6.3 [38, 98].

Generally, Type I neurons are characterized by a steep I-F curve with arbitrarily low firing frequency at firing threshold and by a PRC exhibiting only phase advances in response to a brief, excitatory current pulse. In contrast, Type II neurons are characterized by a more shallow I-F curve with a minimum firing frequency at threshold, and a PRC that exhibits phase delays in response to a brief, excitatory current pulse early in the neuron's firing cycle [114, 21]. Example plots illustrating these differences are shown in Fig 1.8. These neuron classifications are used throughout this dissertation, with the differences in the PRC properties being of particular importance.

Mathematical analysis of dynamical systems using the PRC has yielded a variety of insights that are applicable to neuronal PRCs. In particular, the PRC can serve as an indicator of whether a pair of coupled oscillators, or in the case of neuroscience a network of coupled neurons, might synchronize [40, 38, 95, 52, 94]. Indeed, it has

been shown that Type II neurons have a higher propensity for synchronization than Type I neurons in excitatory networks [40, 52], while these neurons may synchronize via different mechanisms within inhibitory networks [85].

1.1.4 Cholinergic modulation

The properties of individual neurons, including their classification as Type I or Type II, can be altered by a variety of chemical compounds in the brain termed neuromodulators. One of the brain's most potent neuromodulators is acetylcholine (ACh). ACh levels change across sleep and wake states, with high levels during waking contributing to arousal, attention, memory, and motivation.

ACh affects intrinisic neuronal properties as well as synaptic transmission through two major pathways: nicotinic and muscarinic receptors. In individual neurons, ACh blocks the slow, potassium-mediated M-type ionic current via muscarinic channels, which has a three-fold effect on cellular properties: altering the current-frequency (I-F) curve, to increase excitability; decreasing spike frequency adaptation (SFA), the tendency for neurons to fire faster than is typical following a period of quiescence; and finally, altering neuronal phase response curves (PRCs) [4, 91, 38, 98]. In cortical and hippocampal networks, excitatory pyramidal cells and some types of inhibitory interneurons can contain the M-type potassium current and thus are targets for these effects of ACh [98, 92, 69, 82, 73].

In this dissertation, the discussion of neuromodulation and the changing intrinsic properties of the neuron will commonly be done in the context of acetylcholine. This is done given this neuromodulator's ubiquity, its known behavioral correlates, and the direct relationship between its presence and changes in the Type I/Type II classification of individual neurons.

1.2 Neural networks: encoding complex information and behaviors using connected neurons

Just as a lone bit could not perform the complex computations accomplished by a computer, a lone neuron could not possibly be responsible for the complex behaviors made possible by the brain. These behaviors are brought about by the dynamics of neural networks. In such networks, neurons communicate with each other in two primary fashions: via synapses and via gap-junctions.

Gap-junctions utilize electrical signalling to allow neural communication. Facilitated by a specialized membrane protein, two neurons that are connected via a gap-junction contain specialized channels that connect their cytoplasms. Ions and other very small biological compounds are able to travel through this channel, meaning that a change in the membrane potential in one neuron, and the corresponding change in ion concentration inside the cell, will be reflected in any neurons connected via gap-junction [68]. While gap-junctions are common throughout the brain, they are limited to neurons that are located very close to each other, and thus the types of networks that arise solely from gap-junctions are limited. Thus, the networks analyzed in this dissertation do not include gap-junctions.

Synapses, on the other hand, are not limited to close spatial proximities; in fact, axons traverse great distances in the brain to connect distant neurons. This allows for more complex networks to arise, which is why this type of signalling is focused on in this research. Synaptic communication occurs driven by action potentials: when the membrane voltage of a neuron spikes, this triggers the activity of voltage-gated Ca^{2+} channels, and in turn the release of chemicals known as neurotransmitters from the neuron. These neurotransmitters, now free outside of the neuron, can bind to receptor proteins on the membrane of a synaptically coupled neuron. The binding

of the neurotransmitter to these proteins causes a change in this neuron that is normally reflected by a change in its membrane voltage, which will affect the timing of its next action potential firing. A cartoon representation of a typical synapse is shown in Fig 1.4, illustrating the activity of voltage-gated Ca^{2+} channels and the resulting release of neurotransmitter through the fusion of synaptic vesicles with the neural membrane. When discussing synapses, the initial neuron that releases neurotransmitter is referred to as the "pre-synaptic" neuron, while the neuron which receives the signal and the neurotransmitter is referred to as the "post-synaptic" neuron [24].

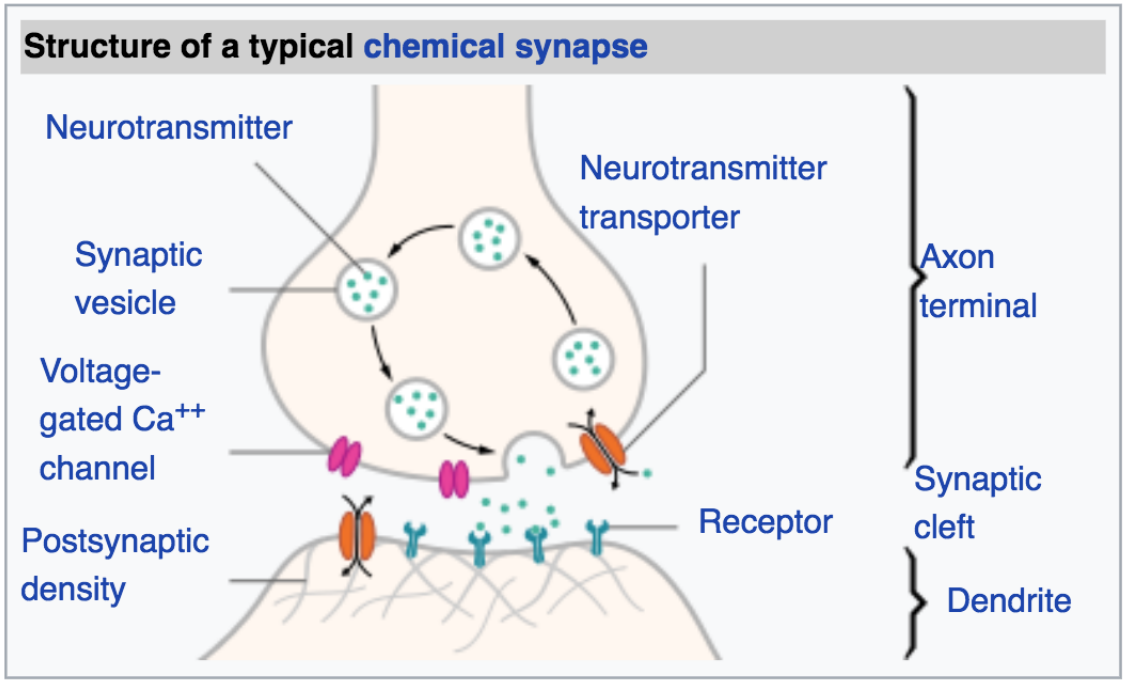

Figure 1.4: A cartoon representation of the typical synapse. When an action potential occurs, the voltage spike activates voltage-gated Ca^{2+} channels. This triggers the release of neurotransmitter through the fusion of a synaptic vesicle with the neuron membrane. The neurotransmitter is now free in the extracellular space between the pre- and post-synaptic neuron and is likely to bind to receptors on the post-synaptic neuron [97].

Synapses can be either excitatory or inhibitory. Excitatory synapses cause the membrane voltage of the post-synaptic cell to rise, and are commonly associated

with the neurotransmitter glutamate. Inhibitory synapses cause the membrane voltage of the post-synaptic cell to decrease, and are commonly associated with the neurotransmitter gamma-Aminobutyric acid (commonly referred to as GABA). Other neurotransmitters, such as the previously discussed ACh, can have more complicated effects on the behavior of the post-synaptic neuron. Neurons that release excitatory neurotransmitters such as glutamate are referred to as "excitatory neurons" while neurons that release inhibitory neurotransmitters such as GABA are referred to as "inhibitory neurons".

Just as for the neuron, there are a variety of mathematical models that are used to model the synaptic current felt by a post-synaptic neuron. In this dissertation, I use what is commonly referred to as the "double-exponential" model, which is described by the following equation,

$$I_{syn}(t) = g_{syn}(V - E_{syn}) \left(\sum_{s_i} e^{-(t-s_i)/\tau_d} - e^{-(t-s_i)/\tau_r} \right) \tag{1.1}$$

where g_{syn} is the maximum conductance for the synapse, V is the membrane voltage of the post-synaptic neuron, E_{syn} is the reversal potential of the synaptic current, s_i are the times of all pre-synaptic spikes occuring before the current time t in ms, and τ_d and τ_r are the synaptic decay and the synaptic rise time constants, respectively (in ms), which affect the "shape" of the synaptic signal. The value of E_{syn} determines whether the synapse is excitatory or inhibitory: it is inhibitory when it is set at -75 mV, and excitatory when it is set at 0 mV. In the various simulations performed in this dissertation, τ_r, τ_d and g_{syn} are varied.

1.2.1 Oscillations and synchrony in neural networks

One of the most important behaviors brought about by synaptically coupled networks of neurons are synchronous oscillations of the neural populations. Such os-

cillations have been detected by electroencephalogram (EEG) recordings since the 1930s, and rhythms with different frequencies are thought to be associated with different brain functions. For example, oscillations in the alpha band, with a frequency between 7.5 and 12.5 Hz, appear to correspond with states where an individual is relaxed and has their eyes closed, while oscillations in the theta band, with a frequency typically between 6 and 7 Hz, appear to correspond with the encoding of memory. Gamma oscillations, which account for rhythms with frequencies ranging from 25 Hz to 100 Hz, are also thought to play a role in memory formation and recollection. Increased power in the alpha and gamma frequency ranges also is seen in tasks requiring selective attention. Finally, some studies imply that gamma oscillations may be crucial for conscious awareness [116]. Given the ubiquity of the gamma rhythm and the numerous computational studies focusing on this frequency range, we will discuss gamma oscillations in more detail in Section 1.2.2.

The study of the mechanisms underlying neural oscillations and synchrony is of great interest to neuroscientists, and is a problem that computational neuroscientists are uniquely qualified to address. Utilizing a variety of mathematical techniques, computational neuroscientists have articulated a diverse set of possible mechanisms by which neural networks might oscillate. This research has revealed that the impetus behind neural oscillations can be either excitatory or inhibitory neurons. As an example, a network of purely excitatory neurons is more predisposed to exhibit synchrony when the neurons have Type II PRCs as opposed to Type I PRCs [52].

However, in this dissertation we focus on the ways that inhibitory interneurons can initiate and influence neural oscillations. In the hippocampus, interneurons mediate rhythms that appear to serve vital roles in memory processing and are affected by sleep-wake activity [4, 9, 109, 64]. Interneurons also play a key role in

generating rhythmic activity in the cortex; in the visual cortex in particular, these rhythms are implicated in the control of attention in the presence of competing stimuli [36, 70, 84, 46, 19].

There are two particularly ubiquitous mechanisms describing how these inhibitory interneurons can drive synchrony in neural networks. One, the Interneuron Network Gamma (ING) mechanism, describes the fashion by which a purely inhibitory network might exhibit synchronous oscillations, while the other, the Pyramidal Interneuron Network Gamma Mechanism (PING), describes how inhibitory interneurons can drive synchronous oscillations in a network containing both excitatory and inhibitory neurons. The computational principles underlying these two mechanisms will be discussed in detail in Section 1.3.

It is important to note the distinction between neural oscillations of the kind detected in EEG recordings and neural synchrony as seen in the classic ING and PING literature. While oscillatory activity in the brain does not manifest the complete synchrony that can be driven by the ING and PING mechanisms (indeed, the existence of completely synchronous neural dynamics is indicative of epilepsy, as discussed in Section 1.2.3), oscillations do arise via "up" states in which neurons are much more likely to fire and "down" states in which much fewer neurons fire. While this more subtle behavior is difficult to match via modeling, ING and PING can model the more idealized behavior represented by full synchrony. As such, computational neuroscientists often study the mechanisms underlying neural synchrony as a means to formulate well-justified hypotheses as to the generation of the oscillatory activity actually detected in EEG recordings.

1.2.2 Gamma rhythms and the potential informational capacity of neural oscillations

Oscillations in the gamma range merit further inspection, not only for their prevalence in diverse brain regions and behaviors, but also because the ING and PING mechanisms, which are the focus of much of this dissertation research, yield oscillations primarily in this frequency range.

The ubiquity of gamma rhythms is supported by a variety of biophysical properties. These include the time scales by which GABA and alpha-amino-3-hydroxy-5-methyl-4-isoxazolepropionic acid (a glutamate receptor commonly referred to as AMPA) receptors operate and the membrane properties of excitatory pyramidal cells. Due to these properties, a hypothesized role of the gamma rhythm is to collect presynaptic spikes into the optimal time window in which to elicit spiking from a postsynaptic neuron [25].

Gamma rhythms may also be uniquely suited to store information. One hypothesis for how this can occur is through the presevation of the ordering of neural firings within a gamma rhythm. In an example with short-term memory, it is theorized that the ordering of excitatory pyramidal cells within a gamma rhythm is preserved, and this ordering is hypothesized to store facets of the memory [116].

Gamma rhythms are also of particular interest because inhibitory interneurons are thought to serve a necessary role in generating these rhythms. Various studies have shown that parvalbumin (PV) positive basket cells, a type of inhibitory interneuron differentiated by the expression of the parvalbumin protein, is essential for the generation of a gamma rhythm. Other interneurons that act over longer spatial distances may be responsible for synchronizing different regions of the brain into a gamma rhythm. Whether these interneurons drive gamma oscillations via the ING or PING mechanism (which are explained in Section 1.3 with cartoon representa-

tions in Figs 1.6 and 1.7), or whether both these mechanisms occur but compete with each other, remains a subject of active research [25]. This open question helps to motivate the continued computational research into the mechanisms underlying gamma oscillations.

It should be emphasized that *in vivo* gamma rhythms tend to be short lived and occur despite irregular firing of the pyramidal cells, and do not exhibit the "complete synchrony" that the classic ING and PING rhythms reveal in computational studies. Instead, *in vivo* gamma rhythms arise on a network-wide basis and are seen via EEG and local field potential (LFP) recordings [25]. If neural networks exhibit complete synchrony that persists for longer time periods, it is often indicative of a neuropathology such as epilepsy, which we discuss in the following section.

1.2.3 Epilepsy and the potential pathology of neural synchrony

Not all forms of synchronous, oscillatory neural activity serve a specific brain function; indeed, sometimes these events can be indicative of neuropathology. The most common example of this is epilepsy, a disease typified by repeated seizures in the patient. Epileptic seizures are detected by EEG recordings that exhibit overactive and synchronous neural activity.

A variety of oscillatory neural dynamics have been implicated in the development of epileptic seizures. Seizures are often initiated by high frequency oscillations (HFOs) in the range of 70 to 120 Hz. Even faster oscillations, referred to as ripples (with a frequency between 120 and 250 Hz) and fast ripples (with a frequency between 250 and 600 Hz) occur in between seizures and are used as markers for brain regions that may be participating in or succeptible to epileptic events. An example experimental recording of fast ripples from the hippocampus (**A**) and a computational model replicating this behavior (**B**) is shown in Fig 1.5. In each case, increased

power in the 250-500 Hz frequency range illustrated by the spectrogram (bottom of each panel) illustrates the development of fast ripples. Typically, epileptiform activity spreads throughout the brain and causes synchronous activity between brain regions [117].

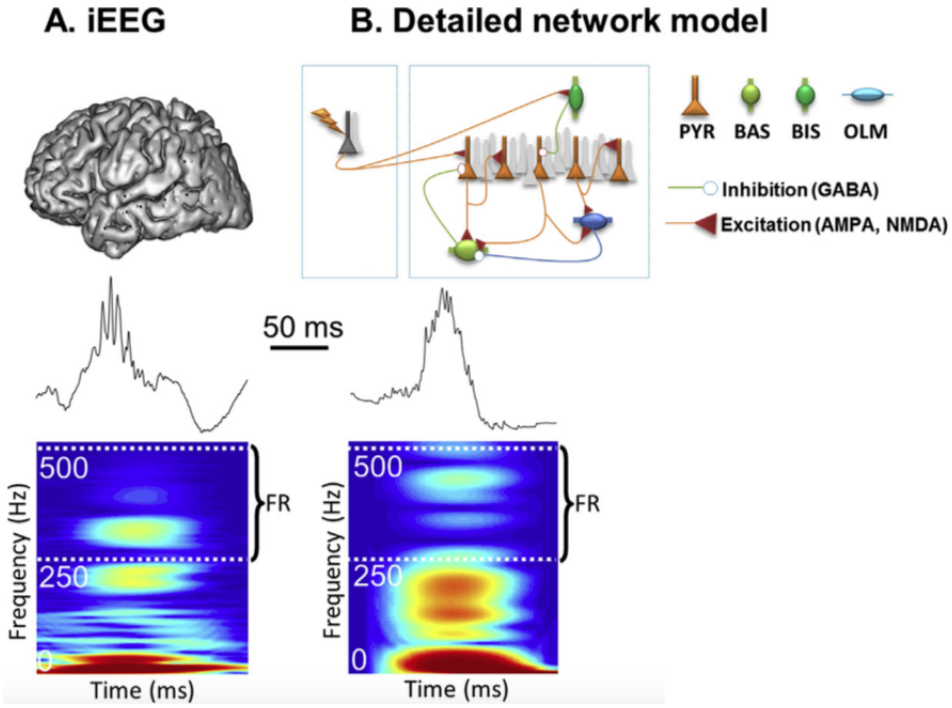

Figure 1.5: **A** An example biological recording revealing fast ripples in the hippocampus. The fast ripples are shown in the spectrogram at the bottom of the panel by the increased power in the 250-500 Hz range. **B** An example computational model that is able to replicate the fast ripples seen experimentally. The model network is represented in an approximate, cartoon fashion in the top of the panel, with the spectrogram at the bottom of the panel showing the presence of fast ripples [117].

Because oscillatory neural activity can be modeled using computational techniques, computational neuroscience has been a particularly powerful tool in the study of epilepsy. A variety of techniques utilizing different degrees of abstraction have been used in creating mathematical models that display dynamics matching those seen in experiments. These models range from complex networks of Hodgkin-Huxley style neurons to neural mass models, which model the overall activity of a neural network with a higher level of abstraction, eliminating the need for the simulation

of individual neurons. Insights from computational studies have been invaluable in decoding the mechanisms underlying the various types of oscillatory dynamics that contribute to this neuropathology, providing a particularly compelling argument for the continued study of neural oscillations using computational methods [117].

1.3 Computational mechanisms explaining synchrony in networks containing inhibitory interneurons

As the discussion in Section 1.2.1 illustrates, the study of neural oscillations consists of a multitude of questions that can be addressed both experimentally and computationally. However, computational neuroscience is particularly adept in providing potential explanations regarding the ability for neural networks to exhibit synchronous oscillations, illustrated by the multitude of studies published in this field over the past quarter century. Indeed, two of the most commonly cited mechanisms explaining the generation of gamma rhythms, ING and PING, were first articulated via computational study.

ING and PING share a common impetus underlying neural synchrony and network oscillations: the activity of inhibitory interneurons. It is for this reason that the focus of this dissertation research is discerning the potential effects of changing interneuron properties on these mechanisms. However, before delving into this research, the ING and PING mechanisms as classically stated must be fully understood.

1.3.1 Interneuron Network Gamma (ING)

The ING mechanism explains how a network consisting only of inhibitory neurons can generate synchronous activity and oscillations in the gamma frequency band [63, 119, 114]. This mechanism was originally articulated utilizing model neurons exhibiting Type I properties and with densely, synaptically coupled networks, justified

by analogy to the ubiquitous PV interneurons [115, 119, 29, 8, 22]. However, as discussed in more detail in Chapter II, the ING mechanism can persist in networks where the neurons are randomly connected in a non-dense fashion.

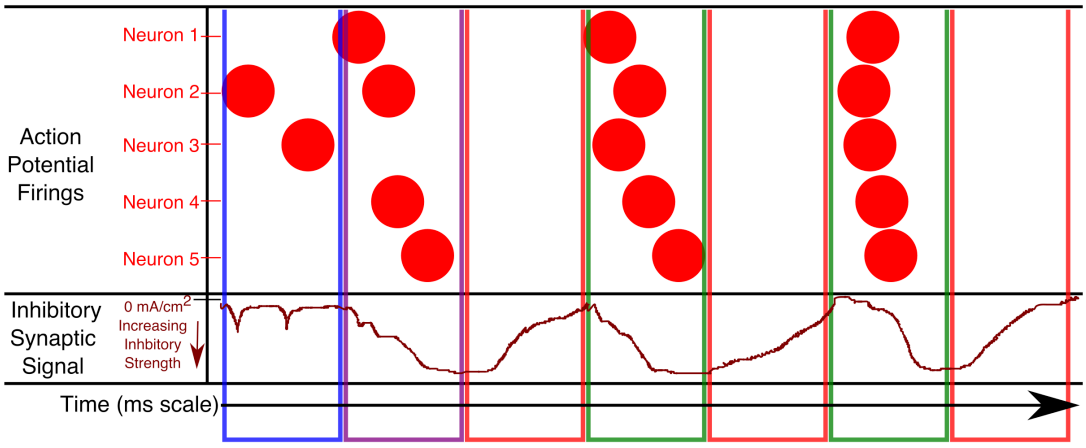

Figure 1.6: An approximated, cartoon representation of a toy network with five all-to-all connected inhibitory cells exhibiting ING synchrony, showing both the firing times of each cell and the inhibitory synaptic signal felt by each neuron. In the regime outlined by the blue bracket, some inhibitory cells fire, but not enough to suppress network activity. In the regime outlined by the purple bracket, enough neurons fire in close enough temporal proximity for the inhibitory signalling to sum and suppress network firing. The regime outlined by the red bracket represents the time window in which firing is suppressed by the resulting large amplitude inhibitory synaptic signals. The regime outlined by the green bracket represents the time window in which firing can occur following the decay of inhibitory signalling. The activities represented by the red and green brackets then oscillate, forming the oscillatory network activity.

The ING mechanism is initiated when a sufficient proportion of the inhibitory neurons in the network fire an action potential in close temporal proximity. The summation of the resulting synaptic signals on each neuron leads to a large hyperpolarizing effect on the neurons' membrane potential, which prevents further firing. The neurons will not be able to fire an action potential until their membrane voltages recover from this hyperpolarized state, which requires the decay of the inhibitory synaptic signals. This creates a small temporal window between the decay of inhibitory synaptic signal and the next instance of large amplitude synaptic inhibition in which neurons can fire an action potential. The creation of this window syn-

chronizes neural firing, while also creating a network oscillation whose frequency is dictated by the timing of these windows, controlled primarily by the duration of synaptic current. A cartoon illustration of this mechanism, illustrating both the spike times and inhibitory synaptic signal in a hypothetical, "toy" network consisting of five all-to-all connected inhibitory neurons, can be found in Fig 1.6.

A major feature of this mechanism is that inhibitory signals promote synchronization by gating the timing of neural firing. As a result, synchrony via the ING mechanism is sensitive to properties of the synaptic currents present in the network and is most robust when networks are densely connected and cellular heterogeneity is low [63, 109, 106, 114, 119]. In particular, the ING mechanism predicts that synaptic inhibition that is sufficiently strong and long lasting should robustly cause synchrony amongst intrinsically firing cells whose firing frequencies are similar.

1.3.2 Pyramidal Interneuron Network Gamma (PING)

The PING mechanism explains the development of gamma frequency synchronous oscillations in a network consisting of both excitatory and inhibitory neurons in which the excitatory and inhibitory neurons are densely inter-connected. Such networks are colloquially termed E-I networks. Computational studies leading to the articulation of this mechanism [108, 63, 119, 42] were spurred by experimental results that implicate interactions between excitatory and inhibitory neurons in gamma rhythm generation [121].

The PING mechanism states that synchronous, rhythmic dynamics of both the excitatory and inhibitory cell populations can be generated if the inhibitory cells spike only in response to excitatory cell activity, if excitatory cell activity quickly induces a synchronous inhibitory population burst, and if the inhibitory burst suppresses all excitatory cells. These requirements ensure that a burst of inhibitory signalling will

only occur directly following excitatory cell activity, which in turn will suppress the excitatory cells in a fashion similar to how inhibitory cells were suppressed in the ING mechanism. Here, though, the inhibitory neurons gate the firing of the excitatory cells, as opposed to their own firing. The impetus behind this mechanism is the firing of a large proportion of the excitatory cells in close temporal proximity, which causes the burst of inhibitory cell firing; once again, this has a close analogue to the initiation of the ING mechanism. A cartoon illustration of this mechanism, illustrating the spike times, E-I synaptic signal, and I-E synaptic signal in a hypothetical, "toy" network consisting of three excitatory and two inhibitory neurons with all-to-all inter-connectivity, can be found in Fig 1.7.

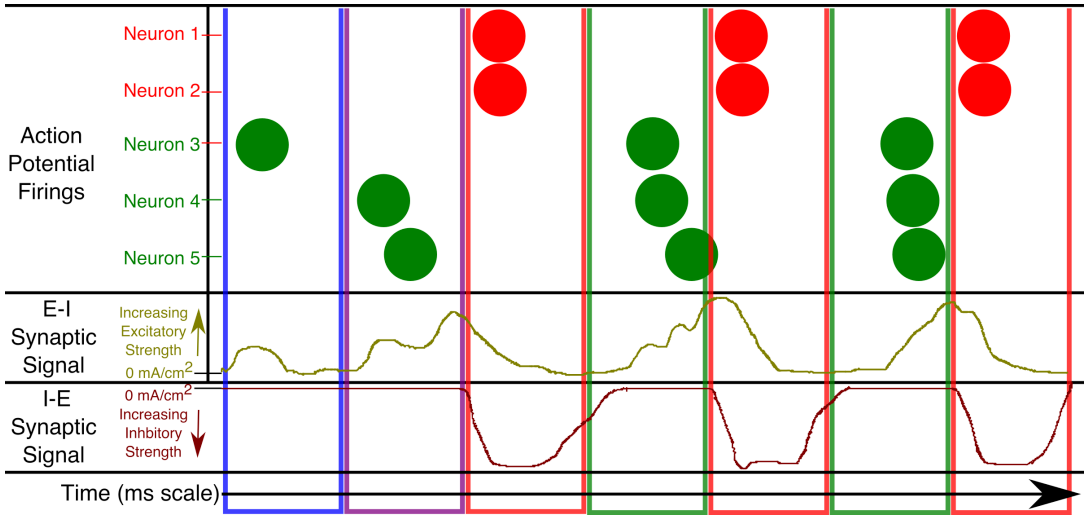

Figure 1.7: An approximated, cartoon representation a toy network with three excitatory cells (green) and two inhibitory cells (red) with all-to-all inter-connectivity exhibiting PING synchrony. The timing of cell firings, the E-I synaptic signal, and the I-E synaptic signal are shown. In the regime outlined by the blue bracket, some excitatory cells fire, but not enough to elicit activity from the inhibitory cells. In the regime outlined by the purple bracket, enough excitatory neurons fire in close enough temporal proximity to cause inhibitory activity. The regime outlined by the red bracket represents the time window in which excitatory firing is suppressed by the activity of inhibitory cells. The regime outlined by the green bracket represents the time window in which firing of the excitatory neurons can occur following the decay of inhibitory signalling. The activities represented by the red and green brackets then oscillate, forming the oscillatory network activity.

PING rhythmicity requires strong inter-connectivity between the excitatory and

inhibitory subpopulations so that the requirements described above are satisfied. Strong intra-connectivity within the inhibitory cell population also plays a role in the PING mechanism by ensuring that the inhibitory population fires a single synchronous burst following excitatory input. While this intra-connectivity has an abundance of biological motivation [44, 59, 104, 82, 73, 76], the research detailed in Chapter IV shows that strong intra-connectivity is not strictly necessary for PING-like rhythms to arise [86], making inter-connectivity between excitatory and inhibitory neurons the paramount aspect of network connectivity underlying PING.

1.3.3 Network versus cellular properties dictating inhibitory synchrony

It bears emphasis that the ING and PING mechanisms rely primarily on network properties, in particular the properties of the synaptic connections, to dictate neural synchrony and oscillatory dynamics. In the ING mechanism, synchrony arises only if the inhibitory signalling is sufficiently strong, long lasting, and uniform across all of the neurons making up the network. In the PING mechanism, the dense and strong synaptic signalling between the excitatory and inhibitory populations precipitates the generation of synchronous oscillations. This similarity manifests itself in the fact that both mechanisms rely upon gating inhibition to synchronize neural activity.

Perhaps driven by this observation, a majority of the studies aiming to probe the robustness of these mechanisms to various forms of heterogeneity and noise have focused on the properties of the synaptic connections. However, this narrow focus neglects the potential role that the properties of the inhibitory interneurons themselves might play in these mechanisms. This is of particular importance given that recent experimental advances have revealed that inhibitory interneurons are an immensely diverse population expressing a variety of neural excitability profiles and synaptic connectivities [61, 23, 10, 7, 96, 62, 51, 11, 47].

This dearth of literature exploring the fashions in which the intrinsic cellular properties of inhibitory interneurons might drive synchrony and oscillatory dynamics in neural networks provides the motivation for the research making up this dissertation. Here, I look not only at the network properties that might underlie oscillatory behavior, but also the potential effects of changing cellular properties on network dynamics. Changes in cellular properties are easily quantified by the Type I/Type II classificiations discussed in Section 1.1.3, and as such I utilize this specific cellular variation in the analysis of interneuronal diversity.

1.4 Outline

Motivated by the distinction between network and cellular properties outlined in Section 1.3.3, in this dissertation I probe how mechanisms other than ING and PING, in particular those driven by cellular rather than network properties, interact and compete with these commonly cited mechanisms to generate synchronous oscillations in neural networks. This research is performed both on purely inhibitory networks, in which the ING mechanism is typically cited, and in E-I networks, in which the PING mechanism is ubiquitous.

In Chapter II, I investigate how changing the cellular properties of the inhibitory interneuron affects synchronous network activity in a purely inhibitory network. The cellular properties are manipulated via the Type I/Type II classifications as well as by analyzing the role of an M-type adaptation current. This research reveals that while networks consisting of Type I interneurons synchronize in fashions accounted for by the ING mechanism, the dynamics of networks of Type II neurons and the distinct behaviors caused by the presence of an adaptation current are not fully accounted for by ING. In fact, mechanisms driven by cellular properties, particularly the distinct

features of the Type II PRC, are likely responsible for the unique dynamics seen in these networks.

Next, in Chapter III, the research transitions to the study of E-I networks and the PING mechanism. In this work, I vary the structure of the E-I network via manipulation of the synaptic strengths of inter-connectivities (synapses between the excitatory and inhibitory neurons) and intra-connectivities (synapses within the excitatory or inhibitory networks themselves). In all of these E-I networks I also manipulate the intrinsic cellular properties between Type I and Type II utilizing the M-type adaptation current and modulation by ACh. My analysis of these simulations reveals three distinct regimes of E-I network connectivities in which modulation by ACh differentially affects synchronous oscillations in the network. When inter-connectivity dominates intra-connectivity, network properties ensure that PING dynamics arise regardless of modulation by ACh. When intra-connectivity dominates inter-connectivity, cholinergic modulation causes significant change in the network dynamics, in which synchronous bursting arises in networks with Type II excitatory neurons but not in networks with Type I excitatory neurons. Finally, when the inter- and intra-connectivities are balanced, mechanisms driven by both network and cellular properties interact, and more complicated dynamics tend to arise.

Finally, in Chapter IV I focus on E-I networks in which PING rhythms tend to occur, namely those with strong inter-connectivity, and analyze the role that changes within the inhibitory cell population can have on PING rhythmicity. This research reveals that networks with Type I and Type II inhibitory cells respond differently to changes in the strength of the inhibitory intra-connectivity; in particular, networks with Type I inhibitory cells and weak inhibitory intra-connectivity display oscillatory dynamics not fully encapsulated by predictions of the PING mechanism. This result

leads to a precise analysis of how patterning in the inhibitory population affects variability seen in oscillatory firing of the excitatory cells.

In the remainder of this introduction, I discuss the neuron models and measures used to quantify network dynamics throughout the three chapters outlined above.

1.5 Neuron models

The networks used in this research are composed of three different model neurons in the Hodgkin-Huxley formalism that display different properties in their I-F curves and PRCs. These models are referred to in this research succinctly as Type I neurons, Type II neurons, and Type II neurons with adaptation.

All model neurons contain Na^+, K^+-delayed rectifier and leak currents. The Type II neuron with adaptation additionally contains a slow, M-type K^+ current [43, 45, 98]. The difference between the Type I and Type II neuron models arises due to the different parameter values for the conductances and the differences in the functions governing the gating variables, primarily a depolarizing shift in the steady-state activation function associated with the delayed rectifier potassium channel. The difference between the Type I and Type II with adaptation neuron arises due to the activity of the slow potassium channel.

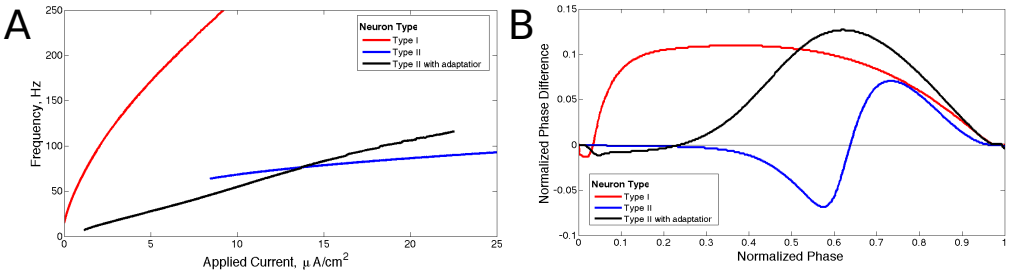

Figure 1.8: Properties of the three neuron models utilized in this dissertation research. **(A)**: Current-frequency curves (I-F curves) of Type I (red), Type II (blue) and Type II with adaptation (black) neuron models. **(B)**: Phase response curves (PRCs) calculated with a brief excitatory current pulse for each model neuron firing at 65 Hz.

1.5.1 The Hodgkin-Huxley model

To model an interneuron exhibiting Type II properties without spike-frequency adaptation, the classic Hodgkin-Huxley equations are used [57, 43]:

$$\frac{dV}{dt} = -g_{Na}m^3h(V - E_{Na}) - g_K n^4(V - E_K) - g_L(V - E_L) + I_{app} - I_{syn} \tag{1.2}$$

$$\frac{dX}{dt} = \alpha_X(V)(1 - X) - \beta_X(V)X, \text{ for } X = m, h, n \tag{1.3}$$

$$\alpha_m(V) = -0.1\left(\frac{V + 40}{e^{-(V+40)/10} - 1}\right) \tag{1.4}$$

$$\beta_m(V) = 4e^{-(V+65)/18} \tag{1.5}$$

$$\alpha_h(V) = 0.07e^{-(V+65)/20} \tag{1.6}$$

$$\beta_h(V) = \frac{1.0}{e^{-(V+35)/10} + 1} \tag{1.7}$$

$$\alpha_n(V) = -0.01\left(\frac{V + 55}{e^{-(V+55)/10} - 1}\right) \tag{1.8}$$

$$\beta_n(V) = 1.25e^{-(V+65)/80} \tag{1.9}$$

V represents the membrane voltage in [mV], while m, n and h represent the unitless gating variables of the ionic current conductances. I_{app} signifies the external applied current to the neuron (described in detail in Section 1.2), in [μA/cm^2], while I_{syn} describes the synaptic current input to the cell from the network (I_{syn} is described in detail above in Section 1.2, while I_{app} will be described in more detail in the following chapters), also with units of [μA/cm^2]. E_{Na}, E_K and E_L are the reversal potentials, with Na symbolizing sodium, K symbolizing potassium, and L symbolizing the leak

current. In this model these constants are set at $E_{Na} = 50$ mV, $E_K = -77$ mV and $E_L = -54.4$ mV. The corresponding maximum conductances g_{Na}, g_K and g_L are set at $g_{Na} = 120$ mS/cm^2, $g_K = 36$ mS/cm^2 and $g_L = 0.3$ mS/cm^2.

The Type II properties of this model neuron are reflected in its I-F curve (Fig 1.8**(A)**) and PRC (Fig 1.8**(B)**) [114]. At current threshold, firing frequency is a discrete, non-zero value and the slope of the I-F curve is shallow for all applied current values. The discontinuity between a zero firing frequency and a non-zero firing frequency arises from the subcritical Hopf bifurcation that leads to periodic firing in this model neuron, and this bifurcation is also historically associated with the classification of this neuron model as Type II [38, 98]. The PRC displays an initial delay region and phase advance when the brief depolarizing current pulse is delivered at later phases.

1.5.2 The Cortical Pyramidal Neuron (CPN) model

Type I neurons and Type II neurons with adaptation are simulated utilizing a model, first articulated to describe cortical pyramidal neurons, in which different values for the conductance associated with the M-type potassium current switch the properties of the neuron between Type I and Type II [45, 98]. The equations are

(1.10)
$$\frac{dV}{dt} = -g_{Na} m_\infty^3 h(V - E_{Na}) - g_{K_d} n^4 (V - E_K) - g_{K_s} z (V - E_K) - g_L (V - E_L) + I_{app} - I_{syn}$$

(1.11)
$$\frac{dX}{dt} = \frac{X_\infty(V) - X}{\tau_X(V)} \text{ for } X = h, n, z$$

(1.12)
$$m_\infty(V) = \frac{1}{1 + e^{(-V-30/9.5)}}$$

(1.13)
$$h_\infty(V) = \frac{1}{1 + e^{(V+53/7.0)}}$$

$$n_\infty(V) = \frac{1}{1 + e^{(-V-30/10)}} \tag{1.14}$$

$$z_\infty(V) = \frac{1}{1 + e^{(-V-39/5)}} \tag{1.15}$$

$$\tau_h(V) = 0.37 + \frac{2.78}{1 + e^{(V+40.5)/6}} \tag{1.16}$$

$$\tau_n(V) = 0.37 + \frac{1.85}{1 + e^{(V+27)/15}} \tag{1.17}$$

$$\tau_z(V) = 75 \tag{1.18}$$

Variables and constants have identical meanings as in the Type II model (see Section 1.5.1), with the new terms g_{K_d} and g_{K_s} representing the maximal conductances associated with the delayed rectifier and slow M-type potassium currents, respectively, and z representing the gating variable governing the M-type potassium current. The constants for this model are as follows: $E_{Na} = 55$ mV, $E_K = -90$ mV, $E_L = -60$ mV, $g_{Na} = 24$ mS/cm^2, $g_{K_d} = 3$ mS/cm^2 and g_L=0.02 mS/cm^2.

When $g_{K_s} = 0$ mS/cm^2 the model neuron is designated Type I because of the properties of its I-F curve (Fig 1.8**(A)**) and PRC (Fig 1.8**(B)**) [114]. The neuron exhibits firing frequencies arbitrarily close to zero at current threshold and the slope of the I-F curve is initially very steep while becoming more shallow as applied current increases. The PRC exhibits phase advance for a brief depolarizing current pulse delivered at essentially every phase. This model neuron achieves repetitive firing via a SNIC bifurcation, which is historically associated with the Type I classification [98, 38].

When $g_{K_s} = 1.5$ mS/cm^2 the model neuron is designated Type II with adaptation because the properties of its I-F curve (Fig 1.8**(A)**) and PRC (Fig 1.8**(B)**) match the

basic properties of a Type II neuron as described previously in Section 1.5.1 [114]. This neuron model achieves periodic firing with a subcritical Hopf bifurcation, a known feature of neuron models with an M-type adaptation current that is associated with the Type II classification [38].

While the equations for the Type I neuron and the Type II neuron with adaptation were initially developed to model a cortical pyramidal neuron modulated by ACh, the properties of this neuron when $g_{K_s} = 0$ closely mirror those of fast-spiking Type I interneurons (such as the ubiquitous PV interneurons). Additionally, the presence of an active M-current when $g_{K_s} = 1.5$ causes this model to act similarly to interneurons with such a current, such as the oriens-lacunosum moleculare (OLM) interneurons.

1.6 Measures quantifying network behavior

While the primary behavior of interest in this dissertation research is synchronous network oscillations, oftentimes this behavior can exhibit complex dynamics that are not completely encapsulated by simply measuring whether or not the network exhibits synchrony. The presence of some type of oscillatory dynamics can most easily be detected by analyzing the propensity for the network to synchronize. However, a major component of this dissertation research is the articulation of additional measures that concisely articulate other crucial properties of the network dynamics. Such measures are used repeatedly in the chapters to follow, and as such are described here.

1.6.1 Synchrony Measure

The Synchrony Measure is an adaptation of a measure created by Golomb et. al. [49, 50] that quantifies the degree of spiking coincidence in the network. Briefly, the measure involves convolving a gaussian function with the time of each action

potential for every cell to generate functions $V_i(t)$. The population averaged voltage $V(t)$ is then defined as $V(t) = \frac{1}{N}\sum_{i=1}^{N} V_i(t)$, where N is the number of cells in the network, which in this work is typically 1000. We further define the overall variance of the population averaged voltage σ and the variance of an individual neuron's voltage σ_i as

$$\sigma =< V(t)^2 > - < V(t) >^2 \tag{1.19}$$

and

$$\sigma_i =< V_i(t)^2 > - < V_i(t) >^2 \tag{1.20}$$

where $< \cdot >$ indicates time averaging over the interval for which the measure is taken. The Synchrony Measure S is then defined as

$$S = \frac{\sigma}{\frac{1}{N}\sum_{i=1}^{N} \sigma_i} \tag{1.21}$$

The value $S = 0$ indicates completely asynchronous firing, while $S = 1$ corresponds to fully synchronous pattern of network activity. Example raster plots differentiating synchronous and asynchronous firing are found in Fig 1.10.

1.6.2 Burst Similarity Measure

To quantify relative overlap in cell participation in subsequent network bursts, where a network burst is defined as a small time window in which a large proportion of the neurons in a network fire action potentials, I constructed a new measure, entitled the Burst Similarity Measure. It quantifies the fraction of active neurons that participate in consecutive bursts of network activity. This measure is calculated in two steps. First, to detect timing and duration of each burst, the spike times of each neuron in the network are convolved with a gaussian function and a cumulative

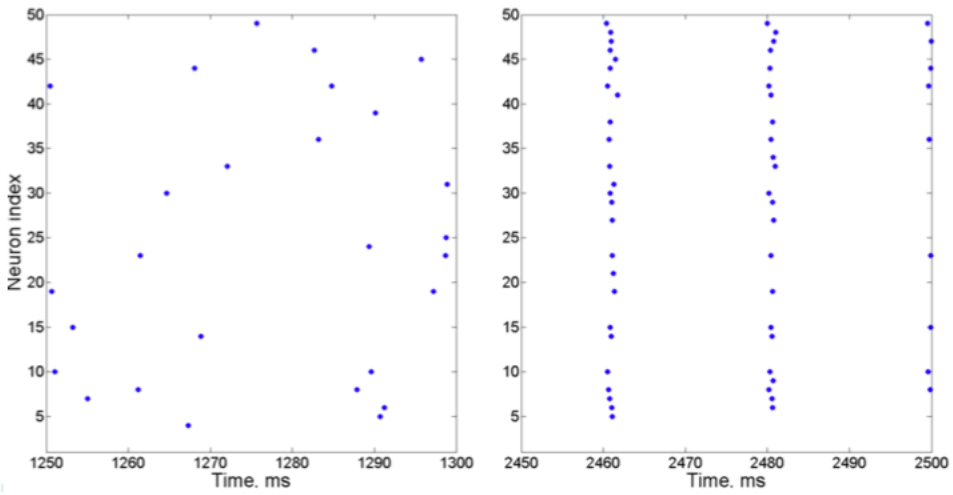

Figure 1.9: Example raster plots differentiating synchronous and asynchronous network activity. Left panel: example neural activity exhibiting asynchrony, which yields a Synchrony Measure near 0. Right panel: example neural activity exhibiting synchrony, which yields a Synchrony Measure near 1.

network activity trace is formed (in the same fashion as described for $V(t)$ in Section 1.6.1. This trace is subsequently thresholded to determine the on and off times for every burst (b_j and e_j, respectively).

For each burst j a binary vector is constructed that quantifies which neurons spiked during the burst, v_j. If neuron i spiked during burst j, meaning it fires at a time t_j such that $b_j \leq t_j \leq e_j$, $v_j(i) = 1$, otherwise $v_j(i) = 0$. The Burst Similarity Measure B is then determined via

$$B = \frac{1}{n-1} \sum_{j=1}^{n-1} \frac{v_j \cdot v_{j+1}}{|v_j||v_{j+1}|} \tag{1.22}$$

where $\cdot$ indicates the vector dot product, $|x|$ indicates the vector norm, and n is the total number of bursts.

A Burst Similarity Measure of $B = 0$ indicates that consecutive bursts contain mutually exclusive populations of neurons, while $B = 1$ indicates that consecutive bursts contain an identical population of neurons.

The measure allows for differentiation of multiple types of behavior reflected by an

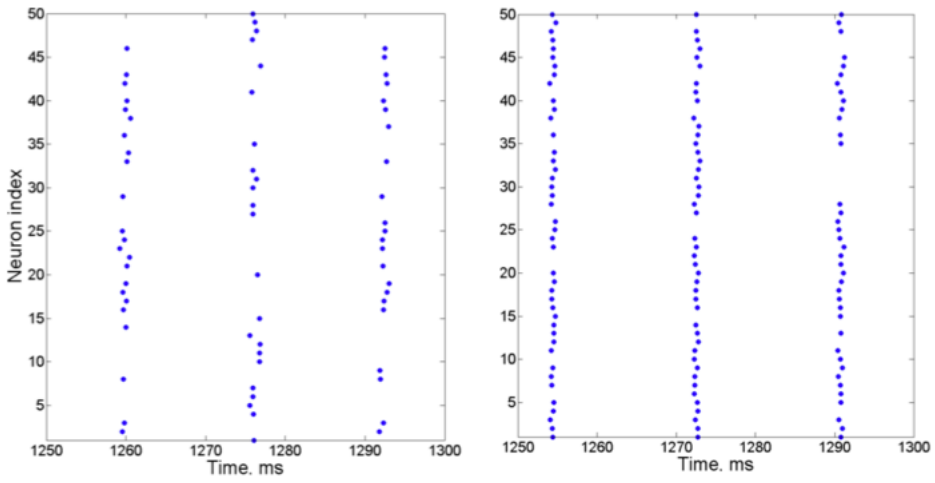

Figure 1.10: Example raster plots differentiating one-cluter and two-cluster network dynamics. Left panel: example neural activity exhibiting two-cluster dynamics, which yields a Burst Similarity Measure of 0. Right panel: example neural activity exhibiting one-cluster dynamics, which yields a Burst Similarity Measure near 1.

intermediate value of the Synchrony Measure. For example, synchronous dynamics for which half the cells in the network are active and participate in each synchronous burst, while the other half of neurons are completely suppressed, exhibits an intermediate value of S and $B = 1$. In contrast, dynamics consisting of bursts of network activity in which consecutive bursts contain mutually exclusive populations of neurons, each containing half of the neurons in the network, also has an intermediate value of S but $B = 0$.

Numerous validation studies were done to confirm that this measurement satisfies the above properties in practice. Toy cases easily confirm the extreme cases of $B = 0$ and $B = 1$ described above; additionally, for a variety of simulations of the networks I confirmed that the dynamics predicted by B matched the dynamics exhibited by the network by visually inspecting the corresponding raster plots. Example raster plots differentiating one-cluster and two-cluster dynamics are shown in Fig 1.10.

1.6.3 Variability Measure

The Synchrony Measure does not detect organization, or lack thereof, within each synchronous burst of network activity, or take into account the periodicity of the bursting dynamics. As such, three additional measures were utilized to quantify the organization and periodicity of excitatory bursting dynamics in E-I networks.

Each of these three additional measures relied upon detecting instances of bursting activity within the excitatory network and identifying which neurons participated in the burst. This was done in an identical fashion to that described for the Burst Similarity Measure in Section 1.6.2.

To analyze the organization of excitatory neurons within each network burst, the Variance of Neuron Order (O) is calculated. For each burst of excitatory network activity in the last second of a given simulation (term k the number of these bursts), the spike time of each firing neuron is detected and temporally ordered. We assign a value $O_{i,j}$ for each neuron i in each burst j that conveys information on the ordering of the firing of neuron i within burst j. The firing order is normalized by the number of unique firing times in each excitatory burst and scaled between 1 and 100 such that the neurons that fire first have a value of 1 and the neurons that fire last (or not at all in a given burst) are given a value of 100. To calculate O, I take the standard deviation of the values $O_{i,j}$ for $1 \leq j \leq k$ for each excitatory neuron i, and then average over the number of excitatory cells to yield O. Low values of O indicate that neurons retain a predictable temporal ordering in each burst of activity; typically neurons with stronger external driving currents fire earlier and those with weaker driving currents fire later (where this variability in driving current is due to implemented heterogeneity in the applied current). High values of O indicate that the ordering of neuron firing within bursts is variable and thus the bursts do not

retain significant ordering.

To analyze the consistency of cell participation in bursts, a measure of burst strength, the Variance of Active Cells (A) is calculated. For each burst of excitatory network activity in the last second of a given simulation, the proportion of excitatory cells active in the burst is calculated, and A is defined as the standard deviation of these values. Low values of A indicate that each burst of excitatory network activity contains a similar proportion of the overall number of excitatory cells in the network, which in turn means that the strength of the excitatory signal sent to the inhibitory cell population is similar for each burst. High values of A indicate the number of active excitatory neurons varies from burst to burst; in turn, this causes significant variation in the strength of the excitatory signal sent to the inhibitory cell population.

Finally, to analyze the consistency of the periodic nature of excitatory network bursting activity, the Variance of Inter-burst Interval (I) is calculated. The inter-burst interval between bursts of excitatory network activity is found for each burst occurring within the last second of a given simulation, and the coefficient of variation is calculated for these inter-burst intervals, giving the measure I. We note that the coefficient of variation in this measure is used because the standard deviation values vary with the average firing frequency of the bursts. Low values of I indicate that the network is periodic with very little variation in the timing between bursts of network activity. High values of I indiate that bursts of excitatory cell activity exhibit significant variability in their timing, which in turn means that the excitatory signal sent to the inhibitory cell population is not strictly periodic.

These three measures are combined together into one measure, dubbed the Variability Measure (V), to quantify the degree to which the excitatory network displays well-organized, periodic bursts typical of classic PING rhythmic activity. The mea-

sure is calculated thusly:

$$V = \sqrt{\left(\bar{O}^2 + \bar{A}^2 + \bar{I}^2\right)} \tag{1.23}$$

where the bar indicates normalized values of each of the measures O, A, and I between 0 and 1.

Each measure is normalized by dividing by a maximal value, X_m for $X = O, A, I$, that is slightly above the highest values of the measure typically achieved in networks exhibiting clear bursting activity amongst excitatory cells. When $S < .2$, which indicates that the network is asynchronous to the point that bursts of network activity do not occur, the value of each normalized measure is artificially set to 1. This ensures that the normalized values of each measure are 1 only in cases without clear bursting patterns. Via this algorithm, the normalized values of each measure are calculated as:

$$\text{for } X = O, A, I\text{: } \bar{X} = \begin{cases} \dfrac{X}{X_m} & \text{if } S \geq .2 \\ 1 & \text{if } S < .2 \end{cases} \tag{1.24}$$

The Variability Measure thus takes the Euclidean Distance of these three measures when their values are scaled between 0 and 1, with 0 indicating minimal variability in the given metric and 1 indicating abnormally high variability or a lack of network bursts. The value $V = 0$ indicates a network in which there is no variability in the order of neurons within each burst, no variability of the number of neurons firing in each burst, and no variability in the inter-burst intervals. V will approach its maximum value of $\sqrt{3}$ in networks when high variability is detected by each of the three measures, and V will achieve its maximum value only if this variability is abnormally high in each measure or if no bursting activity is achieved by the network. Example raster plots differentiating dynamics with low and high Variability Measures

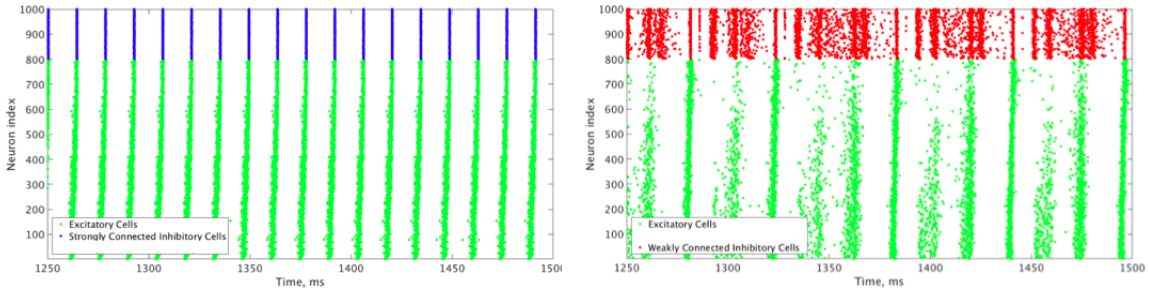

Figure 1.11: Example raster plots differentiating network dynamics with low and high Variability Measures. Left panel: example neural activity in which the excitatory cells exhibit organized firing, consistent cell participation in each burst, and consistent inter-burst intervals, yielding a low Variability Measure. Right panel: example neural activity in which the excitatory cells exhibit variability in the order of firing from burst to burst, inconsistent cell participation in each burst, and inconsistent inter-burst intervals, yielding a high Variability Measure..

are shown in Fig 1.11.

CHAPTER II

Intrinsic cellular properties and connectivity density determine variable clustering patterns in randomly connected inhibitory neural networks

2.1 Introduction

The simplest case in which to examine the variety of mechanisms driving synchronous oscillations in neural networks with inhibitory interneurons is that of a purely inhibitory network. The ING mechanism described in detail in Section 1.3.1 is the most commonly cited impetus behind these networks' tendency to synchronize [63, 119, 114, 118]. A vast majority of the studies articulating and investigating the ING mechanism utilize neuron models with distinctly Type I properties [115, 119, 29, 8, 22]. The PV cells of the hippocampus have been shown via experiment to normally exhibit a PRC only showing phase advance in response to a weak excitatory current pulse and thus are typically classified as Type I; these neurons are also known to exhibit reciprocal synapses to form an inhibitory network primarily containing only this type of interneuron [44, 59], and thus are often analyzed as an archetypical network in which ING might occur.

However, interneurons in the brain are in fact extremely heterogeneous. For example, the oriens-lacunosum moleculare (OLM) cells of the hippocampus contain an M-type potassium current which causes spike-frequency adaptation and is blocked

by the action of ACh on muscarinic receptors [92, 69, 33, 32]. The cholecystokinin-containing basket cells (CCK cells) of the hippocampus also exhibit cholinergic modulation [88, 89]. Moreover, in the cortex, cells exhibiting the PV marker exhibit a wide range of properties, including the possibility of expressing the M-type potassium channel, while somatostatin-expressing interneurons (SOM cells) consistently exhibit spike frequency adaptation much like the OLM cells [82, 73].

Oftentimes, the presence of adaptation currents (like the M-type potassium current) is what imbues a neuron with Type II properties [67]. Hippocampal OLM cells exhibit Type II properties while also exhibiting spike-frequency adaptation, imparted by the M-type potassium current [92, 69, 33, 32], and the SOM cells and some interneurons expressing the PV marker exhibit these properties in the cortex [82, 73]. However, neurons may feature Type II properties without an adaptation current, as is most simply illustrated by the classic Hodgkin-Huxley model neuron which does not exhibit spike-frequency adaptation but does exhibit Type II properties [57, 43]. Interneurons exhibiting Type II properties without strong evidence of an adaptation current have been found in various brain regions including the rat somatosensory cortex [104, 103], the rat barrel cortex [71], the rat cerebellum [30] and the mouse spinal cord [124]. There is evidence suggesting that Type II interneurons in the rat somatosensory cortex synapse onto each other to form an inhibitory network primarily containing only this type of interneruon [104], and the PV cells in the cortex, which sometimes exhibit Type II properties, are also known to be connected in this fashion [82, 73]. However, it is currently unclear whether the OLM interneurons are synaptically interconnected.

The existence of this interneuronal diversity, including a variety of interneurons exhibiting Type II properties, motivates work investigating whether the predictions

of the ING mechanism are robust to changing intrinsic cellular properties. Type II neurons have been analytically shown to synchronize in the case of mutual inhibition in networks of two neurons [112]. Other studies have analyzed larger, all-to-all coupled inhibitory networks of neurons exhibiting these properties, showing that they can either exhibit synchrony or anti-phase clustering [67, 52, 2], while newer studies have begun to investigate the activity of these types of neurons in randomly connected networks [110]. However, this research is much less detailed than the literature probing the ING mechanism and corresponding networks of Type I neurons.

Motivated by the variety of interneurons present in the hippocampus and cortex, evidence that they form inhibitory networks, and the relative dearth of research on purely inhibitory networks with Type II interneurons, in this chapter I investigate spatio-temporal pattern formation in strongly synaptically coupled, randomly connected inhibitory networks of Type I neurons, Type II neurons and Type II neurons containing an M-type potassium current (hereafter referred to as Type II neurons with adaptation). This coupling regime is the focus because networks of this type are not amenable to analytical treatment. Utilizing simulations, it is shown that these networks exhibit different types of synchronous or clustering behavior through multiple mechanisms, which arise from the differing intrinsic cellular properties of these neuron models.

While PRCs generated with a weak excitatory current pulse are used to classify model neurons as either Type I or Type II, a PRC calculated with a perturbation matching the synaptic current profile, which is termed the sPRC and defined in more detail below, is used to more accurately illustrate neural response properties in networks which contain stronger synaptic connections. Neurons that exhibit distinct properties in their PRCs exhibit analagously distinct properties in their sPRCs as il-

lustrated in Fig 2.1, and these sPRC properties are used to articulate the mechanisms underlying the dynamics found in these networks.

Network activity patterns are classified into four major behaviors: asynchrony; full synchrony, in which every neuron in the network fires roughly simultaneously in a stable fashion; one-cluster dynamics, in which some of the neurons in the network fire synchronously in bursts of network activity, but others are silenced; and two-cluster dynamics, in which some, but not all, of the neurons in the network fire synchronously in bursts, but subsequent bursts contain mutually exclusive populations of neurons, providing informational specificity to the burst. While a number of these dynamical patterns have previously been found in computational studies of neural networks [101, 77, 60, 37, 39, 100], I focus on directly comparing network activity in large-scale, synaptically coupled inhibitory networks consisting of neurons with different membrane properties and with differing cellular heterogeneity and connectivity density.

This research shows that the ING mechanism drives one-cluster dynamics via cell suppression [29] and full synchrony in networks of Type I neurons, as has been previously shown [63, 119, 114]. However, I also show that the properties of the sPRC of the neuron, specifically those associated with Type II neurons, can interfere with the ING mechanism and produce two-cluster dynamics. The fact that such networks do not necessarily evolve into one-cluster dynamics as the synaptic decay time constant increases violates the predictions of the ING mechanism and the results indicate that clustering in these networks occurs in a fashion largely independent of synaptic properties. In fact, ING-driven synchrony only appears in networks of Type II neurons when heterogeneity in the intrinsic firing frequency of cells in the network is minimal. Previous studies have shown that the PRC is a useful tool to explain

divergent network dynamics, including the differences between one-cluster and two-cluster firing, although such analysis has not been performed in detail on strongly and randomly connected, strictly inhibitory networks, and has not utilized the features of the PRC focused on in this study [123, 101, 38, 60, 39, 48, 67, 110, 26].

Furthermore, I illustrate that networks of Type II neurons with adaptation exhibit activity patterns similar to either Type I or Type II networks dependent upon the average intrinsic cell firing frequency of neurons in the network and the synaptic decay constant of synapses in the network. The values of these parameters and their interaction with the properties of the adaptation current lead to a change in network dynamics that is associated with a change in properties of sPRC. These results show the importance of the adaptation current in driving network dynamics in strictly inhibitory, randomly-connected networks, further emphasizing the influence of spike-frequency adaptation on network dynamics as shown in other network types [38, 111, 39, 67, 110]. Together, these results detail the important role played by intrinsic cellular properties of neurons, as well as the degree of connectivity in the network, in driving rhythmic behavior in randomly-connected inhibitory networks [1].

2.2 Methods

2.2.1 Neuron properties: Synaptic Phase Response Curves and Spike Frequency Adaptation

For network simulations in this chapter, a constant, though heterogeneous between neurons, external input current is applied to all neurons, inducing continuous periodic firing which allows the PRC to be a useful tool for analyzing neural response properties. However, the PRC computed in response to a brief, weak input (as in Fig 2.1**(B)** and **(C)**) does not accurately describe the cell's response to the inhibitory

[1] Work presented in this chapter has been previously published [85]

synaptic input received within the network, because the synaptic transmission as modeled is not brief and weak. To understand how differences in intrinsic cellular properties affect responses to perturbations received by neurons within the model networks, PRCs with an inhibitory signal approximating the magnitude and profile of the synaptic current received by a single cell following a burst of network activity are computed. To differentiate PRCs calculated with this type of perturbation from those used to classify neuron type, I refer to the PRCs calculated with synaptic currents as sPRCs (as opposed to PRCs calculated with brief, excitatory current pulses which are referred to simply as PRCs). The sPRCs are shown in Fig 2.1**(D)**, **(E)** and **(F)** for Type I neurons, Type II neurons and Type II neurons with adaptation, respectively. For brief synaptic currents, sPRCs show similar properties to their PRC counterparts in Fig 2.1**(C)**, but as the duration of the synaptic current increases, the sPRCs for different cell types become more similar.

The sPRCs for the Type I neuron show a large delay response to perturbations delivered at early phases and exhibit linear properties, with a slope of approximately -1, as the phase of the perturbation increases. The magnitude of the delay depends upon the duration of the synaptic current. The linear properties of these sPRCs indicate that, regardless of timing, all perturbations serve to "reset" the neuron to the beginning of its firing cycle, where the neuron is held until the inhibition decays sufficiently. Furthermore, the neuron is held at the beginning of its firing cycle for the same duration regardless of when the perturbation occurred. The only factor that changes the magnitude of the phase delay, then, is the time elapsed between the initial action potential firing and the delivery of the perturbation. This evolves linearly with the timing of the perturbation. Since the scales of both the timing and the phase delay are normalized to 1, the sPRCs display linear properties with

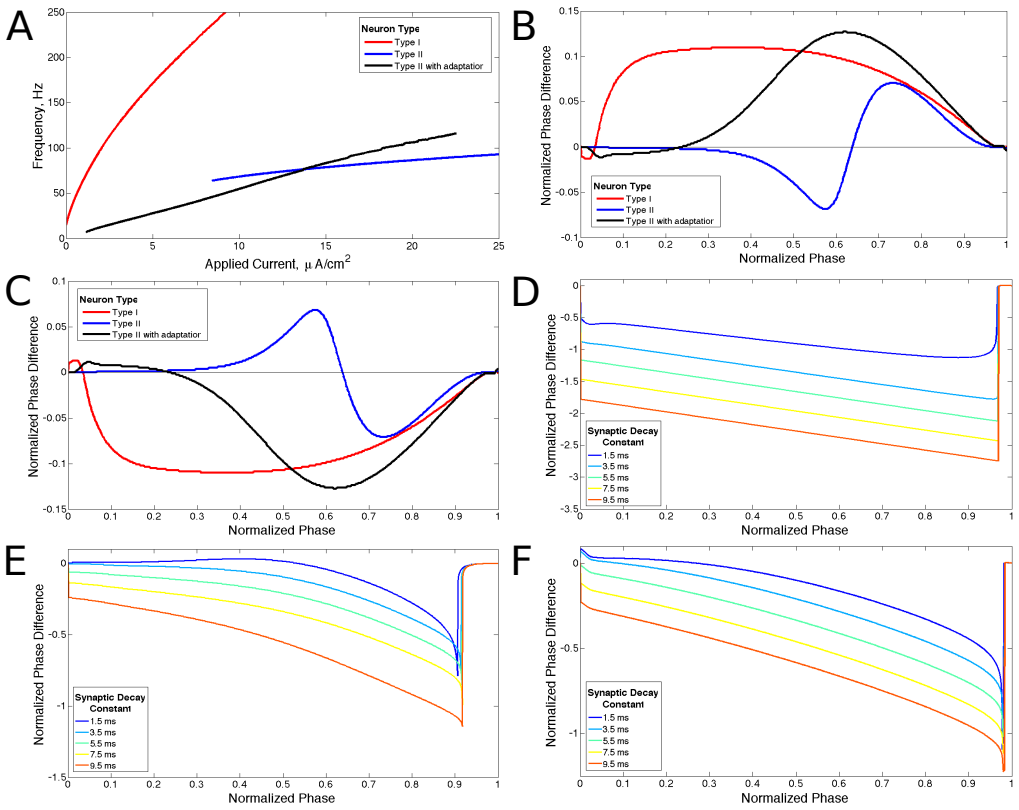

Figure 2.1: **Properties of neuron models. (A)**: Current-frequency curves (I-F curves) of Type I (red), Type II (blue) and Type II with adaptation (black) neuron models. **(B)**: Phase response curves (PRCs) calculated with a brief excitatory current pulse for each model neuron firing at 65 Hz. **(C)**: PRCs calculated with a brief inhibitory pulse for each model neuron neuron firing at 65 Hz. **(D)-(F)**: sPRCs calculated with a perturbation matching the double exponential synaptic current model with various synaptic decay constants for a Type I neuron firing at 44 Hz (**(D)**), for a Type II neuron firing at 70 Hz (**(E)**) and for a Type II neuron with adaptation firing at 30 Hz (**(F)**).

an approximate slope of -1. For these reasons, sPRCs with linear characteristics are classified as having "phase-resetting" properties.

The sPRCs for both the Type II neuron and the Type II neuron with adaptation exhibit a distinctly concave down shape for brief synaptic currents. As the duration of the synaptic current increases, the sPRCs for both of these neurons become more linear and start to resemble the phase-resetting shape. However, even for the longest lasting synaptic currents the sPRCs for the Type II neuron and the Type II neuron with adaptation still retain some concave down characteristics, never achieving the

degree of linearity shown by the sPRCs for Type I neurons.

Another relevant property of the Type II neuron with adaptation is spike-frequency adaptation. When this neuron is quiescent for a sufficient period of time, the gating variable governing the slow potassium current, z, falls below its typical value achieved during repetitive firing. When the neuron begins firing again, the slow time dynamics of z cause its value to rise slowly, allowing faster than normal firing until it fully recovers. These dynamics are displayed in Fig 2.2: in response to an applied current step initiated at $t = 100$ ms from resting membrane potential, action potential firing occurs at higher frequency until the value of z rises to a steady oscillation. Removal of the current step for a moderate period of time allows sufficient decay of z so that frequency is again high when the current step is reintroduced.

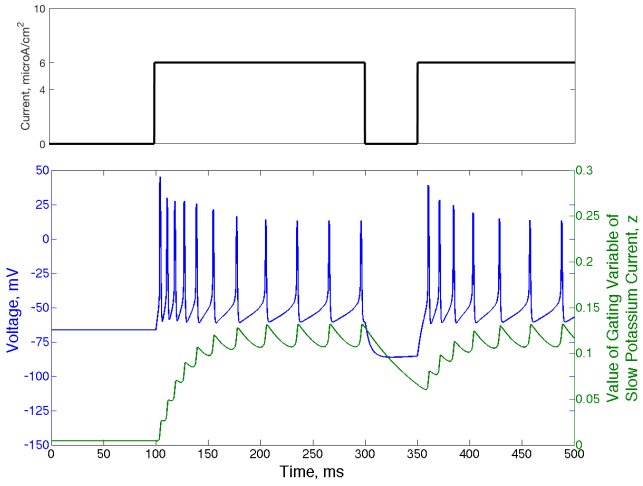

Figure 2.2: **Type II neurons with adaptation exhibit spike-frequency adaptation.** Voltage trace (blue) and value of the slow potassium gating variable z (green) shown for a single neuron that begins with no input current and equilibrium values of the voltage and all gating variables. The current step is shown above the voltage trace in black. The frequency of action potential firing depends upon the rate of previous action potential firing, which is reflected by the value of the gating variable of the slow potassium current.

2.2.2 Network Structure

Simulations in this chapter are performed on networks of 1000 inhibitory neurons. Each neuron received synaptic input from the same number (unless otherwise

specified, 300) of randomly selected pre-synaptic cells.

Cell heterogeneity was implemented by varying the external input current, I_{app}, to each neuron. The input currents were selected from a uniform distribution centered on the current (I_A) that would impart an average intrinsic cell firing frequency to an isolated neuron. Networks with two levels of heterogeneity are studied. For high heterogeneity simulations the input currents are uniformly chosen from the distribution $[.9I_A, 1.1I_A]$, while for low heterogeneity simulations the input currents are uniformly chosen from the distribution $[.99I_A, 1.01I_A]$.

Synapses are modeled using a double exponential profile of the form described in Section 1.2 and Equation 1.1. Here, τ_r is set at 0.2 ms while τ_d is varied in the simulations. In all simulations, g_{syn} is set at 0.010 mS/cm^2.

2.2.3 Simulations

The code underlying these simulations was written in the C programming language and run on the University of Michigan's Flux cluster, a Linux-based high-performance computing cluster.

All simulations were run for 2500 ms from random initial conditions for voltage and gating variables for each neuron. Possible initial conditions for V ranged between -62 and -22 mv, while the possible initial conditions for each gating variable ranged between 0.2 and 0.8. In order to investigate the stability of the network's behavior, at a time of 1400 ms a large amplitude, brief current pulse was delivered to each cell in the network to cause all neurons to fire at the same time. As inhibitory synaptic currents do not directly promote synchronized firing and the ING mechanism achieves synchrony by organizing time windows that allow synchronized firing, this applied current pulse acts to impose an instance of synchrony on the network (analagous to imposing homogeneous initial conditions causing instantaneous spik-

ing of all neurons in the network, as opposed to the randomized initial conditions that begin the simulations). This allows for the comparison of network dynamics established from random initial conditions (Pre Pulse) to those established after the current pulse (Post Pulse), and for differentiation between global convergence and local stability of network synchrony. An illustrative example of a clustered solution that is not globally convergent from random initial conditions but stable locally after the pulse is shown in Fig 2.3.

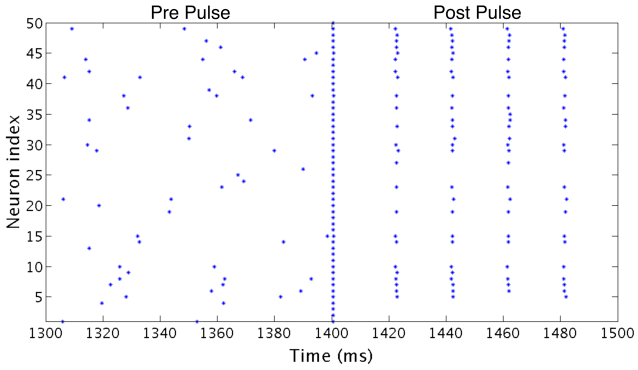

Figure 2.3: **Effect of a synchronizing current pulse in network simulations**. In an example network consisting of Type I neurons with high heterogeneity, a large, brief current pulse delivered at 1400 ms causes every cell in the network to fire synchronously. In response, this network changes behavior and exhibits one-cluster dynamics following the pulse despite firing asynchronously previously.

Model equations are integrated using a fourth order Runge-Kutta technique. Spikes do not trigger synaptic current until 100 milliseconds into the simulation to allow initial transients to decay.

Color plots of the Synchrony Measure and the Burst Similarity Measure display the average of these scores over 10 independent simulations. The Pre Pulse scores (left panels) are calculated based on the network activity from 300 to 1300 milliseconds, and the Post Pulse scores (right panels) are calculated based on the network activity from 1500 to 2500 milliseconds. Simulations (not shown here) were run to ensure that the behaviors indicated by the Synchrony Measure and Burst Similarity

Measure taken over the given interval were indicative of stable behaviors that would persist long past the time interval measured here.

Color plots display measures for the same range of values for the synaptic decay time constant τ_d, while the average intrinsic cell firing frequencies are chosen to sample a majority of the range of frequencies of repetitive cell firing that a given model can attain.

2.3 Results

I investigated global pattern formation in randomly connected inhibitory networks composed of neurons with three cellular excitability types and different levels of cellular heterogeneity, finding that the clustering dynamics were dependent upon cell type, heterogeneity level and the degree of connectivity. This diversity in network activity patterns provides evidence for the importance of intrinsic cell properties in dictating network patterns in randomly connected inhibitory networks, while also allowing for the identification of the mechanisms underlying these dynamics that depend upon these properties.

2.3.1 Effect of Connectivity Density

The computational study of neural networks includes a plethora of studies focusing on all-to-all connected networks. This literature includes many of the papers cited here as relevant to the study of interneuron networks, inhibitory networks, or the role of spike-frequency adaptation in network dynamics [112, 67, 123, 38, 39, 77, 60, 37, 48]. One of the benefits of the study of all-to-all connected networks is the ability to use techniques, including weakly coupled oscillator theory and the phase-reduction technique, in order to mathematically analyze the network dynamics and in turn prove the generality of dynamical results. However, these techniques rely upon the

assumption that the networks have all-to-all network topology [94].

In networks with high heterogeneity in intrinsic cell firing frequency, the level of connectivity density caused significant changes in the patterns of network dynamics. These changes are shown by the changing network dynamics illustrated in Fig 2.4 for networks of Type I (first column), Type II (second column) and Type II with adaptation (third column) neurons, for networks with a connectivity density of 10%, 30%, and 100%, from top to bottom, respectively.

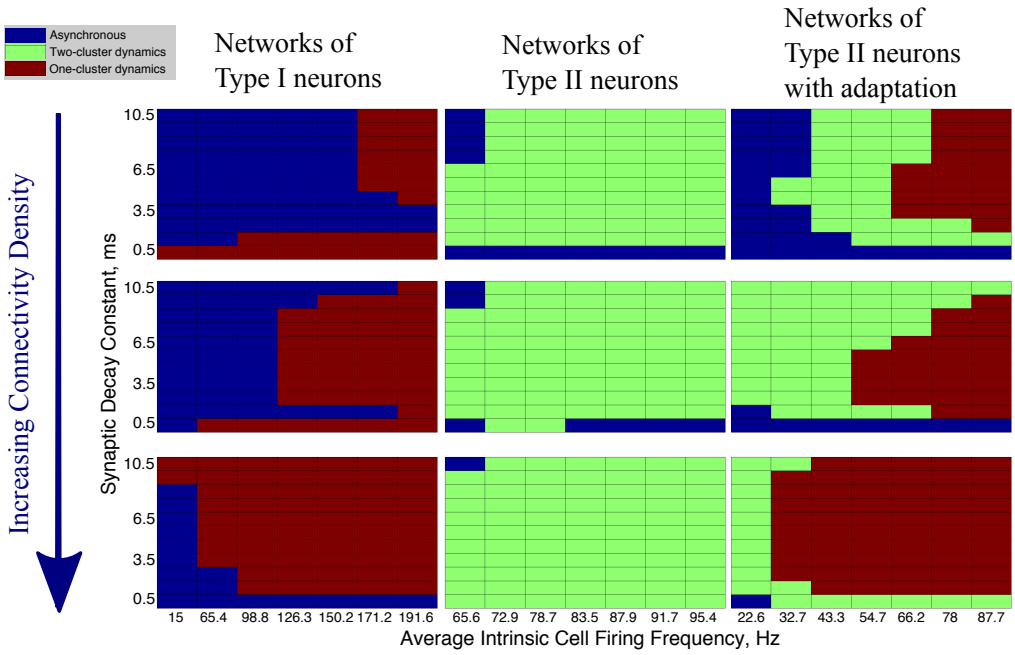

Figure 2.4: **Network activity patterns are dependent upon connectivity density.** Diagrams illustrating the changing network dynamics in simulations as a function of connectivity density and neuron type, with simulations run with a range of average intrinsic cell firing frequencies (horizontal axis) and synaptic decay constants (vertical axis). The connectivity densities shown here are 10%, 30%, and 100%, from top to bottom. Simulations for Type I neurons are shown in the first column, simulations for Type II neurons are shown in the second column, and simulations for Type II neurons with adaptation are shown in the third column.

The values of the Synchrony Measure (S) and Burst Similarity Measure (B), when analyzed jointly, indicate the type of activity in these networks and inform the classification of network dynamics in Fig 2.4. The manner in which S and B are analyzed to yield the classification of network dynamics is described below. For

simplicity, in Fig 2.4 only the changes in overall network dynamics is illustrated.

Regardless of the connectivity density, synchronous activity in networks of Type I neurons was restricted to one-cluster dynamics. The parameter space in which one-cluster firing occurred, as opposed to asynchronous dynamics, moved to include lower intrinsic cell firing frequencies as the connectivity density increased. While networks with 30% connectivity density do not evolve to one-cluster dynamics from randomized initial conditions at low intrinsic firing frequencies, as shown here, it is shown below that these networks can achieve one-cluster dynamics following the synchronizing current pulse.

When connectivity density was less than 30%, networks of Type II neurons with adaptation exhibited one-cluster dynamics for high average intrinsic cell firing frequencies, but displayed two-cluster dynamics or asynchronous activity as cell firing frequency decreased or the synaptic decay time constant increased. As the connectivity density increased, parameter regimes which supported two-cluster dynamics at lower connectivity densities exhibited one-cluster dynamics at the higher connectivity densities. At full connectivity density, two-cluster dynamics were only found for networks with the slowest average cell firing frequencies or shortest synaptic decay constants. Thus, in these networks, lower connectivity density allows cellular and synaptic properties to influence network activity and determine whether two-cluster dynamics or one-cluster dynamics are exhibited. In fully connected networks, cellular and synaptic properties are less influential and network dynamics converge to similar patterns of one-cluster dynamics.

Connectivity density had minimal effect on the type of synchronous dynamics exhibited in networks of Type II neurons. For all densities, networks displayed two-cluster dynamics with little effect due to variations in intrinsic cell firing frequency

and synaptic decay time constant.

In summary, increasing connectivity density limited the contributions of cellular and synaptic properties to network dynamics in simulations. Not surprisingly, full connectivity promoted one-cluster synchronous dynamics, except in the Type II networks. When heterogeneity in intrinsic cell firing frequency was reduced in Type II networks, one-cluster dynamics were exhibited (see further results below).

For the remainder of this chapter, networks with 30% connectivity density are considered. There exists biological evidence for 30% connectivity density among inhibitory neurons based on data from the CA1 region of the rat hippocampus [110, 3]. Additionally, from the above results, networks with this connectivity showed distinct dynamical patterns from both extremely sparsely and extremely densely connected networks, thus making generalizations from the study of these networks to other randomly connected networks reasonable.

2.3.2 Networks of Type I Neurons

Inhibitory networks of Type I neurons manifested full synchrony, one-cluster dynamics, or asynchrony with 30% connectivity density. The particular type of behavior exhibited by the network was determined by the two parameters varied across simulations, the average intrinsic cell firing frequency of neurons in the network and the synaptic decay time constant, as well as the level of heterogeneity. Full synchrony was exhibited only when the level of heterogeneity was low (Fig 2.5); in this case the network exhibited bursts of network activity containing every neuron in the network. In the high heterogeneity case (Fig 2.6), one-cluster dynamics were observed in which bursts contained largely the same group of neurons but not all neurons in the network, which is indicative of cell suppression [29].

The dynamics exhibited by the network were determined by the values of S and

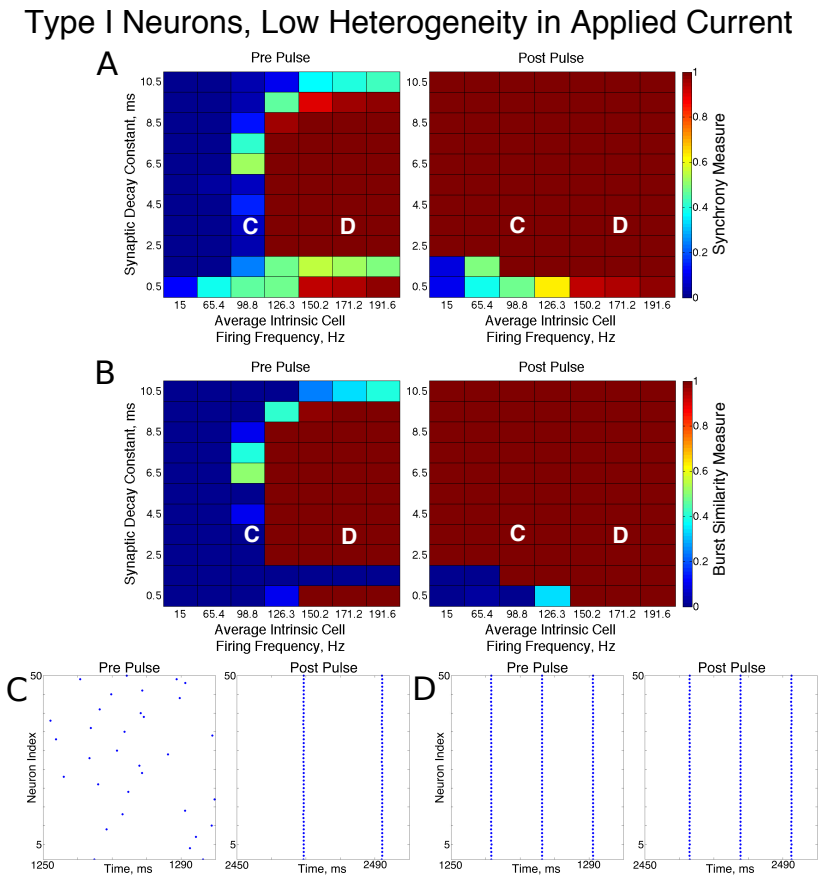

Figure 2.5: **Dynamics of networks of Type I neurons with low cellular heterogeneity. (A)-(B)**: Synchrony Measure (**(A)**) and Burst Similarity Measure (**(B)**) for simulations run with a range of average intrinsic cell firing frequencies (horizontal axis) and synaptic decay constants (vertical axis), averaged over 10 independent simulations before (left panel) and after (right panel) the synchronizing current pulse. **(C)**: Example raster plot for a simulation with an average intrinsic cell firing frequency of 98.8 Hz and a synaptic decay constant of 3.5 ms (whose position in the heatmaps is illustrated by the overlayed C) shows asynchrony occuring from initial conditions but full synchrony following the pulse. **(D)**: Example raster plot for a simulation with an averge intrinsic cell firing frequency of 171.2 Hz and a synaptic decay constant of 3.5 ms (whose position in the heatmaps is illustrated by the overlayed D) exhibits full synchrony before and after the pulse.

B. High values of both measures indicate that the network exhibited one-cluster dynamics: high values of S indicate that some clustering occurred in the network, and high values of B indicate that subsequent bursts of network activity contained similar populations of neurons. After inspecting the values of both S and B corresponding with various network behaviors and visually classifying dynamics in the corresponding raster plots, it was determined that clustering occurs when $S > 0.4$,

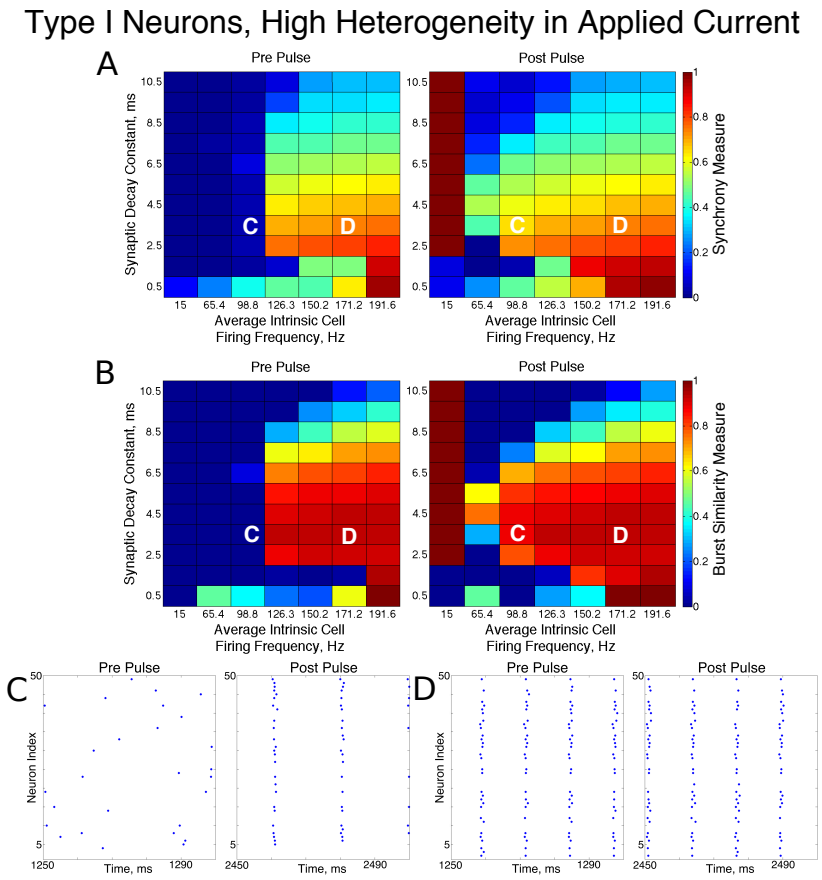

Figure 2.6: **Dynamics of networks of Type I neurons with high cellular heterogeneity. (A)-(B)**: Synchrony Measure (**(A)**) and Burst Similarity Measure (**(B)**) for simulations run with a range of average intrinsic cell firing frequencies (horizontal axis) and synaptic decay constants (vertical axis), averaged over 10 independent simulations before (left panel) and after (right panel) the synchronizing current pulse. **(C)**: Example raster plot for a simulation with an average intrinsic cell firing frequency of 98.8 Hz and a synaptic decay constant of 3.5 ms (whose position in the heatmaps is illustrated by the overlayed C) shows asynchrony occuring from initial conditions but one-cluster dynamics following the pulse. **(D)**: Example raster plot for a simulation with an averge intrinsic cell firing frequency of 171.2 Hz and and a synaptic decay constant of 3.5 ms (whose position in the heatmaps is illustrated by the overlayed D) exhibits one-cluster dynamics before and after the pulse.

and when $B > 0.2$ subsequent bursts are sufficiently similar for the behavior to be deemed one-cluster dynamics (although the values of B observed for one-cluster dynamics were typically much higher than this level). Both measures approaching their maximal value of 1 indicated that the network exhibits full synchrony. Two-cluster dynamics are indicated by a moderate value of S (typically $S \approx 0.6$), but $B = 0$.

The stability of the solutions observed from randomized initial conditions were

investigated by applying a synchronizing current pulse to all neurons approximately midway through the simulation. The current pulse caused all neurons to fire simultaneously which produced a subsequent uniform suppression of all neurons via the synaptic inhibition. The left and right panels of Figs 2.5 and 2.6 display the measures and example raster plots of pre- and post-pulse network activity, respectively.

Networks with low average intrinsic cell firing frequencies exhibited asynchronous activity patterns, regardless of heterogeneity and synaptic decay time constant, when simulated from random initial conditions. However, stable full synchrony or one-cluster dynamics could be induced by the synchronizing current pulse in some of these networks: in nearly all networks with low heterogeneity, the current pulse induced full synchrony, while in networks with high heterogeneity the pulse induced one-cluster dynamics within a range of synaptic decay time constant values. Thus, the current pulse revealed bistable dynamics in these networks characterized by evolution to either asynchronous or clustered dynamics depending on initial conditions. Full synchrony developed following the current pulse in networks with high heterogeneity and an average intrinsic cell firing frequency of 15 because I_A for these networks was 0, resulting in networks with homogeneous external input current to the neurons. Examples of these bistabilities between asynchronous and fully synchronous or one-cluster firing are shown in the raster plots in Figs 2.5**(C)** and 2.6**(C)**.

This bistability is reflective of properties of the ING mechanism. Asynchrony occurred due to the combination of the low firing frequency of neurons and the presence of synaptic inhibition preventing enough cells from firing in close enough temporal proximity to generate sufficient synaptic inhibition to suppress spiking activity in the entire network for a sufficient period. However, the current pulse instantiated a state in which every neuron in the network fired synchronously; following this, every

neuron in the network received identically strong synaptic inhibition, initiating ING-driven activity. Following the pulse, this synchronous activity was fully maintained in most of the low heterogeneity networks, and partially preserved via one-cluster dynamics in many high heterogeneity networks.

Networks with higher average intrinsic cell firing frequencies showed no significant changes in either S or B and after the current pulse, indicating that ING-driven dynamics are globally stable solutions that do not depend on initial conditions. These networks exhibited full synchrony in the low heterogeneity case and one-cluster dynamics in the high heterogeneity case. Example raster plots in this domain, illustrating the similarity in network activity before and after the current pulse, are shown in Figs 2.5**(D)** and 2.6**(D)**. In the high heterogeneity case, the range of computed S values reflect the proportion of cells in the network that participate in the one-cluster dynamics, with lower values of S indicating that fewer cells participated in each burst of network activity. In networks with a lower S, neurons that have smaller input currents either participated in very few bursts or were completely suppressed. This is illustrated by Fig 2.7**(C)**, which shows the relationship between input current and average firing frequency for each individual neuron in an example network illustrating cell suppression. These results match previous results studying analagous networks with heterogeneity [115, 44, 29, 8, 106].

The sPRCs shown in Fig 2.1**(D)** help to explain these networks' tendency to exhibit dynamics driven by the ING mechanism. Regardless of the duration of the synaptic current, the sPRCs for Type I neurons showed strong phase-resetting characteristics. As discussed above, phase-resetting characteristics arise in an sPRC when the synaptic inhibition holds a cell at the beginning of its firing cycle for the duration of the synapse, irregardless of the signal's timing. When all the cells in the network

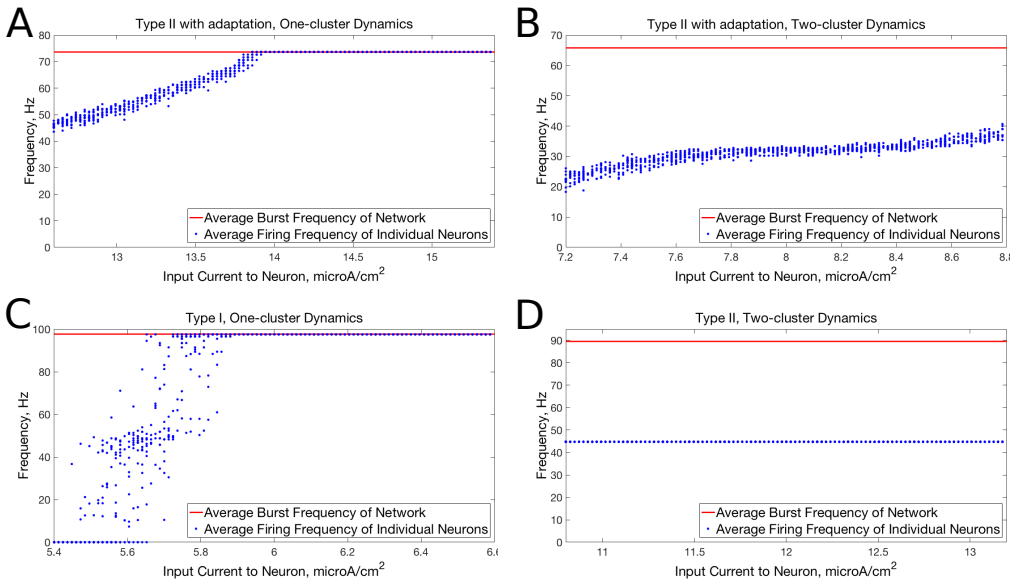

Figure 2.7: **Comparison of relationships between input current and average neuron firing frequencies in one-cluster and two-cluster network dynamics.** **(A)**: Average firing frequencies of individual neurons in a network of Type II neurons with adaptation exhibiting one-cluster dynamics plotted against the input current to the corresponding neuron. **(B)**: Same as **(A)** but for a network of Type II neurons with adaptation exhibiting two-cluster dynamics. **(C)**: Same as **(A)** but for a network of Type I neurons with similar values of S and B as in **(A)**. **(D)**: Same as **(B)** but for a network of Type II neurons with similar values of S and B as in **(B)**.

receive this type of perturbation, they become suppressed until the synaptic signal decays, eliciting a "window" in which cell firing can occur before the next round of action potential firing and the resulting synaptic inhibition suppresses the neurons once again. This is exactly the underlying mechanism of ING, indicating that the tendency for the ING-driven dynamics in these networks can be explained by the phase-resetting characteristics of the sPRC.

Thus, the results in this case agreed with the theory of the ING mechanism, as networks exhibited full synchrony or one-cluster dynamics with the degree of synchrony within these clusters dependent upon heterogeneity, the synaptic decay constant, and the average intrinsic cell firing frequency of neurons in the network. Further evidence for the ING mechanism driving the synchronous activity was in the response of these networks to the current pulse that artificially instantiated synchronous dynamics into

these networks.

2.3.3 Networks of Type II Neurons

The networks of Type II neurons typically exhibited either full synchrony or two-cluster dynamics. The type of behavior displayed depended upon the synaptic decay time constant and level of cellular heterogeneity. Interestingly, for the range of synaptic decay time constants and average intrinsic cell firing frequencies studied here, networks of Type II neurons only exhibited ING-driven full synchrony in the low heterogeneity case. This provides strong evidence that intrinsic cellular properties are important in determining clustering dynamics in networks with non-trivial levels of heterogeneity, which are more biologically plausible than homogeneous networks.

For low values of the synaptic decay time constant, networks with low heterogeneity (Fig 2.8) exhibited two-cluster dynamics. When the decay constant was large, the network evolved to full synchrony from random initial conditions, but for moderate values of the decay constant the synchronizing current pulse was necessary to induce full synchrony. Thus, in this regime the network displayed bistability between a two-cluster solution and full synchrony. Networks of Type II neurons with high heterogeneity (Fig 2.9) almost exclusively exhibited two-cluster dynamics. The current pulse did not induce full synchrony or one-cluster dynamics, but instead the synchronous firing instantiated by the pulse was not maintained and firing evolved back into two distinct clusters.

The fact that low heterogeneity networks showed a response to the current pulse, while high heterogeneity networks did not, implies that ING-driven synchrony plays a role in networks of Type II neurons when the heterogeneity is sufficiently low, but a different mechanism controls behavior in the high heterogeneity case.

Closer analysis of networks of Type II neurons exhibiting two-cluster dynam-

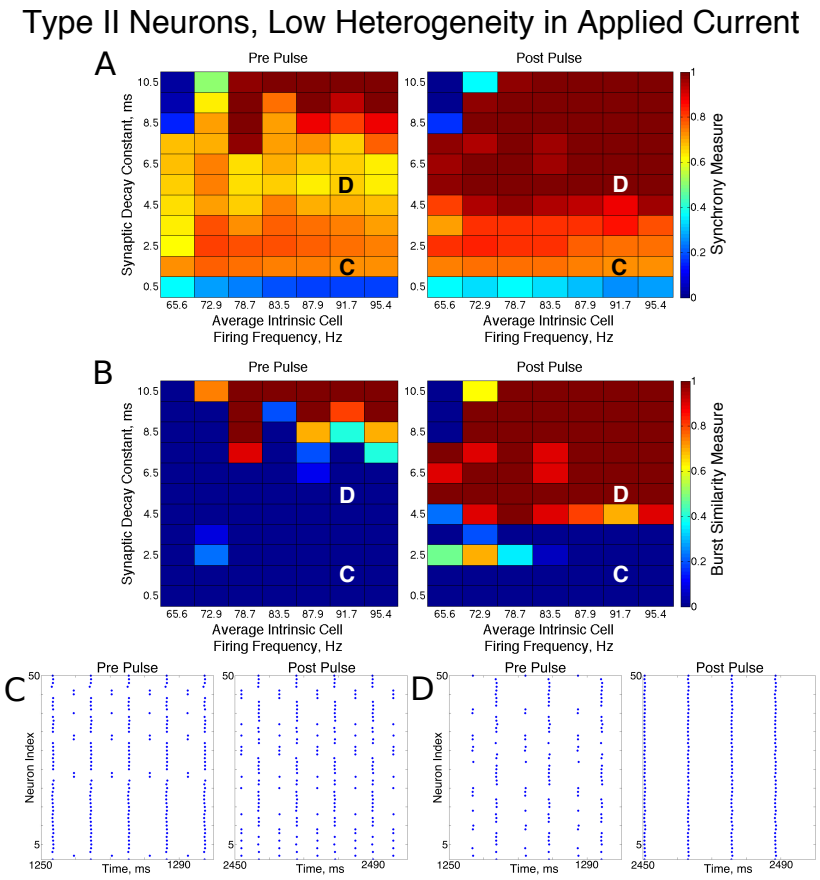

Figure 2.8: **Dynamics of networks of Type II neurons with low cellular heterogeneity. (A)-(B)**: Synchrony Measure (**(A)**) and Burst Similarity Measure (**(B)**) for simulations run with a range of average intrinsic cell firing frequencies (horizontal axis) and synaptic decay constants (vertical axis), averaged over 10 independent simulations before (left panel) and after (right panel) the synchronizing current pulse. **(C)**: Example raster plot for a simulation with an average intrinsic cell firing frequency of 91.7 Hz and a synaptic decay constant of 1.5 ms (whose position in the heatmaps is illustrated by the overlayed C) exhibits two-cluster dynamics before and after the synchronizing current pulse. **(D)**: Example raster plot for a simulation with an averge intrinsic cell firing frequency of 91.7 Hz and and a synaptic decay constant of 5.5 ms (whose position in the heatmaps is illustrated by the overlayed D) exhibits two-cluster dynamics before the pulse but full synchrony after the pulse.

ics showed that the two clusters were easily differentiated: one cluster consisted of neurons with smaller external input currents (I_{app}) and thus lower intrinsic firing frequencies, while the other cluster consisted of neurons with higher input currents and associated intrinsic firing frequencies. Furthermore, the timing of cluster firings was asymmetric. The cluster containing neurons with lower I_{app} values typically fired later in the cycle between firings of the cluster containing neurons with higher I_{app}

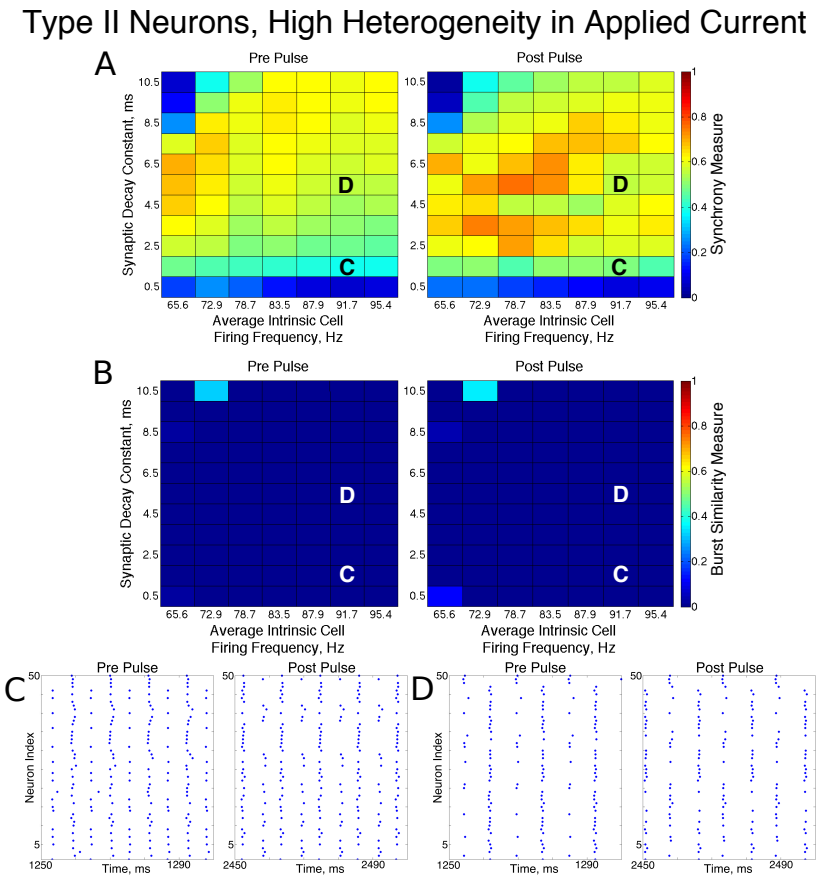

Figure 2.9: **Dynamics of networks of Type II neurons with high cellular heterogeneity. (A)-(B)**: Synchrony Measure (**(A)**) and Burst Similarity Measure (**(B)**) for simulations run with a range of average intrinsic cell firing frequencies (horizontal axis) and synaptic decay constants (vertical axis), averaged over 10 independent simulations before (left panel) and after (right panel) the synchronizing current pulse. **(C)**: Example raster plot for a simulation with an average intrinsic cell firing frequency of 91.7 Hz and a synaptic decay constant of 1.5 ms (whose position in the heatmaps is illustrated by the overlayed C) exhibits two-cluster dynamics before and after the synchronizing current pulse. **(D)**: Example raster plot for a simulation with an average intrinsic cell firing frequency of 91.7 Hz and a synaptic decay constant of 5.5 ms (whose position in the heatmaps is illustrated by the overlayed D) exhibits two-cluster dynamics before and after the synchronizing current pulse.

values, while the cluster containing neurons with higher I_{app} values typically fired earlier in the cycle between firings of the low I_{app} cluster (Fig 2.10).

Properties of the sPRC for Type II neurons explain this phenomenon. When calculated using an inhibitory perturbation matching the synaptic current, the sPRC (red curve in Fig 2.10) is approximately flat for perturbations arriving early in a neuron's firing cycle, but the response begins to change rapidly as the timing of

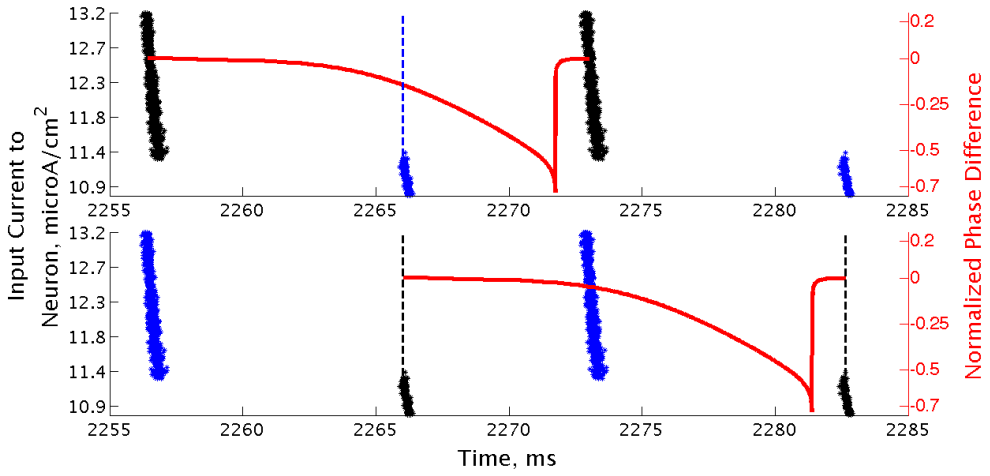

Figure 2.10: **Clusters in networks of Type II neurons are segregated based upon neurons' intrinsic firing frequency.** Raster plot of a high heterogeneity Type II network with an average intrinsic cell firing frequency of 72.9 Hz and a synaptic decay constant of 3.5 ms, with neurons organized based upon their external input current. Overlaid with this plot is a sPRC, generated from analogous synaptic parameters for the neuron firing at a similar frequency to those in the network, showing the timing of firings of the clusters relative to each other (dashed lines added at the beginning of bursts to emphasize these timings). While the raster plots in the bottom and top panels are identical, the overlaid sPRC begins with the black burst in each panel in order to emphasize the timing differences in the cluster firings relative to the effect articulated by the sPRC.

the perturbation occurs later in the neuron's period. As the perturbation to the cells in the high I_{app} cluster from the firing of the low I_{app} cluster occurred at later phases in their firing cycle, these faster firing cells responded with a larger phase delay (top panel). In contrast, since the perturbation to the cells in the low I_{app} cluster from the firing of the high I_{app} cluster occurred at earlier phases, the induced phase delay to these slower firing cells was smaller (bottom panel). This difference in the magnitude of phase delays induced in the two clusters served to balance the frequency differences among their constituent cells, and in turn organized network activity into stable two-cluster dynamics. The properties of the sPRC that underlie this mechanism are distinct from the phase-resetting properties displayed by Type I neuron sPRCs.

This hypothesis was further supported by the timing of firing of cells within each cluster. Within the burst firing of the high I_{app} cluster (the larger cluster in Fig 2.10), the neurons with the highest I_{app} values fired earliest, thus responding with a greater phase delay than the neurons firing later within the cluster. This pattern of cell firing within the cluster balances the effect of the heterogeneity in external input current. This feature holds true for the timing of cell firing within the low I_{app} cluster as well.

The general shape and skew properties of the sPRC shown in Fig 2.10 are present for Type II neuron sPRCs with all but the largest synaptic decay time constants, as shown in Fig 2.1**(E)**. Only for the longest lasting synaptic currents do these properties diminish and phase-resetting properties appear. This helps to explain why for longer lasting synaptic currents, networks with low heterogeneity displayed full synchrony analagous to that seen in similar networks of Type I neurons. The diminished phase-resetting characteristics of the sPRCs calculated for Type II neurons imply that cellular properties play a more important role in determining the dynamics of networks of these neurons as opposed to networks of Type I neurons.

2.3.4 Networks of Type II Neurons with an M-Type Adaptation Current

Networks of Type II neurons with adaptation were found to exhibit all considered types of dynamics: asynchrony, full synchrony, one-cluster and two-cluster dynamics. The exhibited spatio-temporal pattern depended upon the average intrinsic cell firing frequency and synaptic decay time constant. In the low heterogeneity case (Fig 2.11), for higher intrinsic cell firing frequencies there was a bounded range of synaptic decay constant values that led to full synchrony. Outside of this regime, two-cluster dynamics were primarily observed, with a small region of asynchronous behavior for very brief synaptic currents. Networks primarily evolved to these dy-

namics from random initial conditions and the synchronizing current pulse revealed minimal regions of bistability.

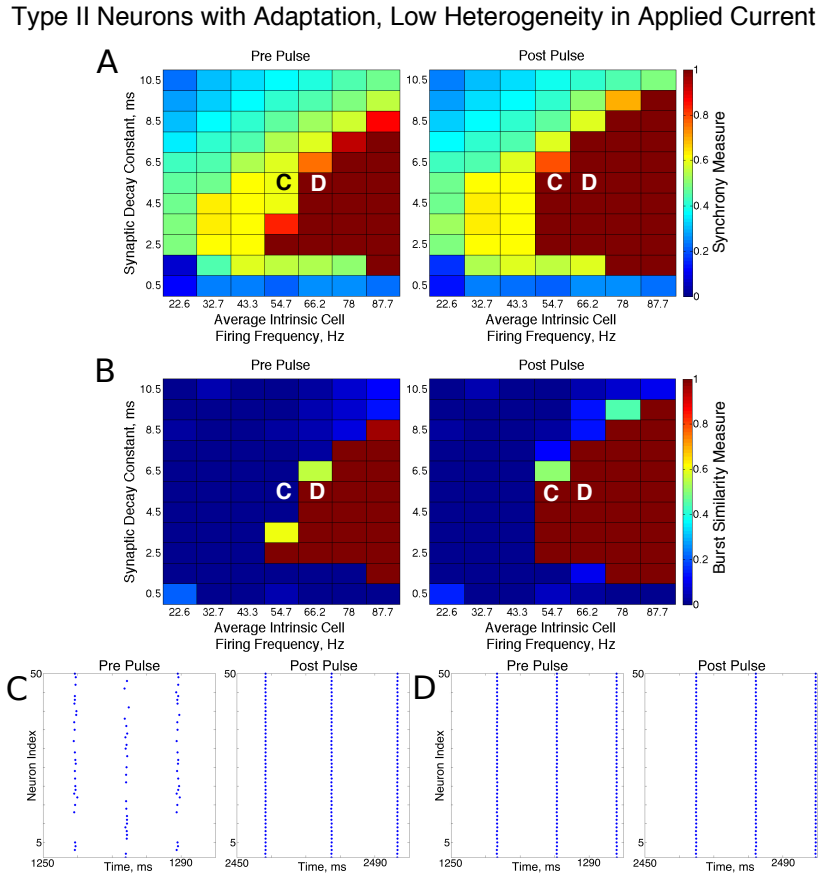

Figure 2.11: **Dynamics of networks of Type II neurons with adaptation with low cellular heterogeneity. (A)-(B)**: Synchrony Measure (**(A)**) and Burst Similarity Measure (**(B)**) for simulations run with a range of average intrinsic cell firing frequencies (horizontal axis) and synaptic decay constants (vertical axis), averaged over 10 independent simulations before (left panel) and after (right panel) the synchronizing current pulse. **(C)**: Example raster plot for a simulation with an average intrinsic cell firing frequency of 54.7 Hz and a synaptic decay constant of 5.5 ms (whose position in the heatmaps is illustrated by the overlayed C) exhibits two-cluster dynamics prior to the pulse but full synchrony following the pulse. **(D)**: Example raster plot for a simulation with an averge intrinsic cell firing frequency of 66.2 Hz and and a synaptic decay constant of 5.5 ms (whose position in the heatmaps is illustrated by the overlayed D) exhibits full synchrony both before and after the pulse.

In these networks, dynamics were robust to cellular heterogeneity. The high heterogeneity case (Fig 2.12) showed very similar results as those observed in the low heterogeneity case, although the region of full synchrony was replaced by a region of one-cluster dynamics in which not every cell participated in each burst. No

bistability between two-cluster and one-cluster firing was observed in response to the synchronizing current pulse for high heterogeneity networks.

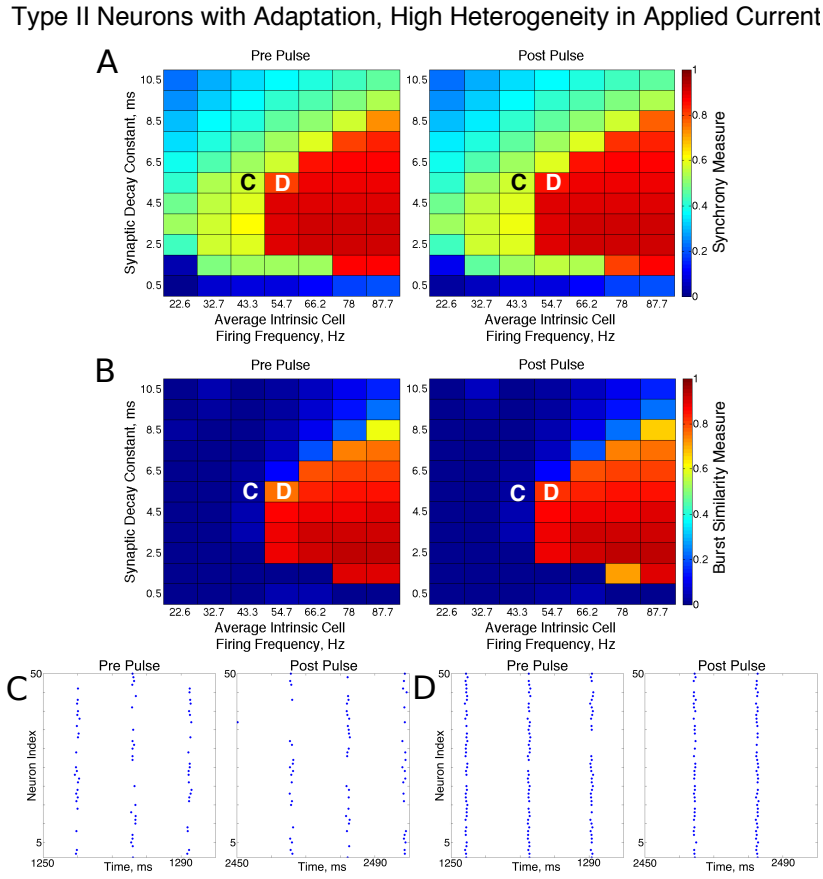

Figure 2.12: **Dynamics of networks of Type II neurons with adaptation with high cellular heterogeneity.** **(A)-(B)**: Synchrony Measure (**(A)**) and Burst Similarity Measure (**(B)**) for simulations run with a range of average intrinsic cell firing frequencies (horizontal axis) and synaptic decay constants (vertical axis), averaged over 10 independent simulations before (left panel) and after (right panel) the synchronizing current pulse. **(C)**: Example raster plot for a simulation with an average intrinsic cell firing frequency of 43.3 Hz and a synaptic decay constant of 5.5 ms (whose position in the heatmaps is illustrated by the overlayed C) exhibits two-cluster dynamics both before and after the synchronizing current pulse. **(D)**: Example raster plot for a simulation with an averge intrinsic cell firing frequency of 54.7 Hz and and a synaptic decay constant of 5.5 ms (whose position in the heatmaps is illustrated by the overlayed D) exhibits one-cluster dynamics both before and after the synchronizing current pulse.

For both high and low heterogeneity simulations, in the regime in which two-cluster dynamics was observed the synchronizing current pulse had minimal effect. Because the effect of the current pulse is to induce ING-driven full synchrony or one-cluster dynamics where possible, this led us to conclude that ING-driven syn-

chrony is not achievable in a large majority of the networks that exhibited two-cluster dynamics.

The transition from two-cluster dynamics to one-cluster dynamics in the high heterogeneity case, or to full synchrony in the low heterogeneity case, as average intrinsic cell firing frequency increased can be explained by changes in the shape of the sPRC. In networks exhibiting two-cluster firing, the average firing frequency of a cell within this network activity pattern was significantly lower than the average firing frequency of a cell in a network exhibiting either one-cluster firing or full synchrony (Fig 2.13**(A)**). The sPRC for these neurons firing at a frequency observed during two-cluster firing (the 12.4 Hz sPRC in Fig 2.13**(B)**) exhibited slope and skew typical of a sPRC calculated for a Type II neuron. In contrast, the sPRC for these neurons firing at a frequency observed during one-cluster firing (the 55 Hz PRC in Fig 2.13**(B)**) showed a strong phase-resetting shape. Thus, both types of network dynamics exhibited in networks of Type II neurons with adaptation are predicted by variations in the shapes of their sPRCs with increasing intrinsic cell firing frequency. The sPRCs for Type I neurons and Type II neurons, on the other hand, do not show significant variation to their overall shapes and skews in response to changes in the cell's firing frequency (Fig 2.13**(D)** and **(F)**), thus predicting the robustness of one-cluster or two-cluster dynamics in these networks, respectively. This frequency-dependence of PRC shape for Type II neurons with adaptation has previously been discussed in relation to the effects of the M-current [45, 67, 38, 39], although the specific effects on the dynamics of inhibitory networks of the type studied here have not.

The behavior of both the one-cluster and two-cluster dynamics exhibited by networks of Type II neurons with adaptation differed in important ways from analagous

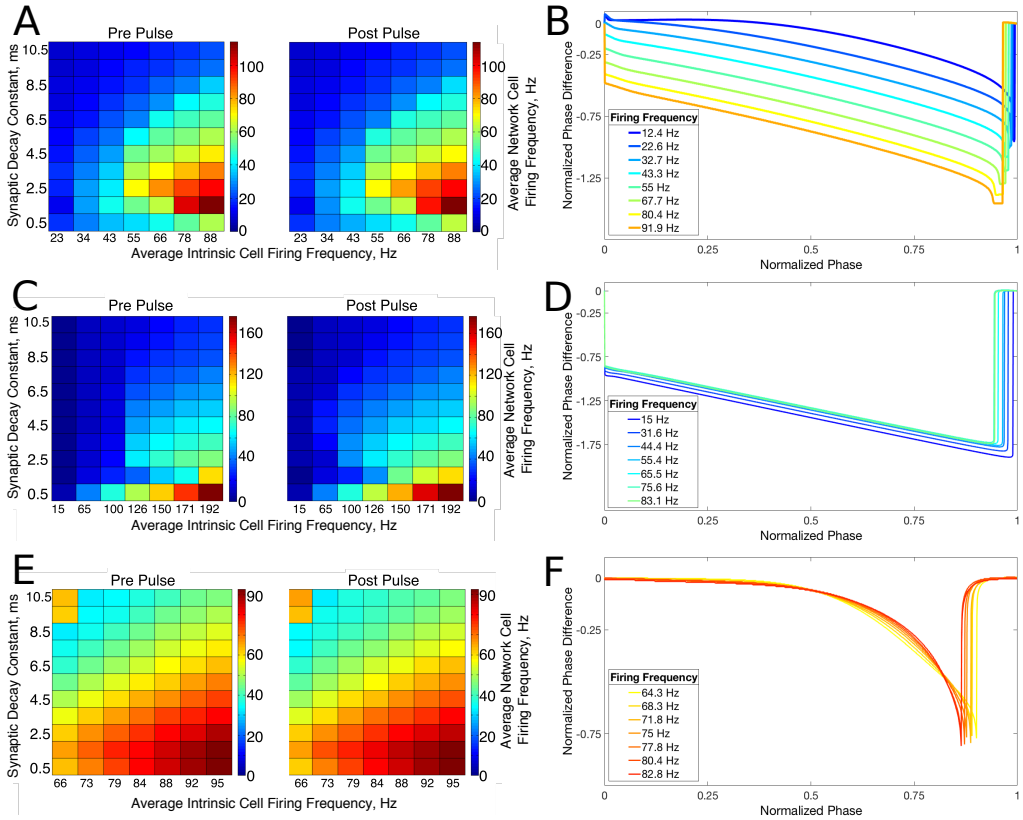

Figure 2.13: **Relationship between average network cell firing frequency and network dynamics is explained by properties of corresponding sPRCs. (A)**: Average firing frequency of neurons in networks of Type II neurons with adaptation in the high heterogeneity case, both before and after the current pulse and averaged over ten independent simulations. **(B)**: sPRCs for a Type II neuron with adaptation naturally firing at various frequencies, calculated with a double exponential synaptic current perturbation with a synaptic decay constant of 3.5 ms. **(C)-(F)**: Same as **(A)** and **(B)** but for Type I neurons (**(C)** and **(D)**) and Type II neurons (**(E)** and **(F)**).

behavior in networks of Type I or Type II neurons, respectively. The adaptation current in the cells of these networks generated unique characteristics of clustered firing. Specifically, networks of Type II neurons with adaptation that displayed one-cluster firing exhibited, on average, clusters containing more neurons than the single clusters in Type I networks in the high heterogeneity case, which is reflected in the higher value of S seen in these networks. Additionally, all neurons fired in a majority of the clusters if the network contained Type II neurons with adaptation, while in networks of Type I neurons many cells fired in every cluster while many others were

completely suppressed. This difference is illustrated by comparing the average firing frequencies of individual neurons as a function of the input current to those neurons in similar example networks shown in Figs 2.7**(A)** and **(C)**.

In Type I networks, since the time interval between cluster firings was primarily determined by the duration of synaptic inhibition, slower firing cells were not able to escape inhibition and fire before the faster firing cells initiated the next cluster firing. As a result, the slower firing cells did not fire in every cluster burst and were often completely suppressed. However, in networks of Type II neurons with adaptation exhibiting one-cluster dynamics, no cells were completely suppressed because deactivation of the slow potassium current makes cells more excitable following extended periods of quiescence. In these networks, cells with lower I_{app} values did not participate in every cluster firing, so the slow potassium gating variable z decayed to lower values between spike firings, as evidenced by their lower average z value compared to cells with higher I_{app} values (Fig 2.14**(A)**). Consequently, at the time of subsequent bursts, these cells were more excitable and were able to escape inhibition and fire with the faster firing cells that initiate cluster firing. Thus, the adaptation current serves to minimize the "effective heterogeneity" of these networks by minimizing the variability in the firing frequencies of individual neurons within the network.

The adaptation current also influenced the pattern of cell firing in two-cluster dynamics. In particular, the clusters in networks of Type II neurons with adaptation were not identical over time, as shown by the fact that neurons in such a network exhibited a range of average firing frequencies dependent upon their input currents, as shown in Fig 2.7**(B)**. In contrast, neurons in networks of Type II neurons that displayed two-cluster dynamics exhibited identical individual neuron firing frequencies irregardless of the neuron's input current (Fig 2.7**(D)**), which indicates that the

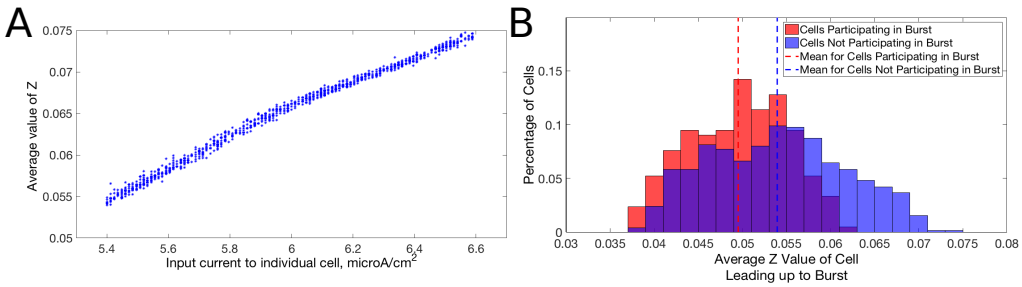

Figure 2.14: **Dynamics of adaptation current explains cell firing activity in networks of Type II neurons with adaptation exhibiting one or two-cluster dynamics (A)**: Average value of the slow potassium gating variable z plotted against the input current to each neuron in a network of Type II neurons with adaptation exhibiting one-cluster dynamics. **(B)**: Histogram of average z values of neurons leading up to a particular burst of activity in a network of Type II neurons with adaptation exhibiting two-cluster dynamics, differentiating neurons participating in the burst (red) and those that are quiescent during that burst (blue).

clusters in these networks were stable.

Furthermore, such networks of Type II neurons with adaptation did not segregate into clusters based upon the neurons' I_{app}, unlike those formed by networks of Type II neurons. Again, effects of the adaptation current on neuron frequency were responsible: frequency of these cells is variable over time, dependent upon the amount of firing that has occurred in the recent past. Cells that participated in a burst had a lower value of the slow-potassium gating variable z leading up to the beginning of a burst compared to cells that were quiescent during that burst. Furthermore, cells with the highest z values did not participate in the burst. This is illustrated by the histograms in Fig 2.14**(B)**: the red histogram shows the average z values of cells participating in a particular burst in the moments before the burst occurred, while the blue histogram shows the average z values of cells not participating in the burst. The offset between these histograms implies that whether a cell fires in a given cluster depends strongly on spike-frequency adaptation and not just a cell's external input current. The large overlap between the two histograms may be due to the randomness in total synaptic inhibitory input arriving at each cell given the

random connectivity.

In summary, the presence of the adaptation current allowed for effective switching between the dynamics exhibited by Type I and Type II networks. Furthermore, the adaptation current minimized the effective heterogeneity present in one-cluster dynamics while preventing neurons from segregating into unique clusters when exhibiting two-cluster dynamics, distinguishing the dynamics in these networks from similar dynamics in networks of Type I neurons or Type II neurons.

2.4 Discussion

The work presented in this chapter shows that intrinsic cellular properties, especially properties of the PRC and the presence of an adaptation current, are of paramount importance in the synchrony and clustering dynamics of a randomly connected network of inhibitory neurons. Furthermore, these intrinsic cellular properties can be the driving force behind potential mechanisms causing these dynamics.

These effects were highly dependent on the degree of connectivity within these networks. Increasing connectivity density limited the contribution of intrinsic cell firing frequency and synaptic decay constant in determining network dynamics. Additionally, increasing connectivity density changed the type of clustering dynamics the networks exhibited. Most crucially, networks of Type II neurons with adaptation exhibited two-cluster firing for networks with low intrinsic cell firing frequencies and lower connectivity densities, but one-cluster dynamics when the network had higher connectivity density. Furthermore, in networks of Type I neurons, lower connectivity density allowed for bistability between asynchronous and one-cluster dynamics when intrinsic cell firing frequencies were low. When the connectivity density was high, networks evolved directly into one-cluster firing.

In this study, networks with 30% connectivity density were the focus since there is evidence for this level of connectivity among interneurons in the hippocampus [110, 3] and this level displayed dynamics distinct from both very sparsely connected and fully connected networks, as shown in Figure 2.4. The focus on this connectivity regime necessitated a numerical study. Previous studies have applied analytical techniques, such as reduction to phase oscillator models, to the investigation of interneuron network dynamics [112, 67, 52, 2, 123, 39]; however, these techniques rely on assumptions of all-to-all connectivity and weak coupling among neurons. The results clearly violate these assumptions: the network regimes focused on exhibit different dynamics from those observed with 100% connectivity density and the suppression of cell firing observed in the one-cluster dynamics of networks of Type I neurons (see Fig 2.7**(B)**) contradicts the hypotheses of the weak coupling regime.

Furthermore, much of the existing literature analyzing networks of interneurons has focused on gap-junctional coupling as opposed to synaptic inhibition [123, 39]. Gap-junctional coupling is instantaneous and can be both excitatory and inhibitory, while synaptic inhibition is purely inhibitory and possesses an intrinsic timescale. These studies also investigate all-to-all coupled networks with weak coupling between neurons, which can be analyzed using techniques such as the phase-reduction method and weakly-coupled oscillator theory [94].

This research illustrates that while networks of Type I neurons exhibit full synchrony or one-cluster dynamics driven by the classical ING mechanism, which relies upon properties of the synaptic current, networks of Type II neurons exhibit two-cluster dynamics driven by neuronal excitability properties (namely, the concave down shape of these neurons' sPRCs). Additionally, networks of Type II neurons with adaptation displayed either one-cluster or two-cluster dynamics dependent upon

the average firing frequency of neurons in the network and the effect this frequency had on the properties of the sPRCs of these cells.

While low heterogeneity networks of Type II neurons fully synchronized via the ING mechanism, these networks exhibited two-cluster dynamics for short lasting inhibitory synapses in low heterogeneity networks and for nearly all values of the synaptic decay time constant with high heterogeneity. Neurons forming these clusters were segregated based upon their natural firing frequencies. The network stabilized two-cluster dynamics by forming asymmetric timing of cluster firings that, due to the skew of the sPRC, led to a different magnitude of delay experienced by each respective cluster. This asymmetry acted to balance the differences in natural firing frequencies of neurons in each cluster.

The tendency for inhibitory networks containing Type II neurons to display the two-cluster dynamics observed here has been previously seen in studies looking at small networks, all-to-all connected networks, and networks containing other methods of signal propagation than synaptic inhibition [112, 67, 110, 52, 2]. However, given the importance of the degree of network connectivity in determining clustering dynamics shown in this study, it can not merely be assumed that these dynamics extend to a larger, randomly coupled network. The simulations justify this extension. Furthermore, analysis reveals that heterogeneity in intrinsic firing frequencies can be compensated for by differences in firing times of each cluster and of individual neurons within in each cluster in order to promote two-cluster dynamics in these networks.

Networks of Type II neurons with adaptation exhibited behavior similar to the one-cluster dynamics of networks of Type I neurons or the two-cluster dynamics of networks of Type II neurons, dependent upon how the average intrinsic cell firing

frequency and synaptic decay constant dictated the average firing frequency of cells in the network. When neurons in the network fired sufficiently fast, the network behaved similarly to networks of Type I neurons, because the sPRC of Type II neurons with adaptation computed at such frequencies mirrored the phase-resetting properties of a Type I neuron. However, the one cluster formed in such a network of Type II neurons with adaptation contained more active neurons, on average, then similar clusters formed in networks of Type I neurons. This difference was caused by the influence of the adaptation current in increasing the excitability of neurons following a period of quiescence.

When cells in a network of Type II neurons with adaptation fired more slowly, the network exhibited behavior similar to the two-cluster dynamics shown by networks of Type II neurons, because the sPRCs calculated for Type II neurons with adaptation firing at this slower frequency matched the shape and skew properties, in particular the concave down nature, of sPRCs of Type II neurons. Here the adaptation current also played a pivotal role in differentiating the dynamics in networks of Type II neurons with adaptation from those of networks of Type II neurons. In particular, the changing cellular excitability of Type II neurons with adaptation brought about by the adaptation current prevented the segregation of neurons into unique clusters based upon their I_{app} values, as was the case in networks of Type II neurons.

Care should be taken when interpreting PRCs for neuron models that contain active currents with slowly evolving gating variables, like the M-current in the Type II neuron with adaptation model. Specifically, perturbations can have effects on firing cycles subsequent to the cycle in which the perturbation occurred. To account for such longer-lasting effects of the perturbation, previous studies have employed higher-order PRCs [80, 102] and functional PRCs [31]. Indeed, for the Type II neuron

with adaptation, the perturbation used to compute the sPRC did result in slightly shorter periods for several firing cycles subsequent to the perturbation cycle due to the influence of spike-frequency adaptation. For Type I and Type II model neurons, on the other hand, firing cycles subsequent to the perturbation cycle showed no effects of the perturbation.

Thus, for networks of Type II neurons with adaptation the focus is on applying the sPRC to explain the transition from one-cluster dynamics to two-cluster dynamics by considering the change in its overall shape as the firing frequency increases: from a more concave down shape to the more linear phase resetting shape as firing frequency increases. As shown in Fig 2.13**(A)** and **(B)**, the correspondence of the change in sPRC shape with the change in network frequency and thus cluster dynamics is remarkably tight: the low network frequency parameter regimes (blue in **(A)**) correspond to concave down sPRCs (blue curves in **(B)**) and display two-cluster dynamics, while the high network frequency parameter regimes (green and warmer colors in **(A)**) correspond to phase resetting sPRCs (green and warmer color curves in **(B)**) and exhibit one-cluster dynamics. Features of the time dynamics of the M-current gating variable are highlighted to explain how cell participation in the one-cluster and two-cluster dynamics differs from the Type I and Type II networks, respectively, in Figs 2.7 and 2.14. For networks of Type II neurons, since the sPRC is the same for all cycles, its use is expanded to understand the segregation of neurons between the two-clusters and to explain the asymmetric timing pattern of the firing of the two-clusters, as shown in Fig 2.10.

The results for networks of Type I neurons paralleled those of previous works in the field, including the work of Wang and Buzsaki [115] and Whittington et. al. [119], as well as more recent, biologically driven simulations of Type I neurons by Ferguson

et. al. [44]. In simulating similar networks of Type I neurons with heterogeneity, Wang and Buzsaki identified a length of synaptic decay that leads to optimal network synchronization. In similar simulations with a model of the PV interneuron (which exhibits distinctly Type I properties), Ferguson et. al. showed that synchrony of these networks improves with faster firing neurons. In these results, the application of the synchronizing current pulse revealed that synchrony and one-cluster dynamics are possible in these networks when intrinsic cell firing frequencies are low, but the network may not evolve to those dynamics from random initial conditions. In particular, if only network dynamics as evolved from random initial conditions are considered, it would appear that there is a strict threshold in intrinsic firing frequency for synchronous or one-cluster firing to occur (left panels of Figs 2.6**(A),(B)** and 2.8**(A),(B)**). The effect of the synchronizing current pulse mimics the conditions for synchronization by the ING mechanism. Specifically, as Whittington states, ING synchrony will occur if enough neural firing occurs in close temporal proximity in order to send a sufficiently strong inhibitory signal throughout the network, which prevents any neuron from firing until this synaptic signal decays [119]. While an instance of enough neurons firing in close temporal proximity is likely to happen when intrinsic neuron firing frequencies are high, it is less likely in networks of slower firing cells. For such networks a single, brief stimulation can be enough to induce stable synchronous dynamics.

A brief synchronizing stimulus may provide a mechanism, both experimentally and computationally, by which the presence of ING can be directly assessed. Indeed, the ING theory predicts that if ING-driven dynamics are at all possible for a given network, the instance of synchronous firing caused by the current pulse should always induce ING-driven clustering or synchrony. The fact that the current pulse had

minimal effect on networks exhibiting two-cluster dynamics, and never induced two-cluster dynamics from a previously asynchronous network, thus suggests that the ING mechanism does not drive two-cluster dynamics in the networks studied here.

Bistability between asynchronous and synchronous solutions in small networks of two mutually coupled inhibitory neurons, where the initial conditions of the network determine the dynamics of the system, has been previously reported [105]. These results serve as a generalization of this phenomena to a larger network with a more complicated connectivity structure.

These results for networks of Type II neurons are similar to those found for pairs of Type II neurons coupled by mutual inhibition studied by Van Vreeswijk et. al. [112]. They analytically showed that for sufficiently long lasting synapses, anti-synchrony is the stable state of these neurons. Anti-synchrony of two neurons corresponds with the two-cluster dynamics seen in these simulations. The work of Achuthan and Canavier on all-to-all coupled inhibitory networks with four Type II neurons also showed the tendency of these networks to exhibit two-cluster dynamics predicted by properties of the PRC [2]. The tendency for larger networks to exhibit these properties has been shown in work by Ladenbauer et. al. and Viriyopase et. al., albeit in networks with different connectivity and heterogeneities than those studied here [67, 110]. This work shows that the results found in these studies can be extended to randomly connected inhibitory networks with heterogeneity in the external input currents to the neurons in the network. This work additionally explains intricacies of the two-cluster dynamics, such as the segregation of neurons into unique clusters based upon their intrinsic firing frequency and the asymmetric timing of the cluster firing.

These results indicate that the clustering properties of Type II neurons, when subjected to high heterogeneity in their external input currents, do not show significant

change in response to a change in average intrinsic cell firing frequency or synaptic decay constant. Given that biologically plausible inhibitory networks typically receive a heterogeneous driving current based upon the drive from a network of excitatory neurons, these results imply that the two-clustering properties of a network of Type II interneurons might prove especially robust to changes in the excitatory drive from the network. This research finds that networks of Type II neurons synchronize fully only when cellular heterogeneity was low and for sufficiently long lasting synapses. This result contradicts previous research that suggested that neurons with Type II properties could not exhibit synchronous behavior in an inhibitory network [52, 2]. Recently, work by Tikidji-Hamburyan et. al. analyzed a randomly connected network of Type II neurons that exhibit post-inhibitory rebound firing (which neither the Type II or Type II with adaptation models exhibit). Their results illustrated that such networks can form synchronous gamma rhythms in a fashion more robust to heterogeneity than similar networks of Type I neurons, driven primarily by the properties of the post-inhibitory rebound firing [107].

The results for networks of Type II neurons with adaptation are of particular biological relevance, considering that the OLM interneurons of the hippocampus exhibit the M-type adaptation current [92, 69, 33, 32], as do some interneurons in the cortex [82, 73]., This work shows that the presence of the adaptation current imbues these neurons with clustering properties and a mechanism driving these dynamics that is distinct from that of Type II neurons without adaptation.

The concentration of ACh in the brain is strongly correlated with sleep state, with the concentrations at their highest during wake and REM sleep. Additionally, the important role of ACh in the hippocampus and its effect on M-type potassium channels has been well studied [4, 91]. These results provide a potential mechanistic explana-

tion for how ACh can affect pattern generation amongst networks of interneurons; in particular, inhibitory networks comprised of neurons containing an M-current are shown to exhibit only one-cluster dynamics when the ACh concentration is high, blocking the M-current and making the neuron Type I, while these networks may exhibit two-cluster dynamics when the ACh concentration is low and the M-current is active. Additionally, the ability for these networks to exhibit either two-cluster or one-cluster dynamics, largely dependent upon how much applied current drives the network, could provide a "gate" by which inhibitory tone to downstream neurons is modulated. These effects on pattern generation might potentially be propagated to pyramidal cells and affect the overall oscillatory behavior of the hippocampus and cortex.

CHAPTER III

Effects of neuromodulation on excitatory-inhibitory neural network dynamics depends on network connectivity structure

3.1 Introduction

The purely inhibitory networks discussed in Chapter II are idealized in order to facilitate computational analysis. One paramount fashion in which these networks diverge from their biological analogues is the tonic excitatory drive provided to the inhibitory interneurons, as biologically this excitatory drive is not tonic and is supplied by excitatory neurons. In computational neuroscience, this idealized network is made more biologically realistic by replacing the tonic excitatory drive with a population of excitatory neurons that is densely inter-connected with the inhibitory interneurons. Such a network is colloquially termed an excitatory-inhibitory (E-I) network. The interactions of excitatory and inhibitory neurons can generate oscillatory bursts of synchronous spiking of excitatory cells which underlie rhythmic electrical activity observed in electroencephalogram (EEG) recordings associated with different brain states and cognition [27, 121]. These networks are ubiquitous throughout the brain [20, 63, 12] and have been the subject of intense study in the computational literature.

In E-I networks, the Pyramidal Interneuron Network Gamma (PING) mechanism is commonly utilized to explain the formation of synchronous rhythms. This con-

ceptual PING mechanism, discussed in detail in Section 1.3.2, has led to research probing the robustness of the mechanism to various forms of randomness and heterogeneity that are likely to occur in the brain. Such studies have investigated the role of sparse and heterogeneous connectivity in PING rhythm formation [15], the role of the strength of interconnectivity between the excitatory and inhibitory neurons in eliciting PING rhythms [14], the effects of noise on these rhythms [16], changes caused by changing the properties of the inhibitory neurons from Type I to Type II [18], and various effects of adaptation currents in the cell models [66, 79]. These studies focus primarily on the interconnectivity between the excitatory and inhibitory cell populations, which according to the PING mechanism is the paramount impetus behind rhythmic activity.

However, the density and strength of the various synaptic connectivities in an E-I network are not the only factor that dictate the network's propensity to exhibit synchronous dynamics. Neuromodulation may also serve a key role in determining network dynamics via multiple pathways. The different types of modulators can wield powerful effects on neural network dynamics, as they can change intrinsic firing properties of neurons as well as alter their effective synaptic strengths. Indeed, while anatomical synaptic connectivity of a neural network plays a primary role in dictating neural activity patterns, the ultimate dynamics exhibited by a network depends critically on which of many neuromodulators are acting on it [5, 72]. One of the brain's most potent neuromodulators is acetylcholine (ACh), which as discussed in Section 1.1.4 and Section 1.5.2 can block an M-type potassium channel and correspondingly shift neuron excitability properties from Type II to Type I. Given the paramount effect cholinergic modulation has on intrinsic cellular properties and a neuron's tendency to exhibit synchrony, it is used as an analogue to analyze neuromodulation in

this work.

In this chapter I analyze how the connectivity of E-I networks affects the influence of cholinergic modulation on the generation of synchronous excitatory bursting. Utilizing computational simulations of E-I networks with neurons modeled in the Hodgkin-Huxley formalism, the effect of ACh is simulated by blocking an M-type potassium current in the neuron models. I investigate all four combinations of modulatory tone of excitatory and inhibitory cells, namely excitatory or inhibitory cells with high (Type I) or low (Type II) modulatory tone. Note that the cases of mixed networks, where one subpopulation exhibits Type I properties and the other exhibits Type II properties, could conceivably arise if cholinergic release is nonuniform or if either subpopulation exhibited the given properties and lacked muscarinic receptors. To vary network connectivity structure, I focus on the effects of the strengths of inter-connections between excitatory and inhibitory cells (E-I synapses and I-E synapses), and the strengths of intra-connections among excitatory cells (E-E synapses) and among inhibitory cells (I-I synapses). These results show that depending on the network connectivity, neuromodulation that changes the cellular propensity for synchronization may or may not affect the generation of network synchrony [1].

3.2 Methods

3.2.1 Cholinergic modulation of CPN neuron model

In this study, only the CPN neuron model is utilized, as it is modulated by ACh (see Section 1.5.2). Two cases of cholinergic modulation are considered: when $g_{K_s} = 0$ mS/cm^2 the neuron displays Type I properties (biologically, due to complete blockade of the slow M-type potassium channel by ACh), and when $g_{K_s} = 1.5$ mS/cm^2 the neuron displays Type II properties (biologically, due to the absence of

[1] Work presented in this chapter has been previously published [87]

ACh that permits maximal activity of the slow M-type potassium channel). These properties are illustrated by the I-F curves and PRCs displayed in Figure 3.1. Note that the only difference between the Type I and Type II neuron models is the activity, or lack thereof, of the M-type potassium channel; thus, the M-current, and the corresponding cholinergic modulation, is entirely responsible for the differences between the Type I and Type II neuron properties. The range of g_{K_s} values used here have been shown to replicate experimentally measured ACh-induced changes in I-F and PRC curves in cortical pyramidal neurons [98, 99]. Also note that in this study only the effect of ACh on this M-current is modeled, and not any of the other potential modulatory effects of ACh.

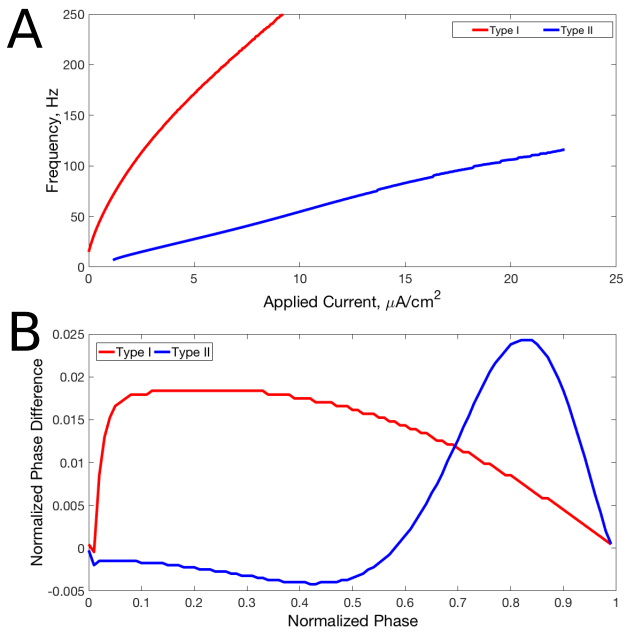

Figure 3.1: **Properties of Type I and Type II neuron models (A)** I-F curves for Type I (red) and Type II (blue) cells. **(B)** PRCs for Type I (red) and Type II (blue) cells.

This model is used for both the excitatory and inhibitory neurons in this study. While these equations were initially developed to model the excitatory cortical pyramidal neuron, the properties of this neuron when $g_{K_s} = 0$ mS/cm^2 closely mirror those of fast-spiking Type I inhibitory interneurons, such as the parvalbumin positive

(PV+) interneurons [44], as well as interneurons containing an M-current blocked by ACh. When the inhibitory interneurons are modeled as Type II with $g_{K_s} = 1.5$ mS/cm^2, their properties mirror those of interneurons like the oriens-lacunosum moleculare (OLM) and somatostatin expressing (SOM) cells, which exhibit an active M-current when ACh concentrations are low [92, 69, 33, 32, 82, 73]. These similarities justify the use of equations that were originally developed to model excitatory cells for inhibitory cells as well.

3.2.2 Network Structure

The E-I networks simulated in this chapter consist of 1000 neurons, 800 excitatory and 200 inhibitory. Excitatory neurons receive an external driving current (described below) and also receive inhibition from the inhibitory cells, where each inhibitory cell has a 50% chance to synapse onto a given excitatory cell. Inhibitory neurons receive a external current (described below) depending upon their cell type in order to ensure they do not fire in the absence of excitatory input and are near their firing threshold. Inhibitory neurons are driven by the excitatory cell population, as each excitatory cell has a 50% chance to synapse onto a given inhibitory cell. Additionally, both the inhibitory and excitatory neurons have a 30% probability of synapsing onto neurons within their subpopulation, forming the intra-connectivity of the network. The choice of this connectivity density is motivated by evidence for this level of intra-connectivity amongst interneurons in the hippocampus [110, 3], and this connectivity density is matched amongst the excitatory neurons for consistency.

Cell heterogeneity was implemented by varying the external input current, I_{app}, to each excitatory neuron. The range of input currents were chosen such that the intrinsic firing frequencies of neurons had a range of 10 Hz. In the results displayed below the average intrisic cell firing frequency for an exciatory cell is 50 Hz, meaning

that the minimum current, $I_{app_{min}}$, is the current that would cause an isolated neuron to fire at 45 Hz, while the maximum current, $I_{app_{max}}$, is the current that would cause an isolated neuron to fire at 55 Hz. The currents are then chosen from a uniform distribution of the form $U(I_{app_{min}}, I_{app_{max}})$.

Inhibitory neurons receive an external current to ensure they will not fire without excitatory input and are near firing threshold. Type I inhibitory cells were given a small external hyperpolarizing current to ensure that the neurons would not fire spontaneously, given that this neuron model exhibits spontaneous firing with no external current. Type II inhibitory cells were given a small depolarizing current such that these neurons were closer to their firing threshold. Variability was implemented in these currents to impart mild heterogeneity to the inhibitory population: the external current for each interneuron was chosen uniformly from the distribution $U(.95I_A, 1.05I_A)$, where I_A is the average current. $I_A = -0.2$ mS/cm^2 for Type I inhibitory cells, and $I_A = 1.0$ mS/cm^2 for Type II inhibitory cells.

Synapses are modeled using a double exponential profile of the form described in Section 1.2 and Equation 1.1. Here, τ_r is set at 0.2 ms for all synapses, while τ_d is set at 3.0 ms for excitatory synapses and 5.5 ms for inhibitory synapses.

The structure of the E-I networks is altered by varying the strength of the various synapses (E-E, E-I, I-I, I-E) in the network. This is done by varying the maximum conductances (g_{syn}) for the corresponding type of synapse. To analyze the role of inter-connectivity (E-I, I-E) versus intra-connectivity (E-E, I-I) the inter-connectivity strengths are varied jointly, as are the intra-connectivity strengths. Since in the networks there are four times as many excitatory cells than inhibitory cells, the E-E synaptic conductance values in the network are 1/4 of the I-I synaptic conductance values shown on the horizontal axis of Fig 3.3-3.6.

The connectivity diagram of the E-I networks studied here is shown in Fig 3.2.

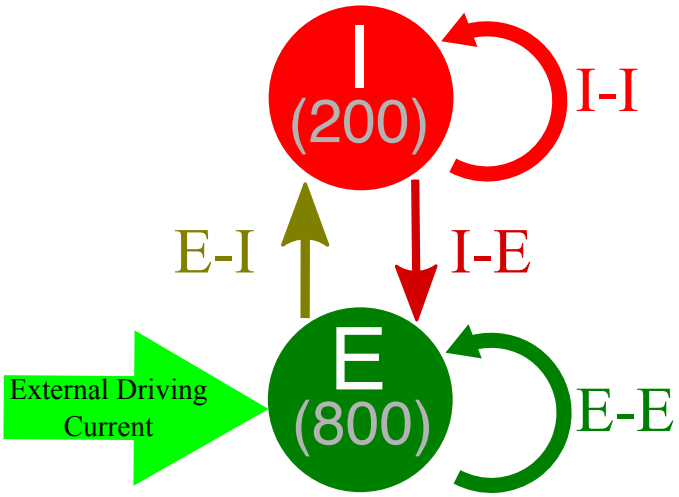

Figure 3.2: **Network diagram for E-I networks.** Network connectivity for E-I networks used for all simulations performed in this work. The various synaptic strengths (E-E, I-I, E-I, I-E) are altered in order to change the network connectivity structure.

3.2.3 Simulations

The code implementing these simulations was written in the C programming language and run on the University of Michigan's Flux cluster, a Linux-based high-performance computing cluster.

All simulations in this chapter were run for 1500 ms from random initial conditions for voltage and gating variables for each neuron. Possible initial conditions for V ranged between -62 and -22 mv, while the possible initial conditions for the gating variables n and h ranged between 0.2 and 0.8, while the initial conditions for the gating variable z ranged between 0.15 and 0.25.

Model equations were integrated using a fourth order Runge-Kutta technique. Spikes do not trigger synaptic current until 100 ms into the simulation to allow initial transients to decay.

Example raster plots shown throughout this chapter are plotted such that the excitatory cells with the highest external driving current are given the lowest Neuron

Index, and thus are plotted towards the bottom of the y-axis, while neurons with lowest external driving current are given the highest Neuron Index, and thus are plotted towards the top of the y-axis. This fashion of organizing the excitatory cells is chosen in order to more clearly illustrate the organization of these cells within a burst and does not reflect their location in the network.

All plots illustrating the various measures used to quantify network dynamics display the average of these scores over five independent simulations, where the measures are calculated over the last second of the simulation.

3.3 Results

The computational study of E-I networks reveals that network dynamics depend jointly on the network connectivity structure, namely the relative strength of inter- and intra-connectivity between and within the excitatory and inhibitory subnetworks, and the neuromodulation of excitatory and inhibitory cells. ACh's effect on both excitatory and inhibitory cells that switches neuronal response properties is considered, as measured by the PRC and I-F curves, from Type II to Type I, thus affecting the cellular propensity of synchronization. Considering the possibility of nonuniform cholinergic release or that excitatory and inhibitory cells exhibit Type I or Type II properties without the presence of an M-current, all four combinations of excitatory and inhibitory cells are investigated, namely excitatory or inhibitory cells with high (Type I) or low (Type II) modulatory tone. To vary network connectivity structure, the focus is on the effects of the strengths of inter-connections between excitatory and inhibitory cells (E-I synapses and I-E synapses), and the strengths of intra-connections among excitatory cells (E-E synapses) and among inhibitory cells (I-I synapses). Figs 3.3 and 3.4 show measures of network dynamics as E-E and

I-I intra-connectivity strengths are varied together (horizontal axes) and E-I and I-E inter-connectivity strengths are varied together (vertical axes) for networks with Type I excitatory cells (Fig 3.3) and Type II excitatory cells (Fig 3.4), and inhibitory cells exhibiting either Type I or Type II properties. Network dynamics roughly divide into three parameter regions in which synchronous bursting of the excitatory cells are differentially affected by a combination of the modulation of cellular properties and network connectivity structure.

3.3.1 High E-I and I-E inter-connectivity promotes synchronous excitatory bursting regardless of cellular properties

When E-I and I-E inter-connectivity strength dominates over E-E and I-I intra-connectivity strength (upper-left corners of heatmaps in Fig 3.3 and 3.4), all networks exhibit synchronous excitatory bursting regardless of the cellular propensity for synchrony modulated by ACh. Values of the Synchrony Measure (panels **A** and **E**) are high in this parameter regime for all modulatory conditions, with networks with Type II excitatory cells (Fig 3.4) reporting higher values due to more coincident spike firing predicted by their cellular properties. Synchronous activity is robust with approximately all cells participating in the activity bursts (panels **B** and **F**) and the frequency of bursts are similar in all networks (panels **C** and **G**). Furthermore, the widths of both the excitatory and inhibitory bursts remain narrow in this regime, with narrower excitatory bursts exhibited by networks with Type II excitatory cells due to the additional synchrony promoted by excitatory intra-connectivity and the properties of Type II PRCs (Figs 3.3 and 3.4**D** and **H**). Note that the detection of excitatory bursts was robust to repeated simulations of these networks, with only one set of network connectivities (whose position in the heatmap is identified by the bolded outline in Fig 3.3**C** and **D**) for which bursts are detected in some, but

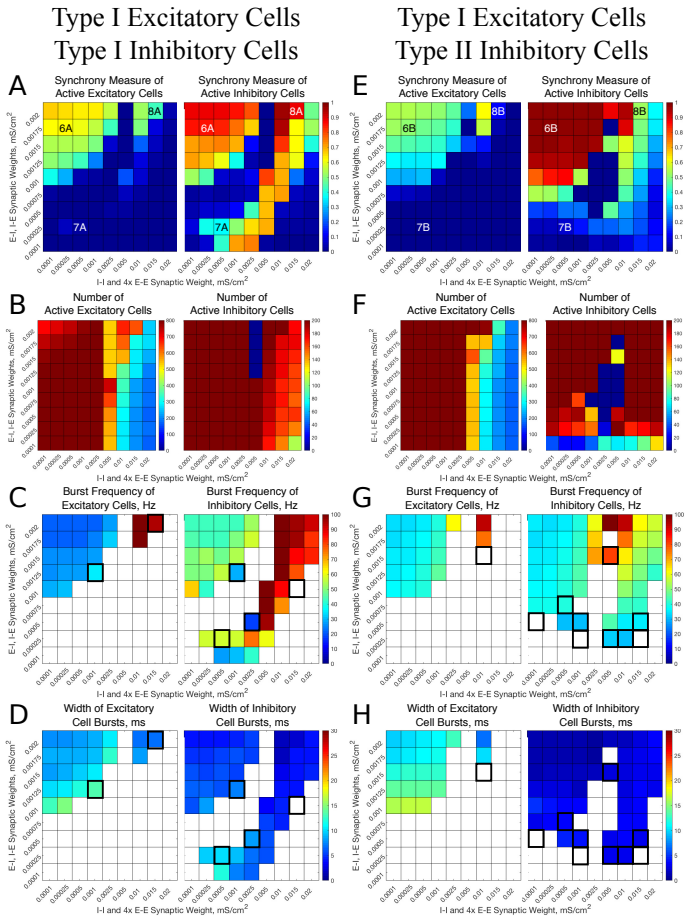

Figure 3.3: **E-I networks with Type I excitatory cells primarily exhibit bursting dynamics of the excitatory subpopulation when the network inter-connectivity dominates network intra-connectivity.** Spatio-temporal dynamics for E-I networks with Type I excitatory cells and Type I inhibitory cells **(A-D)** or with Type II inhibitory cells **(E-G)** as E-E and I-I intra-connectivity strength (x-axis) and E-I and I-E inter-connectivity strength (y-axis) is varied. Dynamics are quantified by the degree of synchrony for active cells **(A, E)**, number of active cells **(B, F)**, the burst frequency **(C, G)**, and the burst width **(D,H)**, where results for excitatory cells are shown in the left panels and results for inhibitory cells are shown in the right panels. Overlaid alphanumeric codes on **(A)** and **(D)** indiate simulations for which an example raster plot is shown in the indicated figure. Panels **(C)**, **(D)**, **(G)** and **(H)** display values (i.e. non-white coloring) only for networks for which the burst detection mechanism identified repetitive bursting for a majority of the simulations, and the value plotted is the average only of networks when repetitive bursting was detected. Networks in which bursting is detected in three or four of the five repetitions run have their colored entry surrounded by a bolded outline. Networks in which bursting is detected in only one or two of the five repetitions run have their white entry surrounded by a bolded outline.

not all, of the simulations run. As shown in the raster plots in Fig 3.5, whether excitatory cells are Type I (Fig 3.5**A** and **B**) or Type II (Fig 3.5**C** and **D**) they fire in synchronous bursts. Thus, for this network connectivity, neuromodulation of cel-

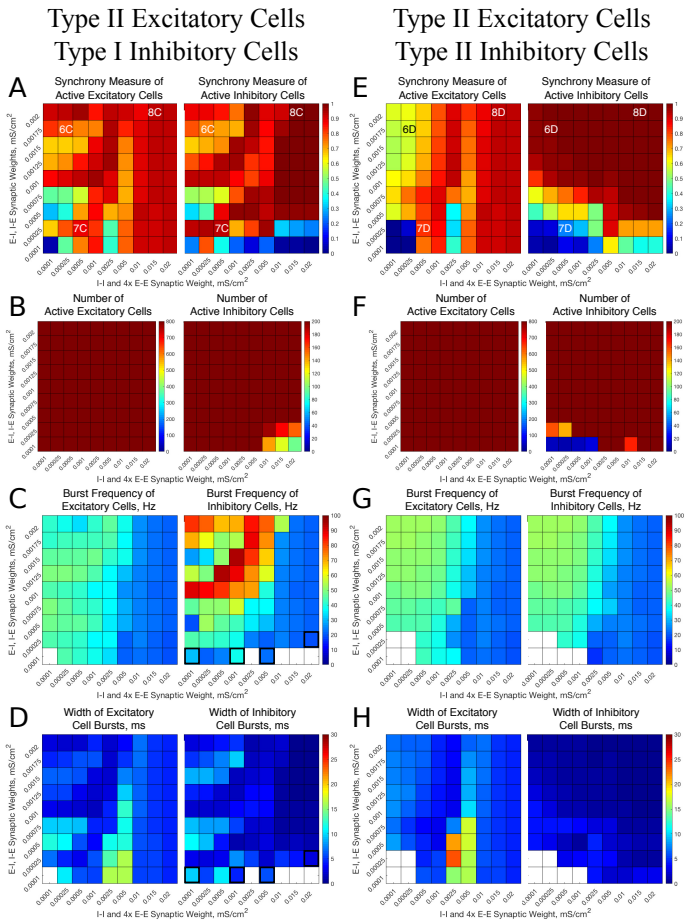

Figure 3.4: **E-I networks with Type II excitatory cells can exhibit bursting dynamics of the excitatory subpopulation not just when network inter-connectivity dominates network intra-connectivity, but also in other parameter regimes driven by the propensity of Type II excitatory cells to synchronize via excitatory signalling.** Spatio-temporal dynamics for E-I networks with Type II excitatory cells and Type I inhibitory cells **(A-D)** or with Type II inhibitory cells **(E-G)** as E-E and I-I intra-connectivity strength (x-axis) and E-I and I-E inter-connectivity strength (y-axis) is varied. Dynamics are quantified by the degree of synchrony for active cells **(A, E)**, number of active cells **(B, F)**, the burst frequency **(C, G)**, and the burst width **(D,H)**, where results for excitatory cells are shown in the left panels and results for inhibitory cells are shown in the right panels. Overlaid alphanumeric codes on **(A)** and **(D)** indiate simulations for which an example raster plot is shown in the indicated figure. Panels **(C)**, **(D)**, **(G)** and **(H)** display values (i.e. non-white coloring) only for networks for which the burst detection mechanism identified repetitive bursting for a majority of the simulations, and the value plotted is the average only of networks when repetitive bursting was detected. Networks in which bursting is detected in three or four of the five repetitions run have their colored entry surrounded by a bolded outline. Networks in which bursting is detected in only one or two of the five repetitions run have their white entry surrounded by a bolded outline.

lular propensity for synchronization has little effect on the generation of excitatory bursting.

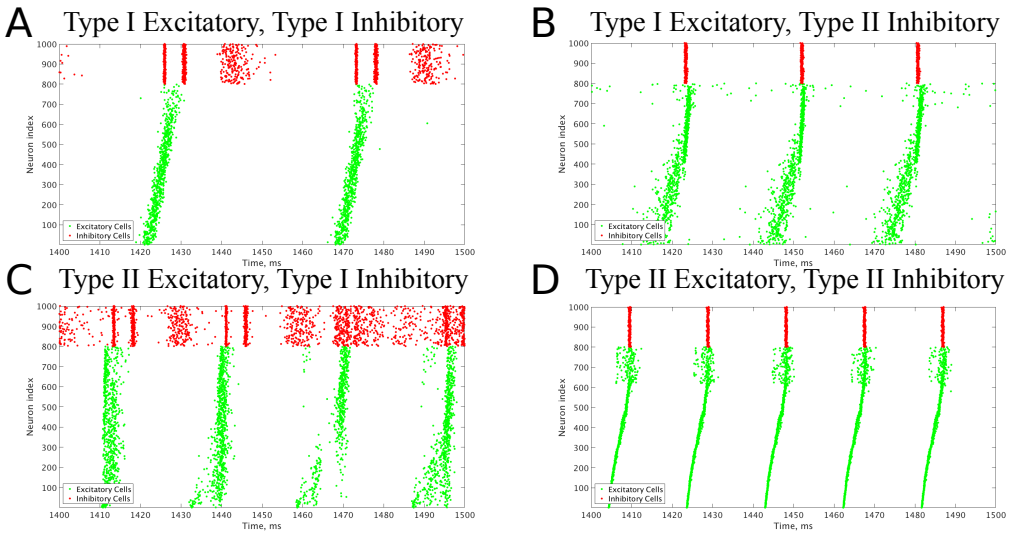

Figure 3.5: **Raster plots from an example network where inter-connectivity dominates intra-connectivity illustrate synchronous excitatory cell dynamics for all combinations of cell types, albeit with varying profiles of the excitatory bursting and inhibitory dynamics. (A-D)** Example raster plots from a network with an E-I and I-E connectivity strength of 0.00175 mS/cm^2, an I-I connectivity strength of 0.00025 mS/cm^2, and an E-E connectivity strength of 0.0000625 mS/cm^2. **(A)** is a network with Type I excitatory and inhibitory cells, **(B)** is a network with Type I excitatory and Type II inhibitory cells, **(C)** is a network with Type II excitatory and Type I inhibitory cells, and **(D)** is a network with Type II excitatory and inhibitory cells. In each case synchronous patterns are apparent in the excitatory network, although the bursting patterns exhibited by the inhibitory cells vary depending on their cell type.

The synchronous excitatory bursting in these networks with high inter-connectivity is predicted and governed largely by the PING mechanism. In the PING mechanism, the inhibitory cells serve to "silence" the excitatory cells following an inhibitory burst, which causes all of the excitatory cells to return to the same point of their oscillatory firing cycle and subsequently fire synchronously when released from inhibition [108, 63, 119, 42]. Evidence of the PING mechanism at work lies in the occurrence of inhibitory cell synchronous bursts near the end of excitatory cell synchronous bursts or immediately following these bursts, and in the effective silencing of excitatory activity by the inhibitory burst.

For additional verification, the same networks are simulated but with all synaptic connections from the inhibitory cells to the excitatory cells (I-E synapses) re-

moved (Fig 3.6). In the parameter region discussed above, no synchronous activity is obtained when excitatory cells are Type I, confirming that synchronous inhibitory signalling is necessary to induce excitatory synchronous bursting in these networks. When excitatory cells are Type II, synchronous activity emerges as intra-connectivity strength increases in this parameter regime, as expected from the propensity for Type II neurons to synchronize in response to excitatory connectivity. However, obtaining synchrony for the weakest intra-connectivity strength values, as obtained in the networks containing I-E synapses, depends critically on inhibitory signalling.

In these networks, cellular properties influence the patterning of spike firing within the PING-driven synchrony. The patterning of inhibitory cell activity in response to an excitatory burst relies heavily on the inhibitory cell type, which in turn can cause subtle changes in excitatory cell dynamics. When the excitatory cells are Type I this effect is primarily seen through the burst frequencies of the excitatory and inhibitory subpopulations (Figs 3.3**C** and **G**). Comparing the example raster plot with Type I excitatory cells and Type I inhibitory cells (Fig 3.5**A**) to that with Type I excitatory cells and Type II inhibitory cells (Fig 3.5**B**), the results show that the slower excitatory burst frequency of the former network is due to the multiple bursts of inhibitory activity in response to a burst of excitatory activity, which provides a longer lasting inhibitory synaptic signal to the excitatory cells. In contrast, when the inhibitory cells are Type II, only one instance of inhibitory activity follows excitatory activity, allowing the excitatory cells quicker release from this inhibitory signal.

The role of inhibitory cell patterning when the excitatory cells are Type II is seen primarily via differences in the Synchrony Measure, and is shown by comparing example networks with Type I inhibitory cells (Fig 3.5**C**) to those with Type II inhibitory cells (Fig 3.5**D**). In the latter case, each excitatory burst elicits a single

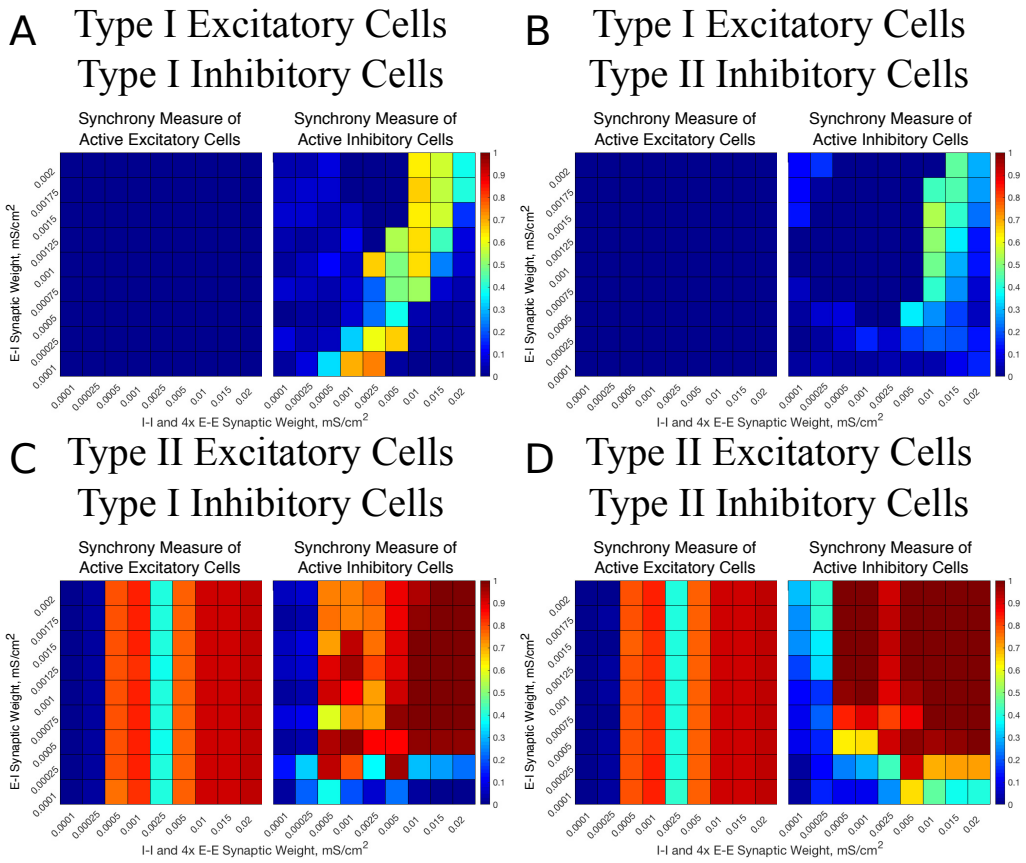

Figure 3.6: **E-I networks with Type I excitatory cells cannot exhibit excitatory subpopulation synchrony in the absence of I-E connectivity, while this connectivity is not necessary to elicit excitatory subpopulation synchrony in most cases when the excitatory cells are Type II. (A-D)** Heatmaps illustrating the degree of synchrony achieved by excitatory (left panel) and inhibitory (right panel) populations in E-I networks without any I-E connectivity for each combination of excitatory and inhibitory cell type. Such networks with Type I excitatory cells, shown in **(A-B)**, exhibit no synchrony in the excitatory cell population, implying that the excitatory bursting patterns achieved in networks with strong inter-connectivity in Fig 3.3 **(A)** and **(D)** are driven by inhibitory signaling to the excitatory population. In contrast, networks with Type II excitatory cells, shown in **(C-D)**, still exhibit excitatory synchrony for a majority of networks (excepting those with the lowest degree of intra-connectivity). The similarities between the parameter regimes exhibiting excitatory synchrony here and in Fig 3.4 **(A)** and **(D)**, where I-E connectivity was active, implies that excitatory intra-connectivity rather than network inter-connectivity may drive synchronous excitatory subpopulation dynamics in these networks.

inhibitory burst of activity including all inhibitory cells, which ensures each excitatory cell receives a near-identical profile of inhibitory synaptic current. This allows the excitatory cells to organize based upon their external driving current, with cells with the highest external current firing earliest in the burst and those with the lowest

firing latest. This organization causes the burst to occur over a longer time interval, slightly lowering the Synchrony Measure. However, when the inhibitory cells are Type I, the results again show that they respond to an instance of excitatory network bursting with multiple instances of activity; importantly, in this case the profile of these bursts varies in response to different instances of excitatory activity due to the randomness in the connectivity of the network as well as the heterogeneity in external drive to the cells. Variations in the inhibitory activity cause a disparity in the inhibitory signal felt by each excitatory cell, which disrupts organization in the excitatory bursts. However, this disorder also allows the burst to occur over a shorter timescale, increasing the Synchrony Measure. Thus, the inhibitory cell type plays a key role in explaining the slight difference in the Synchrony Measure seen in these networks when comparing Fig 3.4**A** and Fig 3.4**E**, while a negligible effect is seen in the frequency of the bursts (Fig 3.4**C** and **G**).

3.3.2 Cellular properties dictate synchronous excitatory bursting when E-E and I-I intra-connectivity is high

When E-E and I-I intra-connectivity dominates over E-I and I-E inter-connectivity, obtaining synchronous excitatory bursting depends on the cellular propensity for synchrony. For the ranges of synaptic strengths considered here, this parameter regime begins when intra-connectivity strength is slightly higher than inter-connectivity strength (near 7A,B labels in Fig 3.3 and 7C,D labels in Fig 3.4). When intra-connectivity is much higher than inter-connectivity (lower-right corners of heatmaps in Fig 3.3 and 3.4), the high I-I synaptic strength acts to slow firing of the inhibitory cells to the point that they cannot fire synchronously, thus minimizing their influence on excitatory subnetwork dynamics. In this regime, networks with Type I excitatory cells have Synchrony Measure values close to zero for excitatory cells (Fig 3.3**A**, **E**

left panels) reflecting asynchronous firing (as seen in the examples in Fig 3.7**A**, **B**), as predicted by their cellular properties. While the majority of excitatory cells are firing (Fig 3.3**B**, **F** left panels), no synchronous excitatory bursts were detected, as reflected by the lack of a burst frequency value (Fig 3.3**C**, **G** left panels). Networks with Type II excitatory cells, on the other hand, display synchronous excitatory bursting (as seen in the examples in Fig 3.7**C**, **D**), as predicted by cellular properties, with high Synchrony Measure (Fig 3.4**A**, **D**), full cell participation in synchronous bursts (Fig 3.4**B**, **E**) and similar burst frequencies (Fig 3.4**C**, **G**). Thus, in this network structure, ACh governs the generation of synchronous excitatory activity.

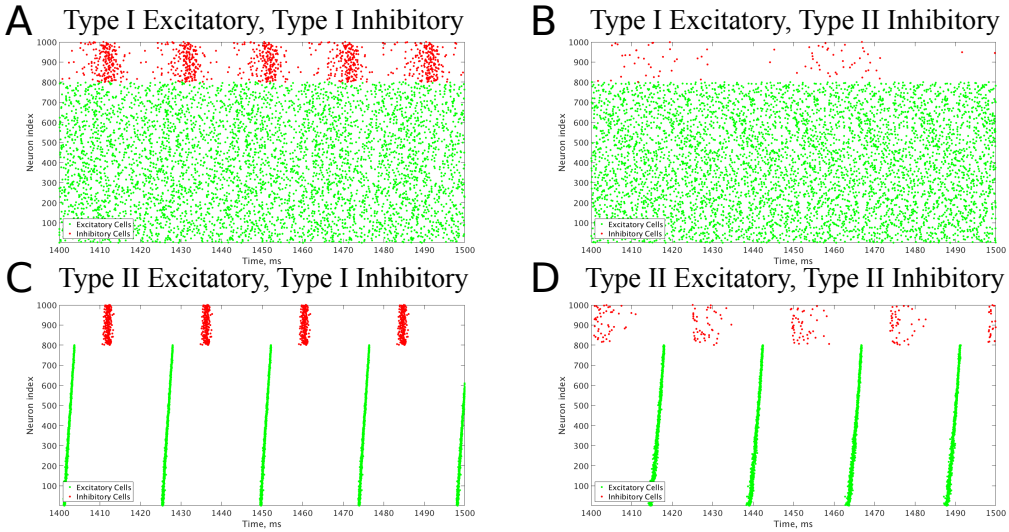

Figure 3.7: **Raster plots from an example network with low inter-connectivity and slightly higher intra-connectivity illustrate that networks with Type I excitatory cells can not achieve synchronous bursting dynamics, while networks with Type II excitatory cells can. (A-D)** Example raster plots from a network with an E-I and I-E connectivity strength of 0.00025 mS/cm^2, an I-I connectivity strength of 0.0005 mS/cm^2, and an E-E connectivity strength of 0.000125 mS/cm^2. **(A)** is a network with Type I excitatory and inhibitory cells, **(B)** is a network with Type I excitatory and Type II inhibitory cells, **(C)** is a network with Type II excitatory and Type I inhibitory cells, and **(D)** is a network with Type II excitatory and inhibitory cells. Only networks with Type II excitatory cells can achieve excitatory synchrony, although inhibitory synchrony is achieved without excitatory synchrony in **(A)**.

The PING mechanism is not involved in generating synchronous excitatory bursts in this parameter regime as evidenced by the long gap between the excitatory cell

burst and inhibitory cell firing. Inhibitory cells fire in bursts, with higher synchrony measure when they are Type I (Fig 3.7**C** and **D**), in response to the oscillatory excitatory signal, but inhibition is not responsible for silencing the excitatory cells after the burst since they stop firing well in advance of the inhibitory bursts. Additionally, the burst frequency is not affected by the different profiles of inhibitory firing when the inhibitory cells are Type I or Type II, reflecting their lack of influence on excitatory bursting. This is confirmed by fully removing the I-E synapses and continuing to see synchronous excitatory cell firing in this regime (Fig 3.6**C** and **D**).

In this regime of dominant intra-connectivity, inhibitory cell type can play a role in the dynamics of the inhibitory cell population without significantly influencing the patterning of the excitatory subpopulation. When excitatory cells are Type I, their asynchronous firing provides a weak, nearly tonic drive to the inhibitory cells. Type I inhibitory cells with weak I-I connectivity can form synchronous patterns in response to such a drive, as shown by the example raster plot in Fig 3.7**A** and discussed in detail in previous work [86]. In contrast, Type II inhibitory cells are less excitable and more susceptible to suppression by inhibitory signalling via the dominant intra-connectivity, preventing them from forming clearly synchronous dynamics, as seen in the example raster plot in Fig 3.7**B**.

Meanwhile, Type II excitatory cells can synchronize driven by E-E connectivity and not network inter-connectivity as discussed above, allowing for the synchronous excitatory subpopulation dynamics seen in Fig 3.7**C** and **D**. Here again, though, the type of inhibitory cell dictates the dynamics of the inhibitory subpopulation in response to this weak, but synchronous, drive to the inhibitory cells. Given that Type I inhibitory cells are more excitable, the weak burst of excitation is sufficient to prompt all of the inhibitory cells to fire in a closely clustered fashion, an example

of which is shown by the raster in Fig 3.7**C**. In contrast, properties of the Type II neuron model lead these inhibitory cells to respond with a more sparse burst to a nearly identical excitatory synaptic drive, an example of which is shown by the raster in Fig 3.7**D**.

Note that the interaction between Type II PRC properties and strong E-E connectivity can cause some complex burst patterns in the excitatory population. This is evidenced in Fig 3.4**D** and **H** by the significantly wider excitatory bursts seen in the middle of the range of network intra-connectivities. However, this behavior does not disrupt the overall oscillatory behavior of the network driven by the network intra-connectivity.

3.3.3 Cellular properties influence ability of inter-connectivity to generate synchronous excitatory bursting when inter- and intra-connectivity are balanced

When E-I, I-E inter-connectivity and E-E, I-I intra-connectivity are both strong in this parameter space, corresponding to the upper-right corner of the heatmaps in Fig 3.3 and 3.4, both cellular properties and network connectivity contribute to the network's tendency to exhibit synchronous excitatory bursting. When excitatory cells are Type I, while their cellular properties resist synchronization, loose synchronous bursting is obtained when inhibitory cells are Type I (example raster in Fig 3.8**A**) but not Type II (example raster in Fig 3.8**B**). This example represents one of the few instances in this parameter regime in which excitatory bursting activity was detected in some, but not all, of the simulations run (as represented by the grid squares with a bolded outline in Fig 3.3**C** and **D**) As reflected in their Synchrony Measures (Fig 3.3**A** and **E**), Type I inhibitory cells synchronize tightly with high I-I intraconnectivity (**A**, right panel), while Type II inhibitory cells do not (**E**, right panel). The strong inhibitory signal provided to the excitatory cells from Type I

inhibitory cells silences their activity and produces a weak synchronous excitatory burst by the PING mechanism. When inhibitory cells are Type II, however, their more sparse firing has little effect on the excitatory subnetwork, and asynchronous excitatory firing persists.

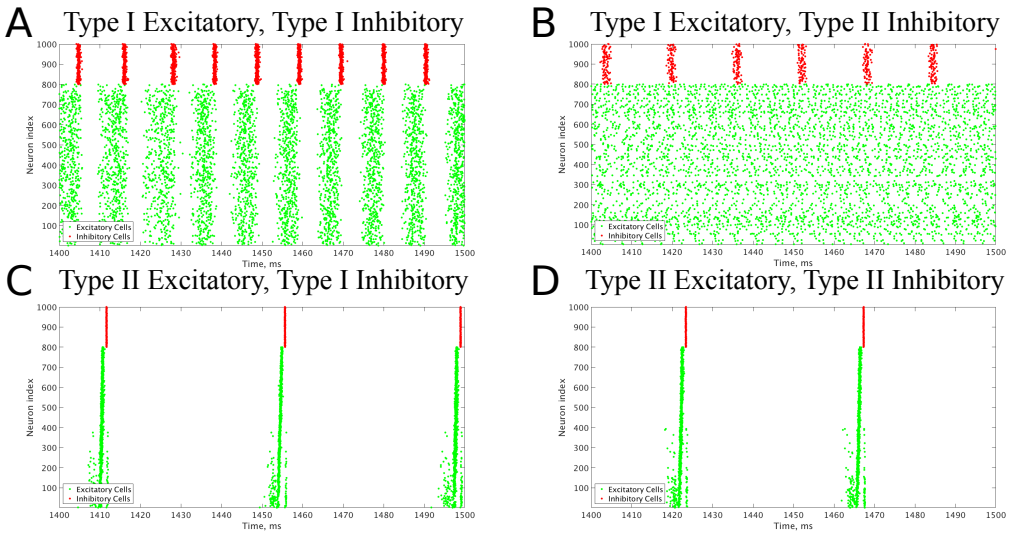

Figure 3.8: **Raster plots from an example network with strong intra-connectivity and inter-connectivity reveal the tendency for high E-E connectivity to elicit depolarization block in some Type I excitatory cells, while consistent bursting patterns remain in networks with Type II excitatory cells. (A-D)** Example raster plots from a network with an E-I and I-E connectivity strength of 0.002 mS/cm^2, an I-I connectivity strength of 0.015 mS/cm^2, and an an E-E connectivity strength of 0.00375 mS/cm^2. **(A)** is a network with Type I excitatory and inhibitory cells, **(B)** is a network with Type I excitatory and Type II inhibitory cells, **(C)** is a network with Type II excitatory and Type I inhibitory cells, and **(D)** is a network with Type II excitatory and inhibitory cells. While networks with Type II excitatory cells exhibit consistent bursting patterns in both the excitatory and inhibitory networks, networks with Type I excitatory cells have some cells shut down due to depolarization block (shown most clearly in **(B)**), which can interfere with the development of synchrony.

When excitatory cells are Type II, their propensity for synchronization strengthens the influence of high inter-connectivity to generate robust excitatory synchronous bursting for both types of inhibitory cells (Fig 3.8**C** and **D**). Indeed, Synchrony Measures for both excitatory and inhibitory subnetworks are the highest in this parameter regime (Fig 3.4**A** and **E**) with full network participation in the bursts (Fig 3.4**B** and **F**). Additionally, values of all measures are the same for Type I and Type

II inhibitory cells. There is conflicting evidence as to whether the PING mechanism or excitatory network intra-connectivity drives this synchrony: while the inhibitory network bursts do closely follow the excitatory network bursts (Fig 3.8**C** and **D**), as predicted by the PING mechanism, the removal of I-E synapses does not eliminate excitatory synchrony (Fig 3.6**C** and **D**), meaning inhibition may not serve a causal role in synchronizing excitatory cells. It is likely that some combination of these two mechanisms is what results in the strong synchrony of the excitatory network seen here.

Thus, in this network structure, cholinergic modulation acts in conjunction with high inter-connectivity to generate synchronous excitatory bursting. Synchronous excitatory bursting fails to exist only when both excitatory and inhibitory populations have a low propensity for synchronization.

In this regime of balanced inter- and intra-connectivity, cell properties contribute to the characteristics of excitatory synchronous bursting, as seen by the example raster plots in Fig 3.8. For Type II excitatory cells, spikes in the synchronous bursts are highly coincident (Fig 3.8**C** and **D**) due to the strong E-E intra-connectivity overpowering the heterogeneity in firing frequency that created more variation in spike timing in the low E-E intra-connectivity regime (examples in Fig 3.5**C** and **D**) This induces a highly coincident burst of inhibitory cells immediately following the excitatory burst. The strong inhibitory signal to all excitatory cells coupled with their previous coincident firing leads to a long silent period between excitatory bursts and low burst frequency (Fig 3.4**C** and **G**). For Type I excitatory and inhibitory cells, burst frequencies are the highest since the high E-E intra-connectivity drives the excitatory cells to recover quickly from the inhibitory signal and initiate the next excitatory burst (Fig 3.3**C**).

The inter- and intra-connectivity strengths can also be balanced at a weak level in this parameter space, which corresponds with the lower-left corner of the heatmaps in Fig 3.3 and 3.4. In this regime networks with Type I excitatory cells exhibit completely asynchronous firing due to an inability to achieve PING rhythmicity, while inhibitory cells may be able to synchronize themselves due to the near-tonic drive provided by the asynchronous excitatory cells (Fig 3.3**A** and **E**). Meanwhile, in networks with Type II excitatory neurons, excitatory synchrony can be achieved in networks with all but the weakest connectivity strengths (Fig 3.4**A** and **E**) driven by the ability for Type II excitatory neurons to synchronize themselves even with weak E-E synapses.

Thus, when the inter- and intra-connectivity strengths are balanced, but at weak levels, the tendency to achieve synchronous excitatory cell dynamics is controlled by ACh. In this regime, synchronous excitatory bursting occurs only due to the tendency of Type II neurons to synchronize due to E-E synapses, even when these synapses may be weak.

3.3.4 Dynamics of inhibitory subnetworks

Across the parameter space of network connectivity structures, there are regimes where activity in the inhibitory subnetwork does not correlate with activity in the excitatory subnetwork. These instances are largely robust to repetition, as there are few instances where inhibitory bursts are detected in some, but not all, of the repetitions for a given network (cases in which this occurs are represented the grid squares with bolded outlines in Figs 3.3 and 3.4 **C**, **D**, **G**, and **H**). For example, as discussed above, Type I inhibitory cells can form oscillatory synchronous bursts independent of synchronous activity in the excitatory subnetwork. This behavior is seen in the networks with Type I excitatory cells when intra-connectivity is larger

than inter-connectivity (diagonal band of high Synchrony Measure in Fig 3.3**A**, right panel). In this regime, the excitatory cells are asynchronous and provide a tonic excitatory drive to the inhibitory cells, inducing repetitive firing. When coupled with inhibitory synapses, repetitively firing Type I cells receiving strong tonic drive have a high propensity for synchronization [85]. As intra-connectivity increases, maintaining synchronous bursting requires increased excitatory input to counteract the increased inhibitory signaling within the inhibitory subnetwork (resulting in the diagonal band). In fact, inhibitory activity becomes sparse and asynchronous when intra-connectivity is much higher than inter-connectivity (Fig 3.3**A**, **B** and **C** right panels, lower right corners).

In other parameter regimes, firing in the inhibitory subnetwork is almost completely suppressed. This occurs in three parameter regimes that are most easily identified in the right panels of Fig 3.3 and 3.4 **B** and **F**, which show the number of active inhibitory cells: a small region of high inter-connectivity strength for networks of Type I excitatory and inhibitory neurons (Fig 3.3**B**), a small region with low inter-connectivity strength for networks of Type II excitatory and inhibitory neurons (Fig 3.4**F**), and a relatively large parameter regime for networks of Type I excitatory neurons and Type II inhibitory neurons (Fig 3.3**F**). The first two cases are easily explained. The first is a case of classic depolarization block of the Type I inhibitory neurons: the moderate intra-connectivity strength is enough to force excitatory cells to fire very quickly due to the E-E connectivity, and the high inter-connectivity strength leads these fast firing excitatory cells to provide excessive excitation to the inhibitory cell population, driving those cells into depolarization block. The second case is the opposite situation, as weak inter-connectivity combined with low excitability of Type II inhibitory cells result in insufficient excitatory synaptic signal to the

inhibitory cells to induce firing.

The final case, that seen in networks of Type I excitatory neurons and Type II inhibitory neurons, is more complex, involving intricacies of the dynamics of the M-type potassium current. The activity of this ionic current not only serves to shift the properties of the neuron PRC from Type I to Type II as discussed previously, but also imbues the neurons with spike-frequency adaptation. Given the slow time-scale of the z gating variable that governs this current when compared to the extremely fast time-scale of the m, n, and h variables governing the currents directly inciting action potential firing, the M-current acts to slow down the firing of the neuron following repetitive action potentials. Thus, the neuron "adapts" its firing frequency given the recent past, firing slower if a quick burst of action potentials occurred previously. This adaptation is reflected by a rise in the value of z as action potential firings occur. As the potassium current is a hyperpolarizing current, larger values of z that arise from action potential firing invoke a larger amplitude of the M-type potassium current which in turn slows down cell firing.

When Type II neurons are provided a tonic excitatory drive that induces repetitive firing, the adaptation current eventually settles into a stable periodic pattern that allows repetitive action potential firing at a constant frequency. However, in these E-I networks, the drive to the inhibitory population is provided by the synaptic drive from the excitatory population, which has a distinctly non-tonic profile. In particular, properties of the reversal potential in the synaptic current term in Equation 1.1 speed up action potential firing when compared to a tonic current with a similar maximum amplitude. This increase in firing frequency prevents z from settling into a stable oscillation, instead causing it to steadily increase. When this gating variable rises too high, the hyperpolarizing current from the M-type potassium channel exceeds the

depolarizing excitatory input current from the excitatory cell population, causing a net hyperpolarizing current and in turn quiescence. In short, in certain E-I networks where the excitatory cells do not synchronize, the adaptation current prevents the inhibitory cells from exhibiting repetitive firing due to the form of the excitatory synaptic current.

3.4 Discussion

The work discussed in this chapter reveals that the development of synchronous excitatory activity in E-I networks depends critically on both the intrinsic cellular properties of the excitatory and inhibitory cells as well as the connectivity structure of the network as described by the inter- and intra-connectivity strengths. These results are summarized in Figure 3.9. In particular, depending on the network connectivity, effects of neuromodulation that change the cellular propensity for synchronization may or may not affect the generation of network synchrony. High E-I and I-E inter-connectivity that dominates over the influence of E-E and I-I intra-connectivity induces synchronous excitatory bursting regardless of the cellular propensity for synchronization. In this regime, the PING mechanism generates the excitatory bursting along with synchronous activity of inhibitory cells. When E-E and I-I intra-connectivity has a larger influence than E-I and I-E inter-connectivity, the propensity of excitatory cells to synchronize determines the generation of excitatory bursting in the networks. Even when inhibitory cells can form synchronous activity due to their cellular properties, weak inter-connectivity does not induce synchronous activity in the excitatory cells. Thus mechanisms for PING-driven synchrony are ineffective in these network topologies.

Networks in which both inter- and intra-connectivity are strong achieve excitatory

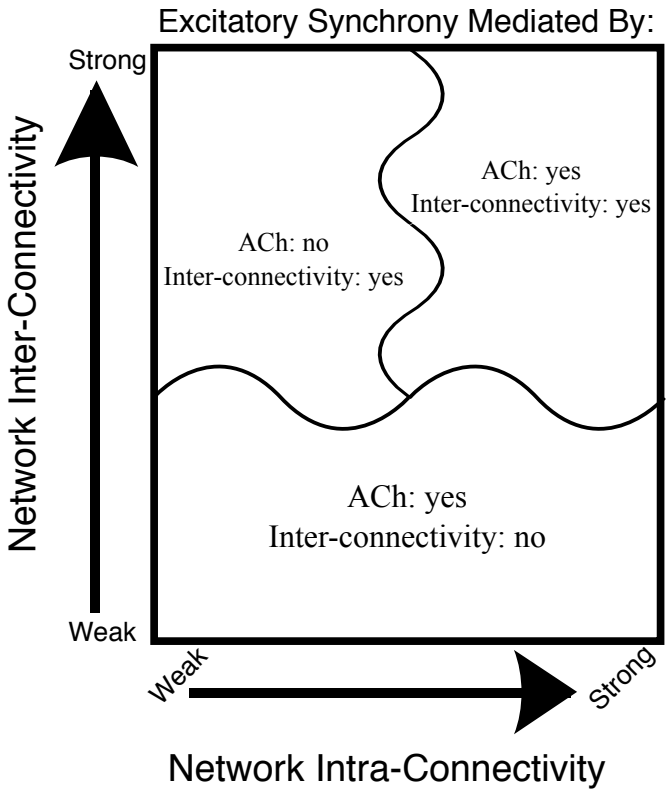

Figure 3.9: **Summary figure illustrating the three regimes in which excitatory synchrony is mediated differentially by cholinergic modulation and network topology.** When network inter-connectivity dominates network intra-connectivity (top-left regime), excitatory synchrony is mediated by network inter-connectivity while cholinergic modulation has minimal effect on dynamics. When network inter-connectivity is weak (bottom regime) exciatory synchrony is mediated by cholinergic modulation's effect on cell type, and not by network inter-connectivity. Finally, when network inter- and intra-connectivity are both strong (top-right regime), cholinergic modulation and network inter-connectivity both influence the tendency for networks to exhibit excitatory synchrony, with these interactions sometimes leading to complex dynamics.

synchrony resulting from a combination of the cellular propensity for synchronization and the network inter-connectivity that drives PING. In this regime, the high propensity for synchronization of Type II excitatory cells, combined with PING-like dynamics driven by strong inter-connectivity, leads to strong synchrony irrespective of inhibitory cell properties. Meanwhile, although Type I excitatory cells resist synchrony driven by intra-connectivity, the ability for inhibitory cells to synchronize permits the PING mechanism to induce weaker synchrony in the excitatory population in some cases. Finally, networks in which both inter-and intra-connectivity

are weak are able to achieve excitatory synchrony only when the excitatory cells are Type II and prone to synchronize even with weak intra-connectivity, while networks with Type I excitatory cells can sometimes elicit synchronous spiking of the inhibitory network due to the near-tonic drive asynchronous firing of the excitatory cells provides.

Computational studies probing oscillatory synchronous activity in E-I networks, and in particular the intricacies of PING rhythms, are prevalent in the literature [108, 63, 119, 42, 15, 14, 16, 18, 66, 79]. These studies pay less attention to the role of intrinsic cellular properties or the impact of more varied network structures, as the conceptual PING mechanism assumes strong E-I and I-E inter-connectivity as well as strong I-I intra-connectivity and burst frequencies are presumed to be dictated by properties of synaptic currents. However, as the biological understanding of the brain rapidly accelerates, the immense diversity of neuron properties, particularly of inhibitory interneurons, and network connectivities among these interneuron populations [20, 63, 12, 61, 23, 10, 7, 96, 62, 51, 11, 47, 34, 53, 54, 93] motivates computational research to investigate and understand dynamics arising from the interaction of cellular properties and network connectivity structures.

Investigating the role of intrinsic cellular properties on E-I network dynamics through the lens of neuromodulation, particularly that achieved via the action of ACh, provides further salience to this work given the important roles this neuromodulator has in the brain. Concentrations of ACh are known to fluctuate based on sleep-wake states: ACh is present in high concentrations during wake and REM sleep, and in low concentrations during slow-wave sleep [4, 91]. Computational research has shown that changing the cholinergic modulatory tone can elicit changes in neural network dynamics that mirror those seen experimentally [90], and this

work shows that the changes brought about by varying ACh concentrations are also affected by network connectivity. Furthermore, ACh also influences how the brain directs attention in response to competing stimuli [36, 70, 84, 46, 19], a behavior whose corresponding neural dynamics might also be explained by analyzing the role of ACh on neural networks as done here. These hypotheses relating ACh concentration to differing neural network dynamics are supported by experiments in which direct manipulation of the M-current causes changes in network dynamics; for example, slow oscillations in excitatory networks in the motor cortex are abolished when the M-current is blocked [28].

More generally, however, it is clear from this study that both cellular as well as structural network properties are intertwined together to dictate which specific dynamical mechanisms generate observed spatio-temporal dynamics. I hypothesize that gross changes in network structure, as those observed for example in the epileptic brain, may lead to transitions among cellular-based and network-based dynamical mechanisms which in turn may result in transitions between cognitive and pathological brain function (see, for example, [13, 81]).

CHAPTER IV

Dichotomous dynamics in E-I networks with strongly and weakly intra-connected inhibitory neurons

4.1 Introduction

As discussed in Chapter III, the classic PING mechanism explains the tendency for E-I networks with strong inter-connectivity between the excitatory and inhibitory neuron populations to exhibit synchronous bursting. As much of the literature examining E-I networks focuses on the PING mechanism [15, 14, 16, 18, 66, 79], in this chapter we analyze in greater detail E-I networks with strong inter-connectivity (corresponding with the "top" regimes in the parameter space seen in Figure 3.9) that are predisposed to exhibit PING-driven dynamics.

Despite the abundance of literature cited above analyzing PING rhythmicity, little work has been done to analyze the role of the intra-connectivity of the inhibitory cell population in affecting the dynamics of E-I networks. Indeed, as classically articulated this inhibitory intra-connectivity is not necessary for PING rhythm generation, but is typically included in the network structure as motivated by numerous experimental studies showing that interneurons tend to be highly connected [44, 59, 104, 82, 73, 76]. Thus, most of the computational studies assume some level of strong synaptic coupling amongst the interneurons, which serves to "slow down" and help prevent disorganized firing of the inhibitory cells that can disrupt

synchronous firing of the excitatory cells [16].

Given the multitude of types of interneurons identified in brain regions where PING rhythms are thought to occur, such as the hippocampus [61, 23] and cortex [10, 7, 96, 62, 51, 11, 47], along with the known connectivity of many of these interneurons with excitatory pyramidal cells as modeled in an E-I network [120], a closer analysis of the role of inhibitory intra-connectivity in PING-driven dynamics will paint a more complete picture of how such rhythmic activity might arise in the brain. In this chapter, the role that the strength of inhibitory intra-connectivity (I-I connectivity) plays in dictating the burst dynamics of excitatory cells in E-I networks is investigated in detail. While some differences in bursting dynamics that arise from weakening the inhibitory intra-connectivity to values well below that typically studied in the PING literature, such as inhibitory spike doublets, have been identified previously [16], this work finds that these differences can have important effects on the spiking properties of the excitatory network.

These results show that, when interneurons have Type I firing properties (similar to those often exhibited by the ubiquitous fast-spiking PV interneuron [44]), there is a distinct difference in rhythmic synchronous dynamics when the strength of I-I connectivity varies from weak to strong. Networks with Type I interneurons are the focus of this work given the preponderance of PV interneurons in the hippocampus and cortex, and also because a majority of PING literature uses inhibitory neuron models with these properties.

When the I-I connectivity is strong, the results closely mirror those of most analyses of PING rhythms. The dynamics of these networks not only include synchrony amongst the excitatory cells, but also lead to organized spike timing within the excitatory bursts, consistent cell participation in each burst, and consistent periodicity of

the bursts. These dynamics are classified as having "low variability" to differentiate them from networks that exhibit synchronous bursting but without this additional spike organization. When the excitatory to inhibitory connectivity (E-I connectivity) is very weak, however, networks with this strong intra-connectivity amongst the inhibitory cells exhibit asynchonous excitatory cell activity, as predicted by the PING mechanism.

On the other hand, when I-I connectivity is weak, E-I networks exhibit alternate dynamics, highlighting the importance of inhibitory cell patterning in dictating excitatory cell dynamics. In this case, synchronous excitatory activity is exhibited at very low values of the E-I connectivity strength, seemingly in opposition to one of the key requirements of PING theory. As E-I connectivity strength increases, these networks tend to exhibit disorganized inhibitory cell firing that follows inhibitory bursts, which in turn leads to degradation of excitatory cell synchrony. Namely, excitatory bursts tend to be disorganized, exhibit variability in the number of cells participating in each burst, and do not exhibit a consistent inter-burst interval.

To determine dependence on inhibitory cellular properties, how changing I-I connectivity affects networks where the interneurons have Type II firing properties is also examined. This work finds that changes to the I-I connectivity in E-I networks do not significantly alter dynamics of the overall network when the interneurons are modeled as Type II. This corresponds with previous work which shows that, unlike strictly inhibitory networks with Type I neurons, such networks containing Type II neurons with and without an M-type slow potassium current do not show significant changes in the propensity for synchrony as the connectivity density, which roughly corresponds with the overall strength of inhibitory signalling in the network, changes [85].

The research presented in this chapter indicates that synchronous, rhythmic, PING activity in E-I networks consisting of Type I interneurons is sensitive to I-I connectivity strength. Specifically, weak inhibitory intra-connectivity allows well-ordered synchronous excitatory activity primarily for low values of the E-I synaptic weight, while networks with strong inhibitory intra-connectivity exhibit such activity for high values of the E-I synaptic weight. This dichotomy motivates the investigation of a network architecture that preserves the advantages of both types of networks, effectively expanding the parameter regime at which PING-like rhythms can be achieved. An E-I network with two inhibitory subnetworks, one weakly intra-connected and one strongly intra-connected, achieves this goal, providing a potential mechanism by which such rhythms can be generated in the brain in a more robust fashion. Numerous studies provide support for the existence of this type of network topology in the brain, where multiple populations of interneurons synapse onto the same excitatory pyramidal cells while connectivity between inhibitory interneurons consists almost exclusively of synapses between similar interneurons [113, 47, 11, 96, 61].

Taken together, these results serve to expand upon the understanding of PING-like rhythms in E-I networks by revealing the important, but often overlooked, role that inhibitory intra-connectivity and inhibitory cell dynamics play in governing the overall network dynamics [1].

4.2 Methods

4.2.1 Network Structure

Simulations of E-I networks presented in this chapter consist of 1000 neurons, 800 of which are excitatory and 200 of which are inhibitory. Excitatory neurons re-

[1] Work presented in this chapter has been previously published [86]

ceive an external driving current (described below) and also receive inhibition from the inhibitory cells, where each inhibitory cell has a 50% chance to synapse onto a given excitatory cell. Inhibitory neurons receive a external current (described below) depending upon their cell type in order to ensure they do not fire in the absence of input from the excitatory cells and are near their firing threshold. Inhibitory neurons are driven by the excitatory cell population, as each excitatory cell has a 50% chance to synapse onto a given inhibitory cell. Additionally, inhibitory neurons receive inhibition from within the inhibitory network, as each inhibitory neuron has a 30% chance to synapse onto a given, different inhibitory cell. The choice of this connectivity density is motivated by evidence for this level of intraconnectivity amongst interneurons in the hippocampus [110, 3]. Diagramatic representations of these networks with strong and weak inhibitory intra-connectivity are shown in Fig 4.1.

Cell heterogeneity was implemented by varying the external input current, I_{app}, to each excitatory neuron. The input currents were selected from a uniform distribution centered on the current (I_A) that would impart an average intrinsic cell firing frequency to an isolated neuron. For excitatory cells, the driving currents are chosen uniformly from the distribution $[.9I_A, 1.1I_A]$. I_A was varied for the excitatory cells in order to study the effects of their intrinsic frequency.

Type I inhibitory cells were given a small external hyperpolarizing current to ensure that the neurons would not fire spontaneously, given that this neuron model exhibits slow, spontaneous firing with no external current. Heterogeneity was implemented in this hyperpolarizing (i.e. negative) current similar to the excitatory cells to impart some degree of heterogeneity to the inhibitory population: the external hyperpolarizing current for each interneuron was chosen uniformly from the distri-

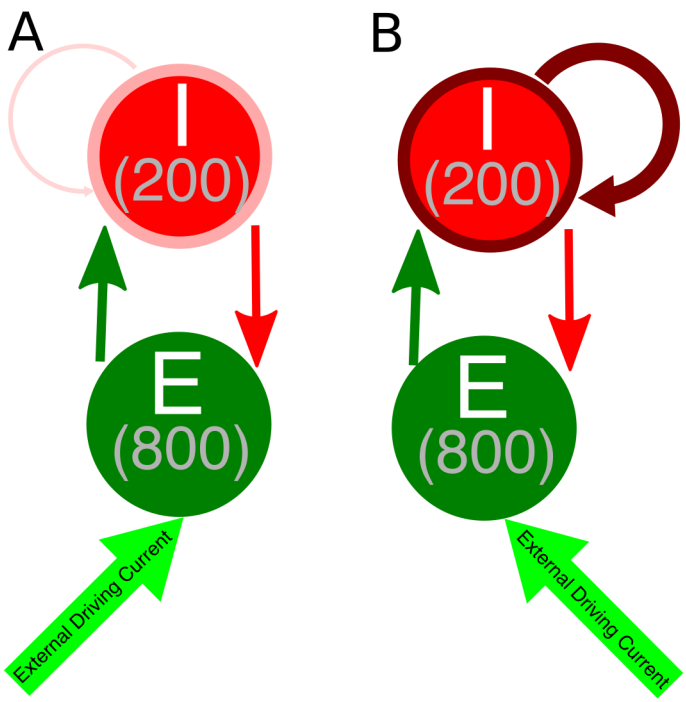

Figure 4.1: **Network diagram of E-I networks. (A)** Connectivity in an E-I network with a weakly connected inhibitory subnetwork. Thin, light red arrow symbolizes the weak intraconnectivity between inhibitory interneurons. **(B)** Connectivity in an E-I network with a strongly connected inhibitory subnetwork. Thick, dark red arrow symbolizes the strong intraconnectivity between inhibitory interneurons.

bution $[1.05I_A, 0.95I_A]$. Here I_A is chosen to be -0.2 $\mu A/\text{cm}^2$ so that all interneurons will not fire action potentials without input from the excitatory cells. This external hyperpolarizing current was not needed when the inhibitory cells were modeled using either Type II formalism, as those model neurons will not fire spontaneously.

Synapses are modeled using a double exponential profile of the form described in Section 1.2 and Equation 1.1. Here, τ_r is set at 0.2 ms for all synapses, while τ_d is set at 3.0 ms for excitatory synapses and 5.5 ms for inhibitory synapses. For I-E synapses, $g_{syn} = 0.003$ mS/cm^2, while the synaptic weight for I-I and E-I synapses is varied in the simulations.

Simulations of strictly inhibitory networks utilize the network connectivity described in Chapter II [85], where 1000 inhibitory neurons are randomly connected

with a 30% connectivity density. Cell heterogeneity is implemented in these simulations by varying the external driving current to the inhibitory neurons in a method analagous to that used for the excitatory neurons in the E-I networks described above. Synapses are also modeled identically to those described above.

4.2.2 Noise

To investigate the effects of noisy perturbations to the network, simulations were run where Poisson trains of brief excitatory stimuli were given to the excitatory neurons in addition to their tonic driving currents and synaptic currents. At each time step, there is a probability $p = 10^{-3}$ that a given excitatory cell receives an excitatory "kick". These kicks are modeled with a temporal profile similar to the excitatory synaptic currents in the network and are thus of the form

$$I_{noise_i}(t) = g_{noise}\left(e^{-(t-s_i)/\tau_d} - e^{-(t-s_i)/\tau_r}\right) \tag{4.1}$$

where s_i is the time of the ith kick to the cell, τ_d and τ_r are the same as for excitatory synaptic currents, and g_{noise} is the amplitude of each kick. The times of the ten most recent kicks are stored and contribute to the drive to the cell, such that

$$I_{noise_{total}}(t) = g_{noise}\left(\sum_{(k-9)\leq i\leq k} e^{-(t-s_i)/\tau_d} - e^{-(t-s_i)/\tau_r}\right) \tag{4.2}$$

where k is the total number of kicks to the given cell at time t. This term is added to the overall current balance equation of the given cell, such that

$$\frac{dV}{dt} = I_{ionic} + I_{app} - I_{syn} + I_{noise_{total}} \tag{4.3}$$

where I_{ionic} denotes all terms besides I_{app} and I_{syn} found in Equations 1.10 and 1.2.

While the frequency of the noise was kept constant (i.e. p was the same for all simulations with noise), g_{noise} was varied in these simulations, as seen in Fig 4.8.

4.2.3 E-I Difference

The difference between the total excitatory and total inhibitory synaptic signalling (E-I Difference) in the inhibitory network was also calculated. It is calculated as a mean difference between the total excitatory synaptic current and total inhibitory synaptic current received by the inhibitory cell population. As with other measures, the final second of the simulations are analyzed using the E-I Difference. Note that this measure is utilized instead of a ratio of excitatory and inhibitory synaptic current, as is common in E/I Balance measures, because such a ratio would tend towards infinity in networks with little or no inhibitory cell activity, which exist in the parameter space.

4.2.4 Simulations

The code implementing these simulations was written in the C programming language and run on the University of Michigan's Flux cluster, a Linux-based high-performance computing cluster.

All simulations presented in this chapter were run for 1500 ms from random initial conditions for voltage and gating variables for each neuron. Possible initial conditions for V ranged between -62 and -22 mv, while the possible initial conditions for each gating variable ranged between 0.2 and 0.8.

Model equations were integrated using a fourth order Runge-Kutta technique. Spikes do not trigger synaptic current until 100 ms into the simulation to allow initial transients to decay.

Example raster plots shown throughout this chapter are plotted such that the excitatory cells with the highest external driving current are given the lowest Neuron Index, and thus are plotted towards the bottom of the y-axis, while neurons with

lowest external driving current are given the highest Neuron Index, and thus are plotted towards the top of the y-axis. This ordering of the excitatory cells was chosen to clearly illustrate the temporal organization of cells within a burst and does not reflect their location in the network.

All plots illustrating the various measures used to quantify network dynamics display the average of these scores over five independent simulations, where the measures are calculated over the last second of the simulation. The lone exception are the results shown in Fig 4.10 for networks with Type II interneurons, for which only three repetitions were performed given the uniformity of the results.

4.3 Results

Previous results from the study of strictly inhibitory neural networks [85], combined with previous work in the field [63, 119, 114, 118] show that synchronous bursting occurs in distinct parameter regimes for strongly connected and weakly connected networks of Type I neurons (see Fig 4.2). From random initial conditions, only networks with very weak inhibitory synaptic weight exhibit synchronous activity when average intrinsic cell firing frequency is low. As average intrinsic cell firing frequency increases, such networks exhibit asynchrony or weaker synchrony. In contrast, networks with stronger inhibitory synaptic weight synchronize only when average intrinsic cell firing frequency is high.

These results motivate the work in thi chapter in which I describe how changing the I-I connectivity strength in an E-I network is the impetus behind changing pattern formation in the inhibitory network, which in turn affects the dynamics of the excitatory network. The PING dynamics that have been analyzed in the literature typically are analogous to those seen in Fig 4.3**D**, **F** and **H**, where the inhibitory

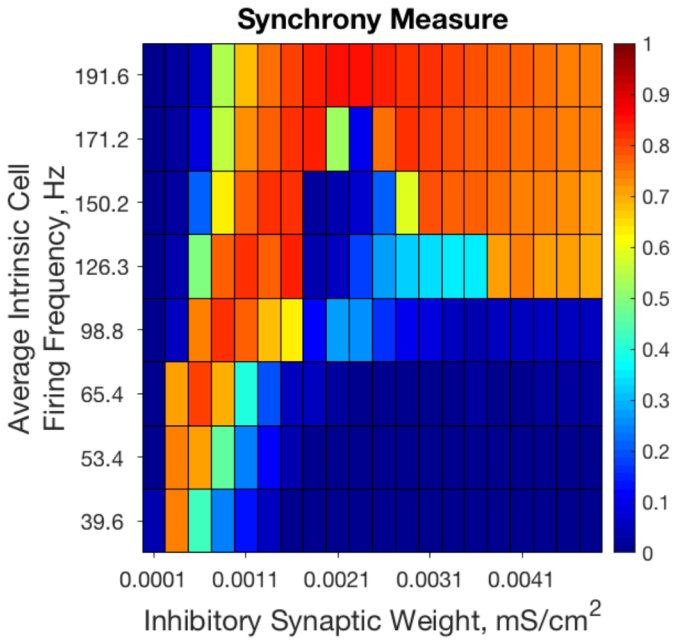

Figure 4.2: **Randomly connected strictly inhibitory networks of Type I neurons with strong and weak inhibitory connectivity synchronize in divergent parameter regimes.** Synchrony measure computed from dynamics of strictly inhibitory networks consisting of Type I neurons as synaptic weight (x-axis) and average intrinsic cell firing frequency (y-axis) are varied. Only networks with very weak inhibitory synaptic weight exhibit synchronous activity when average intrinsic cell firing frequency is low. Networks with stronger inhibitory synapses only synchronize when average intrinsic cell firing frequency is higher. Inhibitory synaptic weights stronger than those shown here simply continue the pattern of synchronous behavior shown for networks with an inhibitory synaptic weight above 0.0041 mS/cm^2.

network is strongly intra-connected and exhibits one instance of activity per oscillatory cycle. However, by weakening the I-I connectivity, different types of dynamics can arise amongst the inhibitory cells that affect the profile of excitatory network bursts, as seen by the examples in Fig 4.3**C**, **E**, and **G**. The focus is on the effects that multiple firings of inhibitory cells and the consistency and organization of these bursts have on the temporal organization of firing in excitatory cell bursts.

4.3.1 E-I Networks with Strong and Weak I-I Synaptic Strength

I analyze E-I networks with two I-I connectivity strengths in detail: an E-I network with strong intra-connectivity amongst the inhibitory subnetwork (entitled "Strong

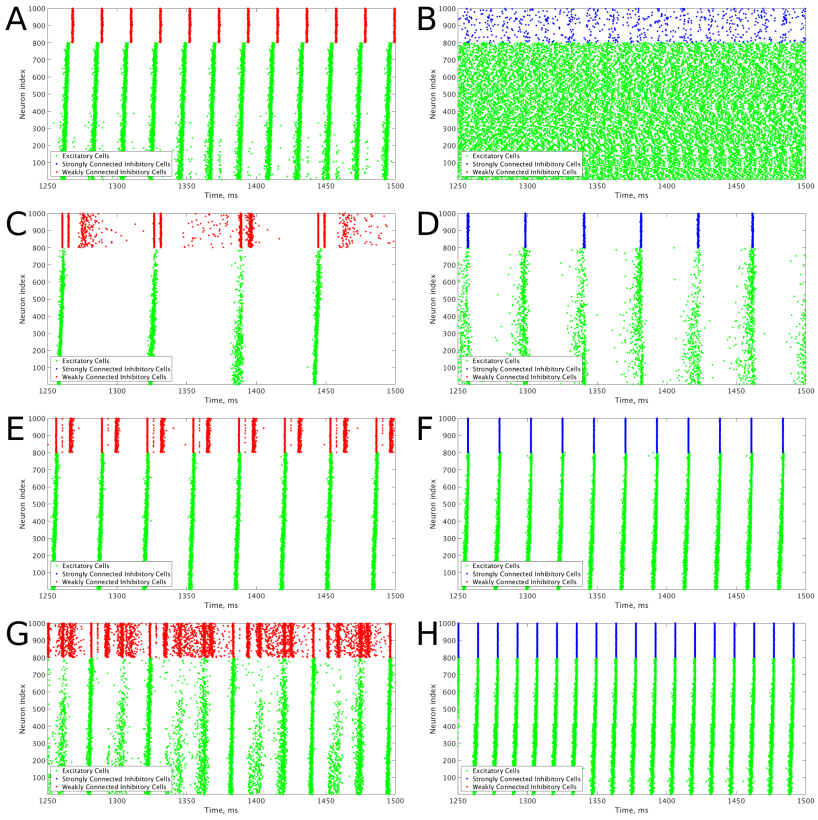

Figure 4.3: **Example raster plots illustrate the differences between dynamics in networks with weakly connected and strongly connected inhibitory subnetworks. (A-H)** Example raster plots with the excitatory cells (green dots) in these raster plots organized such that cells with the highest external drive are given the lowest Neuron Indices with the rest of the neurons organized such that decreasing external drive corresponds with increased Neuron Index. Panel letter corresponds with overlaid labels in Figs 4.4 and 4.5 indicating the parameters of the given network. Panels **A, C, E and G** are from networks with weakly connected inhibitory subnetworks, while panels **B, D, F, and H** are from networks with strongly connected inhibitory networks. Panels **A** and **B** are raster plots from a network with an E-I synaptic weight of 0.0004 mS/cm^2 and an average intrinsic excitatory cell firing frequency of 98.8 Hz. Panels **C** and **D** are raster plots from a network with an E-I synaptic weight of 0.00235 mS/cm^2 and an average intrinsic excitatory cell firing frequency of 39.6 Hz. Panels **E** and **F** are raster plots from a network with an E-I synaptic weight of 0.00235 mS/cm^2 and an average intrinsic excitatory cell firing frequency of 80 Hz. Panels **G** and **H** are raster plots from a network with an E-I synaptic weight of 0.00235 mS/cm^2 and an average intrinsic excitatory cell firing frequency of 126 Hz.

Networks" for brevity) and an E-I network with weak intra-connectivity amongst the inhibitory subnetwork (entitled "Weak Networks" for brevity). Strong Networks have an I-I synaptic weight of 0.025 mS/cm^2, which was chosen in order to be analogous to the strong inhibitory synaptic weights used in the study of strictly inhibitory

networks [85] (where scaling from 1000 inhibitory neurons in the strictly inhibitory networks to 200 inhibitory neurons in the E-I networks is taken into account). Weak Networks have an I-I synaptic weight of 0.0015 mS/cm^2.

For both Strong and Weak Networks the average intrinsic excitatory cell firing frequencies and E-I synaptic weights are varied. The I-E synaptic weight as well as connectivity densities (I-I, E-I and I-E) are kept constant in all simulations.

To summarize network dynamics, the Variability Measure is shown for Strong Networks in the left panel of Figs 4.4**(A)** and 4.5**(A)** and for Weak Networks in the left panel of Figs 4.4**(B)** and 4.5**(B)**. For moderate values of the E-I synaptic weight, both Strong and Weak networks show synchronous rhythmic bursting with low Variability Measure reflecting periodic, well-organized excitatory cell bursts. For low E-I synaptic weight and high E-I synaptic weight there is a significant difference that requires further investigation. The right panels of Fig 4.4**(A)** and **(B)** investigate networks with low E-I synaptic weight in more detail by showing the Synchrony Measure as well as the three measures that are used in the formation of the Variability Measure individually. The same is done for networks with high E-I synaptic weight in the right panels of Fig 4.5**(A)** and **(B)**.

These results indicate that Strong Networks do not display any form of excitatory bursting activity in most networks with the lowest E-I synaptic weights. This is illustrated by the Synchrony Measure in the right panel of Fig 4.4**(B)**. A raster plot showing an example of this asynchronous activity is shown in Fig 4.3**(B)**. In contrast, Weak Networks achieve excitatory bursting for many networks with the lowest E-I synaptic weights as shown by the Synchrony Measure in the right panel of Fig 4.4**(A)**. The raster plot in Fig 4.3**(A)** shows a network with identical parameters to that shown in Fig 4.3**(B)** with only the I-I synaptic weight weakened which exhibits

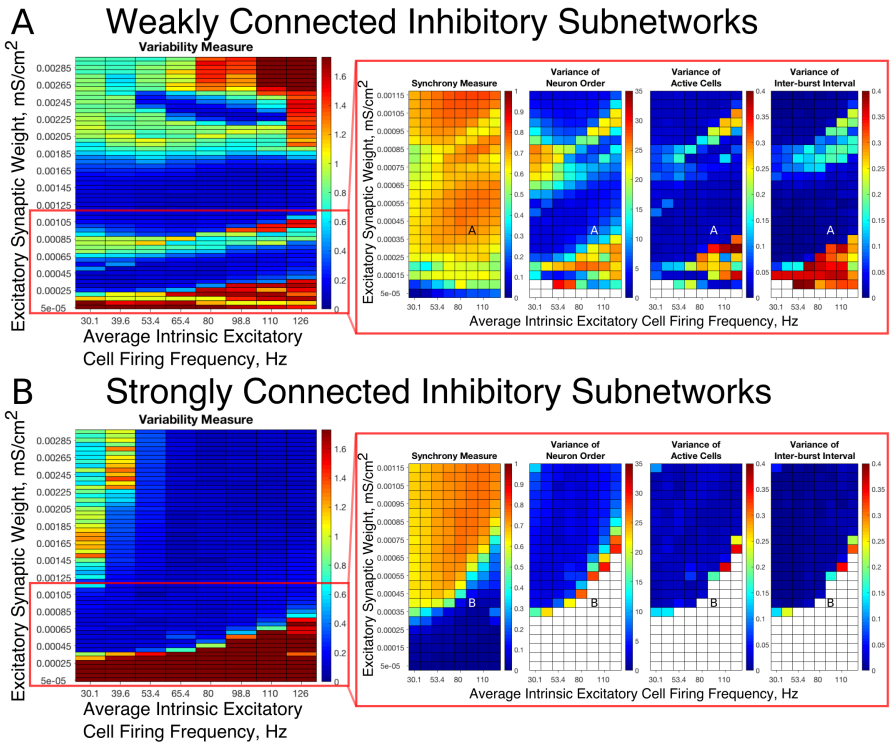

Figure 4.4: **E-I networks with weakly connected inhibitory subnetworks are able to achieve synchrony for low values of the E-I synaptic weight, while E-I networks with strongly connected inhibitory subnetworks are unable to achieve any sort of excitatory bursting activity for many of these networks. (A-B)** Variability Measure (left panel) calculated over the entire parameter range studied, with the parameter regime of particular interest outlined in red. For this parameter regime of interest, the Synchrony Measure is shown along with the three measures that are used to calculate the Variability Measure (Variance of Neuron Order, Variance of Active Cells, and Variance of Inter-burst Intervals) in the red box making up the right panel. White entries in the heatmaps indicate that the excitatory network did not achieve sufficient synchrony for the given measure to be accurately calculated for that network. Overlaid letters indicate parameter values of example raster plots in Fig 4.3. Results for E-I networks with weakly connected inhibitory subnetworks are shown in **(A)**, while results for E-I networks with strongly connected inhibitory subnetworks are shown in **(B)**. In the parameter regime of interest, networks with weakly connected inhibitory subnetworks achieve synchrony of the excitatory subnetwork for many network parameters for which networks with strongly connected inhibitory subnetworks are completely asynchronous.

clear bursting activity. Additionally, there is a consistent ordering of the excitatory cells in each burst, along with periodic firing and the same level of participation of excitatory cells in each burst, leading to low values of the Variability Measure.

When E-I synaptic weight is strengthened, strong inhibitory intra-connectivity plays a significant role in controlling network dynamics. For a large majority of the

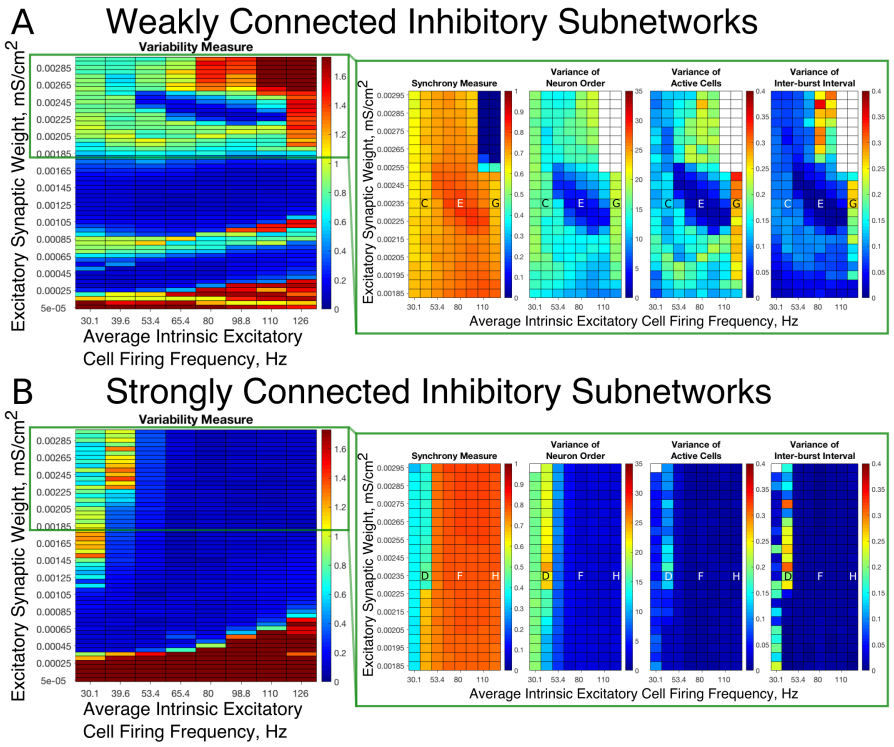

Figure 4.5: **E-I networks with weakly connected inhibitory subnetworks exhibit excitatory bursting with high variability for high values of the E-I synaptic weight despite exhibiting synchrony in this parameter regime; in contrast, E-I networks with strongly connected inhibitory subnetworks exhibit mostly low variability firing in this parameter regime. (A-B)** Variability Measure (left panel) calculated over the entire parameter range studied, with the parameter regime of particular interest outlined in green. For this parameter regime of interest, the Synchrony Measure is shown along with the three measures that are used to calculate the Variability Measure (Variance of Neuron Order, Variance of Active Cells, and Variance of Inter-burst Intervals) in the green box making up the right panel. White entries in the heatmaps indicate that the excitatory network did not achieve sufficient synchrony for the given measure to be accurately calculated for that network. Overlaid letters indicate parameter values of example raster plots in Fig 4.3. Results for E-I networks with weakly connected inhibitory subnetworks are shown in **(A)**, while results for E-I networks with strongly connected inhibitory subnetworks are shown in **(B)**. In the parameter regime of interest, networks with strongly connected inhibitory subnetworks almost exclusively exhibit bursting patterns with low variability, while networks with weakly connected inhibitory subnetworks show a much higher Variability Measure due to the higher values of the Variance of Neuron Order, Variance of Active Cells, and Variance of Inter-burst Intervals for most networks in this parameter regime.

networks with high E-I synaptic weight (highlighted in Fig 4.5**(B)**), Strong Networks show well-organized synchronous bursting with very low Variability Measures, with behavior typified by the example raster plots shown in Fig 4.3**(F)** and **(H)**. In contrast, a majority of Weak Networks show a significantly increased Variability Measure

in the regime of high E-I synaptic weight, despite still exhibiting synchronous excitatory activity. As shown in the right panel of Fig 4.5**(A)**, these networks show noticeable increases in each of the measures making up the Variability Measure. High values of the Variance of Neuron Order indicates that the timing of individual excitatory neuron activity within each burst is not consistent (shown by the "wider" excitatory bursts without a clear slope and outlier firings in the raster plots displayed in Fig 4.3**(C)** and **(G)**); high values of the Variance of Active Cells indicates that the number of excitatory cells in each excitatory burst fluctuates significantly from burst to burst (again illustrated by Fig 4.3**(C)** and **(G)**); increased values of the Variance of Inter-burst Interval indicates that excitatory burst firing is not strictly periodic (best illustrated by Fig 4.3**(G)**). All three of these issues, reflected by an increase in the Variability Measure, imply that for high E-I coupling, Weak Networks lose the organization, consistency and strict periodicity of excitatory bursts that have classically typified PING rhythmicity.

The cause of the changes in excitatory bursting dynamics in the Weak Networks is the disorganization of inhibitory cell firing. As illustrated by the example raster plots in Fig 4.3**(C)** and **(G)**, the combination of weak I-I and strong E-I synaptic strength leads to multiple instances of inhibitory cell activity in response to a burst of excitatory cell activity. Due to the randomness in network connectivity and cell heterogeneity, these multiple bursts are not consistent across different instances of inhibitory activity; in extreme cases, inhibitory bursts may not exhibit clear synchrony. The specific form of the inhibitory network activity changes throughout the simulation, altering in turn the modulation of the excitatory network's activity. Thus, while these dynamics might not disrupt the formation of synchronous excitatory bursts, they do disrupt the organization, consistency and periodicity of these

bursts.

However, there is a parameter regime within the highlighted high E-I synaptic strength region for which Weak Networks retain a low Variability Measure. Such networks, an example of which is shown by the raster in Fig 4.3**(E)**, still exhibit multiple bursts of inhibitory activity in response to excitatory activity, but do so in a consistent and organized fashion in response to each instance of excitatory activity. The existence of such networks shows that it is the disorganization of inhibitory cell firing, and not necessarily the existence of multiple inhibitory network bursts, that causes significant changes to the properties of excitatory bursts.

An additional parameter regime of interest is networks with a low average intrinsic cell firing frequency but a high E-I synaptic weight. Here, Strong Networks exhibit a significantly increased Variability Measure similarly to Weak Networks, albeit driven by a different mechanism. While the increased variability in Weak Networks in this regime can be attributed to overactivity and disorganization amongst the inhibitory cells (as illustrated by the raster in Fig 4.3**(C)**), the increased variability in this regime for Strong Networks is caused primarily by the dynamics of the excitatory cells.

A combination of two factors leads to these dynamics in Strong Networks, typified by the behavior shown by the raster plot in Fig 4.3**(D)**. First, for networks with the slowest average intrinsic excitatory cell firing frequencies, following an inhibitory burst, the excitatory cells are slow to fire leading to a longer interval between inhibitory bursts. This allows the burst of excitatory activity to occur over a longer period of time (see example in Fig 4.3**(D)**). Thus, the possibility of more variability in the excitatory bursts arises. In contrast, for networks with faster firing excitatory cells, the excitatory cells fire shortly after the inhibition decays, causing the next

inhibitory burst to occur quickly as well. This, in turn, creates a very small time window in which excitatory activity can occur and thus less possibility for significant variability in firing times.

Second, with high E-I synaptic weight, even strongly intra-connected inhibitory networks can receive sufficient excitatory signal to burst without a majority of the excitatory cells firing. Excitatory cells that fire before the burst of inhibition are suppressed following the burst of inhibition, while cells that have not fired are typically past the threshold for action potential firing at the time of the burst of inhibition, and thus their firing pattern is not significantly affected by the inhibition. Thus, cells that fire prior to the burst of inhibition on one cycle will fire later, if at all, on the following cycle. This causes disorganization in the neuron order from cycle to cycle, as the driving current to the excitatory cells is now not the only factor determining when in a burst they fire, since each neuron is not receiving similar inhibitory delay as is typical in PING rhythmicity.

These two factors cooperatively lead to the disorganization of the excitatory bursts as reported by the Variability Measure. This is shown in the raster in Fig 4.3**(D)** by the lack of a clear slope in the excitatory burst, as well as the bursts occurring over a longer timespan. Additionally, the number of cells participating in each burst varies significantly by the same reasoning.

In summary, in most cases high values of the E-I synaptic weight require stronger inhibitory intra-connectivity in order to preserve consistent inhibitory response to excitatory activity in an E-I network, which in turn preserves well-ordered and consistent bursting of the excitatory population. However, investigation into these networks also reveals that Weak Networks may exhibit well-organized and consistent excitatory bursting when the inhibitory network exhibits multiple bursts, as long

as such bursts are themselves well-organized. Additionally, Strong Networks exhibit increased variability for high E-I synaptic weight when intrinsic excitatory cell firing has lower average frequency.

A further explanation as to the differences underlying the Strong and Weak Networks lies in the synaptic E-I Difference in the inhibitory subnetwork. As shown in Fig 4.6, there is a stark difference between the E-I Difference for Weak Networks (Fig 4.6**(A)**) and Strong Networks (Fig 4.6**(B)**). In particular, the E-I Difference for Strong Networks is always negative, meaning that the inhibitory intra-connectivity dominates the excitatory drive to the inhibitory cells, and shows minimal change in response to altering network parameters. In contrast, the E-I Difference for Weak Networks increases as the E-I synaptic weight increases and is always positive, meaning that the excitatory drive dominates the inhibitory intra-connectivity within the inhibitory subnetwork.

This dichotomy provides a more quantitative explanation for the dynamical differences exhibited by these networks. The dominance of inhibitory intra-connectivity over the excitatory synaptic drive in Strong Networks ensures that following a burst of inhibitory activity, the inhibitory synaptic drive dominates the excitatory synaptic drive and ensures that inhibitory cells are silent following the burst. This explains the tendency for Strong Networks to only exhibit the 1:1 bursting ratio that is a hallmark of classic PING theory, as well as the minimal differences in network dynamics seen as the E-I synaptic weight increases. However, in Weak Networks, increasing E-I synaptic weight cannot be counteracted by the weaker inhibitory synapses as illustrated by the increasing and positive E-I Difference, which allows for multiple bursts of inhibitory activity that are often disorganized and in turn lead to an increase in the Variability Measure.

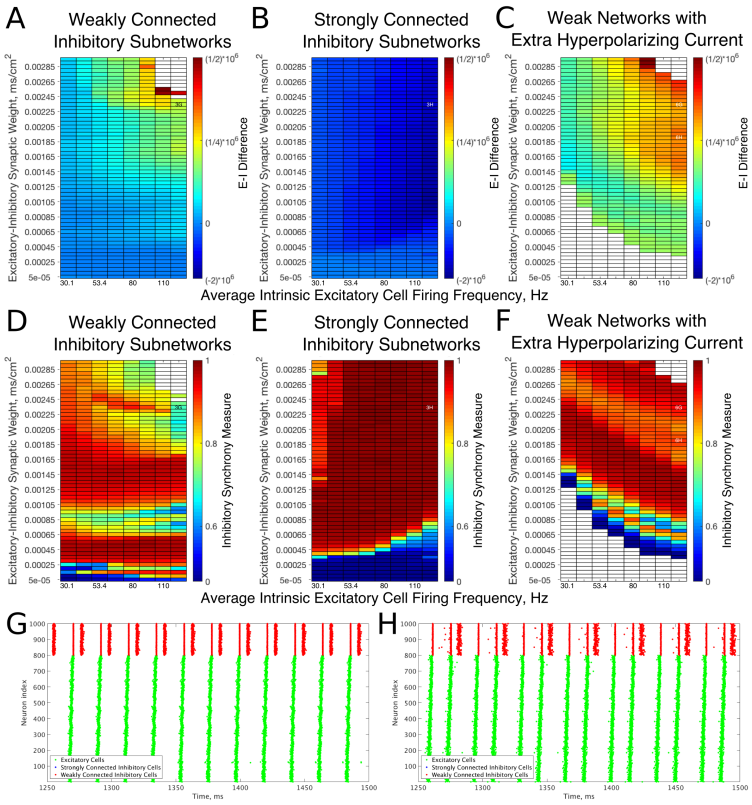

Figure 4.6: **Dynamical differences between networks with weakly connected and strongly connected inhibitory subnetworks are reflected in differences in E-I Difference and Inhibitory Synchrony Measure, even with changes to the external hyperpolarizing current.** **(A-C)** Synaptic E-I Difference for Weak Networks **(A)**, Strong Networks **(B)**, and Weak Networks where the external hyperpolarizing current is increased from -0.2 to -3.0 μA/cm^2 **(C)**. **(D-F)** Inhibitory Synchrony Measure for the same three network types. White entries in the heatmaps indicate that the measure could not be calculated due to insufficient inhibitory activity, and overlaid alphanumeric codes indicate position of example raster plots seen in Fig 4.3 (for comparison to those shown here) and in this figure. **(G-H)** Example raster plots for Weak Networks with Extra Hyperpolarizing Current; both examples are for a network with an average intrinsic excitatory cell firing frequency of 126 Hz, with Panel **(G)** an example from a network with an E-I synaptic weight of 0.00235 mS/cm^2 while Panel **(H)** is an example from a network with an E-I synaptic weight of 0.00190 mS/cm^2. Weak Networks, both with and without additional hyperpolarizing current, show a dominance of excitatory synaptic activity reflected in positive E-I Difference values that increase as the E-I synaptic weight increases, while Strong Networks show a dominance of the inhibitory synaptic activity reflected in largely uniform negative values of the E-I Difference. Moreover, Weak Networks with Extra Hyperpolarizing Current retain distinct behaviors from Strong Networks as illustrated by the Inhibitory Synchrony Measure and example raster plots.

Additionally, analyzing the E-I Difference cements the importance of the I-I connectivity in dictating overall network dynamics. Fig 4.6**(C)** illustrates the E-I Dif-

ference for a Weak Network where the hyperpolarizing current to the inhibitory cells is increased from -0.2 to -3.0 μA/cm^2. In this network paradigm, the inhibitory cells are "less excitable" than those in the Weak Networks due to the external current, but the synaptic E-I Difference in the inhibitory subnetwork retains similarity to that seen in the Weak Network, namely retaining positive values that increase with increasing E-I synaptic weight. Importantly, the E-I Difference remains entirely distinct from that of Strong Networks, which can be considered to have "less excitable" inhibitory cells given the stronger I-I connectivity. This result indicates that the net excitability of the inhibitory cells and the strength of inhibitory intra-connectivity are distinct features that have differing effects on network dynamics. Indeed, multiple and sometimes disorganized inhibitory bursts are seen in Weak Networks with this additional hyperpolarizing current, as shown by the example raster plots in Fig 4.6**(G)** and **(H)**, while Strong Networks never show inhibitory double bursts. This again shows that making the cells less excitable through an external hyperpolarizing current does not have the same effect as doing so by increasing the I-I synaptic weight. The differences in dynamics of the inhibitory cells between these networks and Strong Networks are confirmed by comparing the Synchrony Measure computed for the inhibitory subnetwork, shown for all three types of networks discussed above in Fig 4.6**(D-F)**. Thus, regardless of the hyperpolarizing current to the inhibitory cells, the weak I-I synaptic weight is not sufficient to balance increasing excitatory signal, preventing them from achieving the very synchronous bursts exhibited in Strong Networks for all values of the E-I synaptic weight.

To study the robustness of these behaviors, the I-I synaptic weights are varied between the values used in the Weak and Strong Networks. The results are illustrated in Fig 4.7, in which the I-I synaptic strength is varied along the y-axis and the E-

I synaptic strength along the x-axis while keeping the average intrinsic cell firing frequency fixed. Examples are shown for slow firing excitatory cells in panels **(A)**, **(C)**, **(E)** and **(F)** and for fast firing excitatory cells in panels **(B)**, **(D)**, **(F)** and **(G)**.

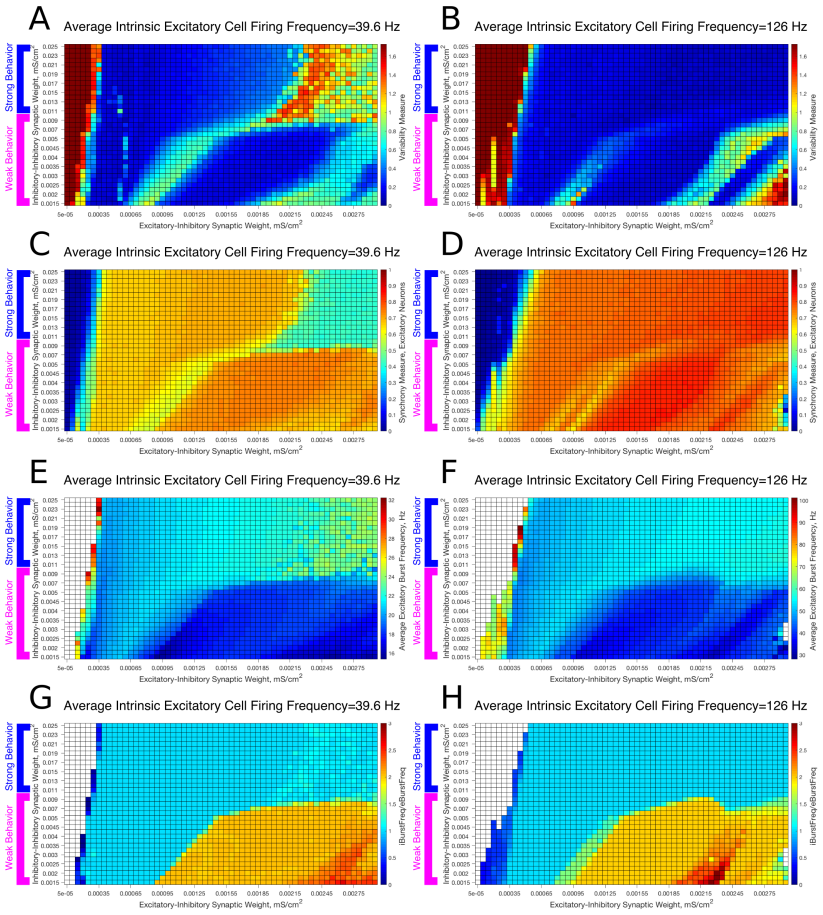

Figure 4.7: **Varying the I-I synaptic weight reveals that E-I networks display two distinct dynamical patterns directly analagous to those seen in the networks with weakly connected or strongly connected inhibitory subnetworks. (A-H)** Heatmaps varying the E-I synaptic weight on the x-axis and I-I synaptic weight on the y-axis for networks with an average intrinsic excitatory cell firing frequency of 39.6 Hz **(A, C, E, G)** and 126 Hz **(B, D, F, H)**. Four measures are shown: the Variability Measure **(A-B)**, the Synchrony Measure for Excitatory Neurons **(C-D)**, the Average Excitatory Burst Frequency in Hz **(E-F)** and the ratio of the Average Inhibitory Burst Frequency over the Average Excitatory Burst Frequency **(G-H)**. White boxes in the heatmaps indicate that the excitatory network did not achieve sufficient synchrony for the given measure to be accurately calculated for that network. Values of I-I connectivity strength that exhibit behavior corresponding with that seen in the network with a weakly connected inhibitory subnetwork are highlighted by the pink bracket, while values that exhibit behavior corresponding with that seen in the network with a strongly conected inhibitory subnetwork are highlighted by the blue bracket.

As the I-I connectivity is varied, there are two distinct dynamical regimes, one with dynamics analogous to the Strong Network (blue bracketed values) and one with dynamics analogous to the Weak Network (pink bracketed values), with an abrupt transition between the two. This result justifies the study of the Strong Network and Weak Network as their activity is representative of dynamics for a range of I-I synaptic weights in the E-I network topology. For the values of the I-I synaptic weight in the weak regime, the Variability Measure (panels **(A)** and **(B)**) increases non-monotonically as E-I synaptic weight increases as discussed for the Weak Network. These regimes of high and low Variability Measure shift as the I-I synaptic weight increases since the E-I synaptic weight for which a given behavior is achieved likewise increases; for example, when the I-I synaptic weight is increased, a correspondingly higher E-I synaptic weight, which provides a stronger drive to the inhibitory cells, is required to achieve the "parameter balance" necessary for these networks to achieve a low Variability Measure despite a high E-I synaptic weight. Additionally, these networks display a non-zero Synchrony Measure (panels **(C)** and **(D)**) for lower values of the E-I synaptic weight. In contrast, the values of the I-I synaptic weight in the strong regime display a consistently low Variability Measure (with the exception of high E-I synaptic weight for the slower firing network, the unique situation discussed in detail above) but completely asynchronous activity (shown by the Synchrony Measure) for low values of the E-I synaptic weight.

The presence of two distinct dynamical regimes is also apparent from analyzing the average excitatory burst frequency (panels **(E)** and **(F)**) and the ratio of inhibitory bursts to excitatory bursts (panels **(G)** and **(H)**) in these networks, properties that reveal the network dynamics in more detail. Networks with inhibitory intra-connectivity in the strong regime show a monotonic increase in their average

excitatory burst frequency as the E-I synaptic weight increases, while networks with inhibitory intra-connectivity in the weak regime show an overall decrease in their average excitatory burst frequency as the E-I synaptic weight increases, with some instances of increasing burst frequency that correspond with networks that exhibit low variability. Additionally, networks in the strong regime exclusively exhibit a 1:1 ratio between inhibitory and excitatory bursts, while networks in the weak regime can exhibit two or even three inhibitory bursts for each excitatory burst. Through these measures it is apparent that activity closely matching classic PING rhythms is seen over the majority of the values of the E-I synaptic weight for the range of I-I synaptic weights that yield behavior analogous to the Strong Network studied above, while unique dynamics are seen over the range of I-I synaptic weights that yield behavior analogous to the Weak Network studied above.

These results reveal the robustness of the dichotomous dynamics displayed by excitatory cells in the Strong Network and Weak Network studied above. Indeed, it appears that slight heterogeneities in the I-I synaptic strength should not lead to major changes in network dynamics in an E-I network, while larger heterogeneities (where I-I synaptic weights include those inducing both weak and strong behavior) may lead to antithetical dynamics. This motivates the construction of E-I networks with heterogeneous inhibitory populations, described below.

4.3.2 E-I Networks with Noisy Excitatory Cells

To confirm the robustness of these results to more realistic biological conditions, analogous networks are simulated while adding Poisson trains of excitatory synaptic input to the excitatory neurons. These simulations were performed with a range of noise amplitudes: the lowest amplitude noise slightly accelerates the next firing of the perturbed neuron, while the highest amplitude noise causes the perturbed neuron

to fire with a probability of nearly 1 in a 5 ms window following the perturbation.

The results of these simulations for an illustrative choice of the average intrinsic excitatory cell firing frequency, for both Strong Networks and Weak Networks, are illustrated in Fig 4.8. For both types of networks, the network dynamics are quantified via the Variability Measure (Fig 4.8 **(A)** and **(B)**) and Synchrony Measure (Fig 4.8 **(C)** and **(D)**). Overall, it is observed that slight increases in the Variability Measure are seen as the noise amplitude increases, but this increase is largely uniform across all values of the E-I synaptic weight, preserving the relative pattern of well-organized and less organized excitatory bursting dynamics. These patterns only break down in the presence of large amplitude noise, in which many simulations lose synchronous excitatory activity, shown by the maximal Variability Measure values and near-minimal Synchrony Measure values.

In particular, Weak Networks (Fig 4.8 **(A)** and **(C)**) still exhibit pockets of lower Variability Measure amidst the simulations with higher E-I synaptic strength that tend to exhibit higher Variability Measure. In contrast, Strong Networks ((Fig 4.8 **(B)** and **(D)**) retain their more consistent pattern of exhibiting low Variability Measure in nearly every case where excitatory synchrony is achieved. In both scenarios, the Variability Measure increases in a largely consistent manner as the amplitude of the noise increases, with exceptions for the scenarios when excitatory network synchrony is completely lost.

These results taken together illustrate that the introduction of noise does not significantly alter the previously identified dynamical regimes of the Strong and Weak Networks, as each retains their unique properties that differentiate network dynamics dependent upon the strength of inhibitory intra-connectivity.

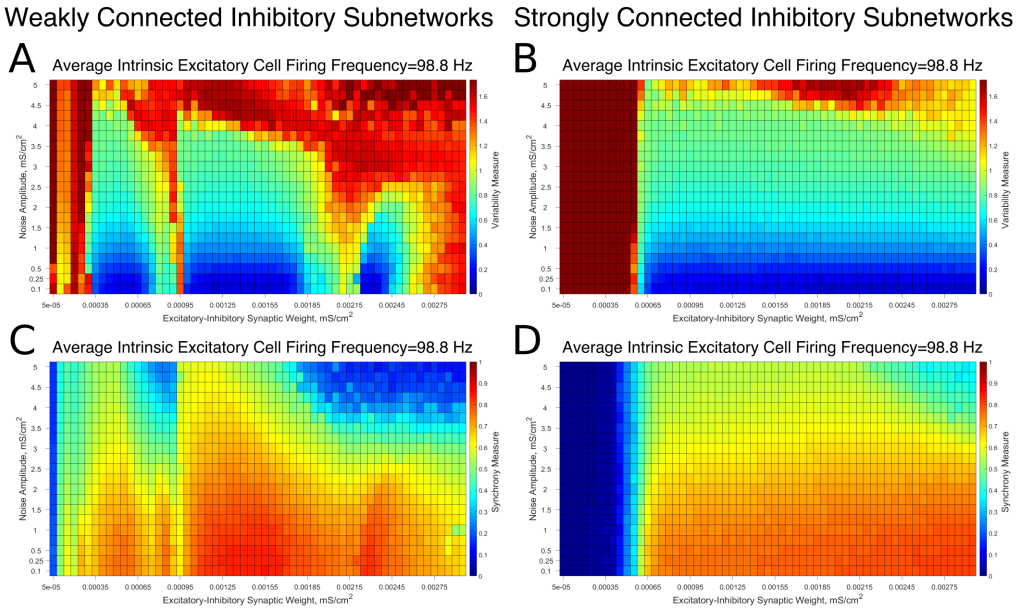

Figure 4.8: **Differences in dynamical patterns between Weak and Strong Networks are preserved in the presence of noisy drive to the excitatory cells. (A-D)** Variability Measure **(A,B)** and Synchrony Measure **(C,D)** shown for Weak Networks **(A,C)** and Strong Networks **(B,D)** with an average intrinsic excitatory cell firing frequency of 98.8 Hz in the presence of noise with varying amplitudes (y-axis). E-I synaptic weight is varied along the x-axis. Distinct differences in the dynamics articulated by the Variability Measure and Synchrony Measure are still seen between Weak and Strong Networks, with the major similarity being that both networks similarly devolve into asynchronous excitatory cell firing with high-amplitude noise.

4.3.3 E-I Networks with Heterogeneity in I-I Synaptic Strength

To construct a network that incorporates properties of networks with weak I-I connectivity and networks with strong I-I connectivity, networks with heterogeneous inhibitory synaptic strengths were created (which for brevity are refered to to as Strong/Weak Networks, Fig 4.9**(B)**).

Strong/Weak Networks contain 800 excitatory cells and 200 inhibitory cells as before, but the inhibitory cells are divided into two subnetworks of 100 cells each. One of the subnetworks has a strong I-I synaptic strength of 0.05 mS/cm^2, while the other has a weak I-I synaptic strength of 0.003 mS/cm^2. The values of the I-I synaptic strength are scaled from the values used in the Strong Networks and Weak

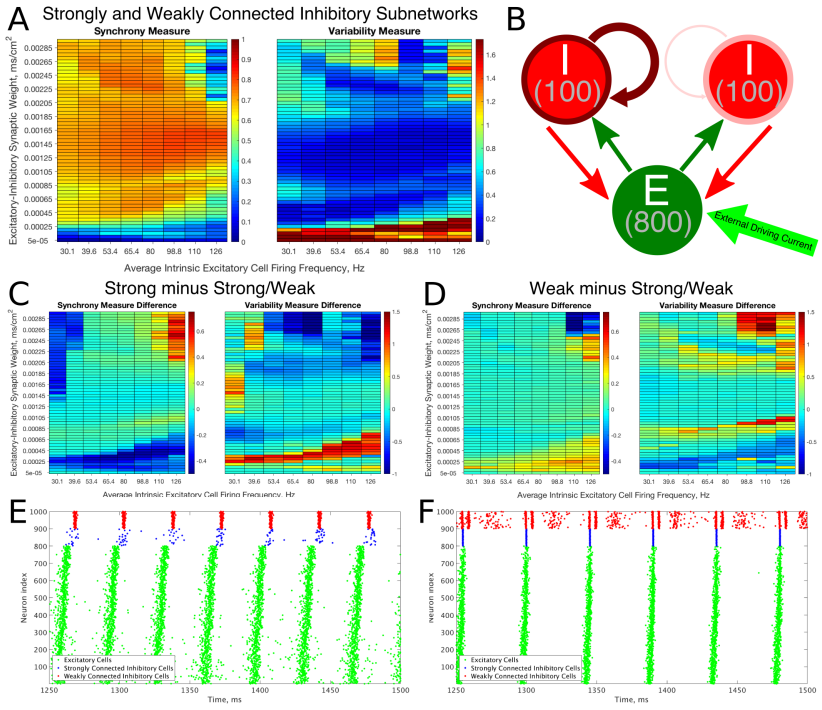

Figure 4.9: **Constructing an E-I network that contains both strongly connected and weakly connected inhibitory subnetworks decreases burst variability in networks with strictly weakly connected inhibitory subnetworks while also expanding the parameter regime in which any synchrony is achieved in comparison to networks with strictly strongly connected inhibitory subnetworks.** **(A)** Synchrony Measure (left panel) and Variability Measure (right panel) for a network with both strongly connected and weakly connected inhibitory subnetworks (hereafter referred to as Strong/Weak networks). **(B)** Diagram representing the connectivity for the Strong/Weak network. The thicker and darker red curve connecting the inhibitory cells to themselves for the population on the left illustrates the strong interconnectivity of those interneurons, while the thinner and lighter red curve connecting the inhibitory cells to themselves for the population on the right illustrates the weak interconnectivity of those interneurons. **(C-D)** Difference between the Synchrony and Variability Measure of a strictly weakly connected inhibitory subnetwork **(C)** and strictly strongly connected inhibitory subnetwork **(D)** with the Strong/Weak network with networks show the parameter regimes in which the Strong/Weak Networks show a higher Synchrony Measure and lower Variability Measure compared to networks with only one strength of inhibitory interconnectivity. **(E-F)** Example raster plots from Strong/Weak Networks. Panel **(E)** is a network with an intrinsic cell firing frequency 53.4 Hz and an E-I synaptic weight of 0.0003 mS/cm^2, and is from a parameter regime similar to the network shown in Fig 4.5**(B)**. Panel **(F)** is a network with an intrinsic cell firing frequency 53.4 Hz and an E-I synaptic weight of 0.00225 mS/cm^2, and is from a parameter regime similar to the network shown in Fig 4.5**(C)**.

Networks for a network of 100 as opposed to 200 cells. Each of these subnetworks has 30% intra-connectivity density, just as for the inhibitory subnetworks in previously studied E-I networks, but these inhibitory neurons only synapse onto other inhibitory

neurons within their subnetwork. Interneurons have the same likelihood of receiving synaptic input from an excitatory cell or sending synaptic output to an excitatory cell as in the networks studied above.

The Synchrony and Variability Measures for the excitatory neurons in Strong/Weak Networks are shown in Fig 4.9**(A)**. For ease of comparison the difference between these measures in the Weak and Strong Networks (Figs 4.4 and 4.5) and the Strong/Weak Networks are shown in Figs 4.9**(C)** and 4.9**(D)**. As Fig 4.9**(C)** illustrates, compared to the Strong Networks, Strong/Weak Networks achieve a higher Synchrony Measure and lower Variability Measure for low values of the E-I synaptic weight. A raster plot exhibiting such a network is shown in Fig 4.9**(E)**, where despite sparse, asynchronous activity of the strongly connected interneurons, the weakly connected interneurons exhibit synchronous bursting that provides the necessary inhibition to the excitatory cells to promote synchronous bursting. In contrast, Strong Networks in this parameter regime are typified by the behavior shown by the raster in Fig 4.3**(B)**, which is completely asynchronous. Additionally, Strong/Weak networks exhibit higher values of the Synchrony Measure and lower values of the Variability Measure in the regime of high E-I synaptic weight and low average intrinsic cell firing frequency for which Strong Networks show less organized bursting.

Furthermore, as illustrated in Fig 4.9**(D)**, compared to Weak Networks, Strong/Weak Networks show a significant decrease in the Variability Measure for high values of the E-I synaptic weight, as well as in a thin parameter regime with moderate E-I synaptic weight for which Weak Networks showed increased variability in excitatory bursting. Fig 4.9**(F)** displays an example raster plot of a Strong/Weak network with high E-I synaptic weight where the organization and consistency of excitatory bursting is largely maintained thanks to consistent synchronous bursting from the

strongly connected inhibitory neurons, which in turn helps to maintain a more consistent firing pattern amongst the weakly connected inhibitory neurons by gating excitatory cell activity. This can be compared to the Weak Network illustrated in Fig 4.3**(C)** which displays distinctly unorganized and variable bursting patterns.

Indeed, Strong/Weak Networks achieve the proverbial "best of both worlds", exhibiting synchrony for very low values of the E-I synaptic weight like Weak Networks while preserving the organization and consistency of excitatory bursting for high values of the E-I synaptic weight like Strong Networks. This new type of E-I network with heterogeneity amongst the inhibitory interneurons thusly generates well-organized and consistent excitatory bursting over a wider parameter range than a network with homogeneous inhibitory intraconnectivity, regardless of the strength of that intraconnectivity. The biological motivations for creating such a network and the implications of this mechanism are discussed in more detail in the Discussion below.

4.3.4 E-I Networks with Type II Interneurons

Previous work revealed that intrinsic cellular properties, typified by the Type I and Type II neuron classifications, play a pivotal role in determining network dynamics in strictly inhibitory neural networks [85]. The importance of interneuron cell type in those networks begs the question of whether E-I networks with different inhibitory cell types will exhibit different responses to a change in the I-I synaptic weight.

To probe this topic, E-I networks with the same topology as those studied above while replacing the Type I interneuron with either a model neuron exhibiting Type II properties without spike frequency adaptation (hereafter simply referred to as Type II neurons) or Type II properties with spike frequency adaptation (hereafter simply referred to as Type II neurons with adaptation) are studied.

It is observed that networks with either Type II interneuron do not exhibit significant changes in dynamics as the I-I synaptic weight changes. For slow firing networks there is essentially no change in the excitatory bursting properties as the I-I synaptic weight changes, as displayed in Fig 4.10**(A)** and **(C)**; indeed, even though networks with Type II neurons show a significantly increased Variability Measure for high values of the E-I synaptic weight, this increase is not dependent upon the I-I synaptic weight.

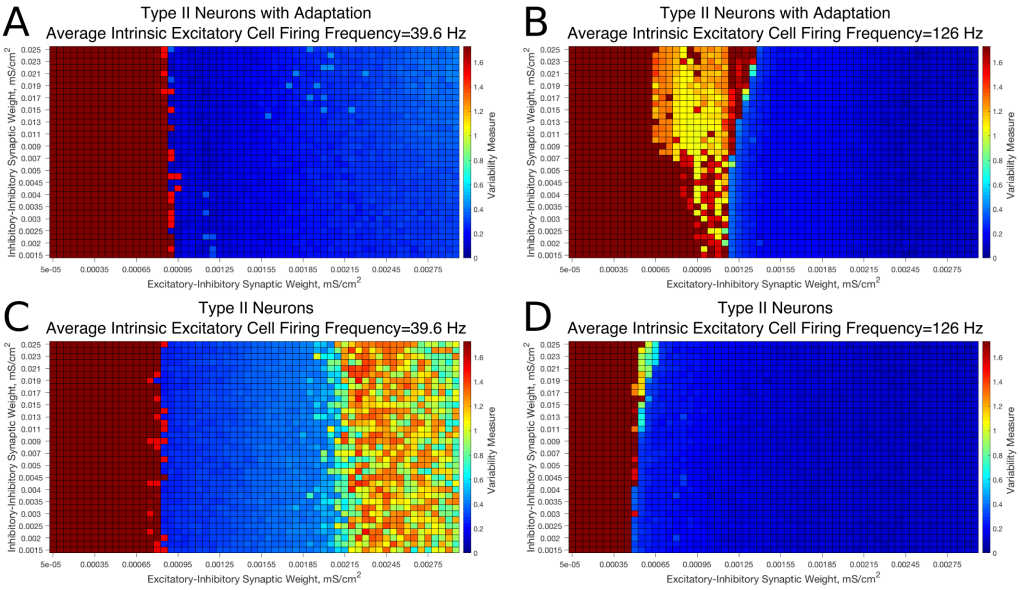

Figure 4.10: **E-I networks with Type II interneurons, both with and without an adaptation current, do not show significant change in dynamics as a function of I-I synaptic strength, unlike E-I networks with Type I interneurons. (A-D)** Heatmaps showing the Variability Measure for networks with varying E-I synaptic strength on the x-axis and varying I-I synaptic strength on the y-axis. The average intrinsic cell firing frequency of the networks are set at 39.6 Hz in panels **(A)** and **(C)** and 126 Hz in panels **(B)** and **(D)** . Results with inhibitory neurons modeled as a Type II neuron with adaptation are shown in **(A-B)**, while results with inhibitory neurons modeled as a Type II neuron without adaptation are shown in **(C-D)**. Neither networks with Type II with adaptation or Type II interneurons show the significant changes in dynamics as a function of the I-I synaptic weight that typified networks with Type I interneurons.

Faster firing networks with Type II neurons, shown in Fig 4.10**B** and **(D)**, also exhibit minimal change in network dynamics as a result of changing I-I synaptic weight. For the faster firing networks with Type II neurons with adaptation shown

in Fig 4.10**(B)**, networks with high values of the I-I synaptic weight exhibit a regime with a moderate value of the Variability Measure whereas networks with weaker values of the I-I synaptic weight are less likely to do so; however, all networks, regardless of I-I synaptic strength, with moderate to high E-I synaptic weight still show similar bursting properties, unlike in Type I networks.

These results imply that classic PING rhythmic bursting, which typically yield low values of the Variability Measure, are more robust to changes in I-I synaptic weight when the interneurons are Type II (with or without adaptation) then when the interneurons are Type I. This provides further evidence for the important role that cell type plays in networks with inhibitory neurons. Furthermore, these results also match the intuition gained from varying the connectivity density in strictly inhibitory networks with these types of neurons, as unlike networks of Type I neurons, networks of Type II neurons showed little if any change in dynamics as the synaptic strength changed [85].

4.4 Discussion

The work presented in this chapter shows that the strength of intra-connectivity amongst inhibitory neurons in a E-I network plays a pivotal role in controlling rhythmic PING-like dynamics. Changes to this connectivity can cause the inhibitory network to display dynamics beyond the single burst per oscillatory cycle typically seen in PING rhythms. Analyzing networks that do not satisfy this largely artificial constraint reveals that changing dynamics amongst the inhibitory cells are the impetus behind patterns formed in the excitatory cells that diverge from the classic PING predictions. Changes in the dynamics of the excitatory network are of paramount importance in biological networks where the excitatory pyramidal cells serve to output

the signal generated by an E-I network to other brain regions.

Such networks with strong I-I connectivity display behavior largely explained by the conceptual PING model. For example, the inability for these networks to exhibit any excitatory synchrony for low E-I synaptic weights follows directly from the classical PING theory [63]. In this case, the strong intra-connectivity between inhibitory cells, combined with a weak excitatory drive to the inhibitory cells due to the weak E-I synaptic weight, prevents enough net drive from accumulating in the inhibitory cells to elicit a synchronous burst. This parallels the behavior seen in strictly inhibitory networks with strong inhibitory connectivity, in which networks with a low average intrinsic cell firing frequency, analogous to the excitatory drive to the inhibitory cells seen here, exhibit complete asynchrony. This behavior is explained in greater detail in previous work, as the synaptic weight values analyzed in those strictly inhibitory networks are in an analogous range to the strong inhibitory intra-connectivity in the Strong Network here [85].

Furthermore, in Strong Networks with increased E-I synaptic weight, which results in a stronger drive to the inhibitory cells, the strong inhibitory intraconnectivity ensures only a single inhibitory burst occurs in response to excitatory cell activity. This provides for nearly identical levels of inhibition to each excitatory cell, which leads to classic PING activity [63].

However, networks with weak I-I connectivity display divergent dynamics that have not been thoroughly analyzed by existing PING literature. These networks exhibit synchrony amongst the excitatory cells for very weak values of the E-I connectivity, contrary to the conceptual PING model [108, 63, 119, 42]. When the I-I synaptic weight is weak, less inhibition accumulates as a result of inhibitory intra-connectivity; this means that less excitatory drive is required to elicit a synchronous

burst of inhibitory cell activity, which in turn leads to an excitatory burst. Here again the parallels to strictly inhibitory networks with weak inhibitory connectivity are apparent, as such networks were able to synchronize for low average intrinsic cell firing frequencies for which strongly connected networks were asynchronous.

Additionally, as the E-I connectivity strength increases, Weak Networks exhibit inhibitory cell dynamics beyond the single synchronous burst typically seen in PING networks. These dynamics can include multiple inhibitory bursts, as well as asynchronous inhibitory firing. Furthermore, the inhibitory patterning may differ in response to each excitatory burst. While such networks can still exhibit synchronous activity amongst the excitatory cells, the inconsistency of the inhibitory cell activity combined with the heterogeneous connectivity between neuron populations will cause a loss of well-organized and consistent bursting in the excitatory cell population, a feature which is reflected in the Variability Measure but not the Synchrony Measure.

With high E-I connectivity strength, Weak Networks do exhibit excitatory bursts with low Variability Measure in some cases. In these instances multiple inhibitory bursts occur, but the profile of these bursts is consistent and well-organized in response to each excitatory burst. The behavior of E-I networks with multiple inhibitory bursts, in particular the differences in excitatory network dynamics seen in response to disorganized versus well-organized patterns of multiple inhibitory bursts, is not investigated in detail by the conceptual PING model.

The dichotomy between networks deemed "strongly" intra-connected and "weakly" intra-connected is in fact a robust feature when the I-I connectivity is varied. Indeed, by varying the strength of inhibitory intra-connectivity two distinct regimes of activity are revealed: networks exhibiting "strong behavior" show a low Variability Measure for a vast majority of networks in which any form of excitatory synchrony

is achieved, while networks exhibiting "weak behavior" show synchronous excitatory activity at significantly lower values of the E-I connectivity strength but also exhibit increased variability in the excitatory bursting patterns as the E-I connectivity strength increases. Analysis of networks with various values of the I-I connectivity also reveals that these two types of dynamics correspond with features in other important network properties. While networks exhibiting strong behavior show a monotonic increase in their average excitatory burst frequency as the E-I connectivity strength increases, networks exhibiting weak behavior show an overall decrease in this frequency, albeit with some upticks in frequency corresponding to networks where well-organized bursting is recovered thanks to consistent patterning in the inhibitory population. Additionally, in the parameter regime studied here networks exhibiting strong behavior will only exhibit a 1:1 ratio between inhibitory and excitatory bursts, while networks exhibiting weak behavior can achieve 2:1 and 3:1 burst ratios.

Perhaps most interestingly, these results highlight that the patterning of inhibitory activity, as influenced heavily by the I-I connectivity strength, controls the consistency of excitatory burst rhythmicity. When the inhibitory bursting pattern is consistent following each excitatory burst, be that pattern a single burst of activity as is classic in PING activity or multiple inhibitory bursts as occured in networks with weak I-I connectivity, well-organized and consistent excitatory cell bursting is common and rhythmicity is periodic. However, when the inhibitory bursting pattern varies in response to each excitatory burst, different magnitudes and profiles of inhibitory current are generated. When the inhibitory input to the excitatory neurons varies from burst to burst, this disrupts the ability for these cells to exhibit consistent organization, leading to increased rhythm variability. Indeed, the importance

of I-I connectivity in controlling inhibitory dynamics plays a crucial role in preserving consistent excitatory bursting and rhythmicity, revealing both the role of the I-I connectivity and inhibitory patterning to be of more importance in E-I network dynamics than previous studies of PING-like dynamics indicate.

Note that some of the behaviors of E-I networks focused on in this work, including multiple bursts of the inhibitory network, have been identified in previous PING literature without a thorough analysis [16]. This research shows that when E-I networks display patterns of inhibitory behavior slightly beyond the classic restrictions of PING, such as the requirement that the inhibitory network only be active once per oscillatory cycle, the effect on the dynamics of the excitatory network can be more salient than previously suggested.

Furthermore, the same work by Börgers and Kopell identifies a broad "suppression boundary" between a regime of strict PING rhythms and a regime of asynchrony of the inhibitory cells that is affected by the strength of the I-I connectivity [16]. Thus, it stands to reason that networks that exhibit patterns of multiple inhibitory bursts that are messy or inconsistent, such as the examples shown in Fig 4.3**(C)** and **(G)**, may exist in the region of bistability between strict PING rhythms and complete asynchrony of the inhibitory cells identified by Börgers and Kopell; by this interpretation, one can contextualize this work as expounding upon the dynamics of E-I networks in this regime where E-I network behavior is neither strictly rhythmic nor strictly asynchronous.

Finally, note that all E-I networks studied here tend to exhibit more asynchrony and higher variability for networks with a stronger external drive to the excitatory cells. A clear example of this at work is seen in the differences between the example raster plots in Fig 4.3**(E)** and **(G)**. This result fits the predictions of more analytical

work done by Börgers, Krupa and Stan [17].

The focus of this work was on networks containing Type I interneurons given the evidence that fast-spiking, PV+ interneurons, which often display Type I properties [44], make up a majority of the interneuron population in various brain regions [78, 83]. Additionally, a majority of the computational studies analyzing PING rhythms utilize Type I interneurons. However, given the important role intrinsic cellular properties play in determining inhibitory dynamics [85], E-I networks were simulated with interneurons modeled as Type II neurons with and without an M-type adaptation current to see if cell type plays a similarly important role in E-I networks. Strictly inhibitory networks of such neurons did not exhibit significant changes in dynamics in response to changing the inhibitory intraconnectivity, unlike such networks containing Type I interneurons; as expected, neither did E-I networks with Type II interneurons. This result indicates that PING-style networks with Type II interneurons exhibit more consistent activity in response to changes in the I-I connectivity.

The dichotomy between the dynamics of E-I networks with weakly intra-connected Type I interneurons and strongly intra-connected Type I interneurons motivated the creation of a E-I network utilizing heterogeneity in the I-I connectivity. Various studies have shown that heterogeneities can be used in neural networks to improve the network's ability to exhibit features such as rate coding [74], gain control [75], synchrony [65], and robust oscillations [122]. While many of these studies look at E-I networks similar to the ones analyzed here, the heterogeneities studied are not in the I-I connectivity.

The Strong/Weak Network created in this study implements heterogeneity in the I-I coupling by creating two inhibitory subnetworks, one that is strongly intracon-

nected and one that is weakly intraconnected. Given the vast diversity in cellular properties amongst interneurons [61, 23, 10, 7, 96, 62, 51, 11, 47], heterogeneity in the strength of inhibitory intra-connectivity amongst a population of interneurons is likely. Furthermore, numerous studies have shown that interneurons tend to intra-connect preferentially to those exhibiting similar properties [113, 47, 11, 96, 61], in a sense forming the "subnetworks" modeled in the Strong/Weak Network. In addition, many of these same studies show evidence for these different types of interneurons connecting with the same excitatory pyramidal cells, forming a network similar to that modeled here. Thus, there is biological motivation for creating a network not only with heterogeneity amongst the interneuron intra-connectivity, but also with inhibitory subnetworks without interconnectivity that synapse onto the same excitatory cell population.

Indeed, the heterogenous network structure broadens the parameter regime in which well-organized and consistent excitatory bursting patterns are achieved. While Strong Networks did not achieve any sort of synchronous dynamics amongst excitatory cells for low values of the E-I connectivity, Strong/Weak Networks do. Additionally, while Weak Networks exhibited excitatory bursting without well-organized or consistent excitatory bursting for high values of the E-I synaptic weight, Strong/Weak Networks decrease the Variability Measure in this parameter regime significantly. Thus, the Strong/Weak Networks provide a potential mechanism by which PING rhythms might be generated more robustly for a variety of external drives to the excitatory cells and E-I synaptic weights.

CHAPTER V

Conclusion

5.1 Summary and conclusions

Perhaps the most daunting task facing neuroscientists is understanding how the brain can encode all of human consciousness, thought, and emotion while being comprised of a single fundamental unit, the neuron. Given that an individual neuron mimics a binary variable, with the spike of an action potential analogous to an "on" state and resting voltages analogous to an "off" state, it is extremely unlikely that individual neurons alone could store such complex information. Instead, all indications are that the neural correlates of complex behaviors lie in networks of communicating neurons, which as a network can achieve a much greater variety of states than just the binary "on" or "off". Indeed, it appears to be no coincidence that modern computing is made possible by communicating binary bits just as our brain accomplishes complex tasks via communicating neurons.

Network oscillations, which are typically driven by some degree of synchronous neural firing, are one type of neural network dynamic that is thought to serve a vital role in a variety of important functions performed by the brain. The fashions in which these oscillations arise has been a subject of intense scrutiny by neuroscientists for decades, and has made use of the interdisciplinary tools brought to bear by

computational neuroscientists. In particular, computational techniques have led to the precise articulation of a variety of potential mechanisms by which these rhythms, particularly those in the gamma frequency band, might be generated. However, historically the articulation of these mechanisms has been facilitated by a variety of idealizations that, while making computational study possible, sometimes overlook crucial features of biologically accurate neural networks.

Two such mechanisms, ING and PING, propose that neural synchrony driving rhythms in the gamma range are caused by gating inhibition provided by inhibitory interneurons. However, given the immensely diverse properties displayed by such interneurons, both in their excitability profiles and in the fashions that they communicate with each other, it remains an open question whether the predictions of these mechanisms are robust to changing interneuronal properties. The research presented in this dissertation studies less idealized networks than typically seen in the ING and PING literature to identify what, if any, dynamical changes are caused by changing interneuron properties and, where necessary, articulate new mechanisms explaining novel dynamics.

In Chapter II, I probe the classic ING mechanism, which describes the tendency for purely inhibitory networks to synchronize themselves, to see whether changing intrinsic cellular properties affects the tendency for such networks to oscillate. This research reveals that the predictions of ING theory are often violated in networks containing neurons with Type II excitability profiles. Instead, a mechanism relying upon properties of the Type II PRC, rather than properties of the network connectivity like in ING, explains the dynamics of these networks. Interestingly, networks with neurons containing an M-type potassium current modulated by the concentration of ACh, display unique dynamics that include a “switch” between two dynamical

behaviors as a function of the driving current to the network. This feature might provide a potential mechanism by which this ubiquitous neurotransmitter causes changes in neural dynamics that correspond with its known behavioral effects.

Next, in Chapter III this investigation transitions to the study of E-I networks and the PING mechanism. Here, I explore the interacting effects of changing network connectivity and changing cellular excitability type on overall network dynamics. This research shows that networks predisposed to exhibit PING rhythms will do so regardless of the cellular properties of either the excitatory or inhibitory cells; however, the dynamics of networks with weaker inter-connectivity between the excitatory and inhibitory populations depends critically on excitatory cell type and the corresponding propensity for synchrony. As these changes in cellular properties are often caused by differing ACh concentrations, these results provide another hypothesis for the fashion by which cholinergic modulation might cause major changes in neural network dynamics corresponding with changes in behavior.

Finally, Chapter IV focuses on E-I networks with dense and strong inter-connectivity that are predisposed to exhibit PING rhythms, analyzing how changing the inhibitory cell type and strength of inhibitory intra-connectivity affects the dynamics of excitatory network oscillations. This work reveals that networks with different inhibitory neuron types respond differently to changes in the inhibitory intra-connectivity; in particular, networks with Type II inhibitory cells adhere to the predictions of the PING mechanism more robustly in response to such changes than networks with Type I inhibitory cells. Indeed, networks with Type I inhibitory cells and weak inhibitory intra-connectivity are able to achieve oscillatory dynamics for weak excitatory-to-inhibitory signalling, while the rhythms achieved with strong excitatory-to-inhibitory signalling are often very irregular in nature. Both of these dynamics are not ac-

counted for by the classic PING literature. Finally, and perhaps most interestingly, an altered E-I network architecture, consisting of one inhibitory population that is strongly intra-connected and one which is weakly intra-connected, exhibits more robust oscillatory dynamics than seen in the classic networks.

Taken together, these results reveal that the properties of inhibitory interneurons serve a paramount role in dictating the characteristics of synchronous dynamics achieved both in purely inhibitory and E-I networks. These specific intricacies have not been the subject of intense scrutiny in the computational literature, as much of this work still utilizes inhibitory interneurons with the same idealized properties as those used in the classic articulation of the ING and PING mechanisms. However, the discovery of interneurons with varied excitability profiles and connectivity tendencies continues at a rapid pace, necessitating broadening our understanding of the dynamics of neural networks containing inhibitory interneurons to reflect interneurons exhibiting these diverse properties. In this vein, this work identifies the pivotal fashions in which modulation by the neurotransmitter ACh can affect the features of oscillatory neural network dynamics through changing the properties of inhibitory interneurons. It stands to reason that the known behavioral changes affected by varied concentrations of ACh should correspond with some change in neural dynamics, and the work presented in this dissertation provides potential explanations as to how such dynamical changes, brought about via altered properties of neural network oscillations, might arise.

While the work presented in this thesis focuses primarily on an analysis of the potential computational mechanisms underlying synchronous oscillations in simulated neural networks, it is important to place this work in the context of existing biological experiments. Rhythms in the gamma frequency band, particularly around 40 Hz,

have been observed in both the cortex and hippocampus, and experiments by Whittington et. al. have provided convincing evidence that inhibitory interneurons play a role in driving these dynamics [121]. Further experiments in both the hippocampus and cortex confirmed that interneurons in these regions tend to be connected to each other in the fashions necessary for the ING or PING mechanisms to be viable [119]. Thus, while the networks studied here are idealized to some extent from their biological counterparts, there exists convincing evidence that these mechanisms acting in these idealized networks may also be playing a role in dynamics seen in the brain.

Many of the manipulations to the neural networks studied in this dissertation also have experimental analogues. For example, in Chapter IV I manipulate the strength of inhibitory intra-connectivity and study the resulting changes in network dynamics. Experimental results have found the magnitude of the synaptic inhibition between inhibitory interneurons to be key modulators of dynamics potentially driven by ING or PING, and have manipulated this magnitude via the use of anesthetics, sedatives, and sex steroids, amongst other neuromodulators [119]. Furthermore, in the work presented in Chapters II and IV the external driving current to the modeled neurons is manipulated to see its effect on the development of synchronous oscillations. This too has an analogue to experimental manipulations in which this drive is altered by differential release of the neurotransmitter glutamate or differential expression of the metabatropic glutamate receptor on neurons [119]. In both cases, the parameters of interest in my simulated networks have been shown via experimental manipulation to serve a key role in modulating dynamics that are potentially driven by ING or PING.

Additionally, it is worth emphasizing that the work presented in this dissertation involves the direct study of large scale spiking neural networks, while other studies

of the ING and PING mechanims often utilize analytical techniques to idealize and simplify the computational costs of such analysis. Such techniques, while useful, require the networks studied to be idealized to a further degree than what was done here. By studying the large scale spiking neural networks directly, this research was able to analyze more complex, and likely more biologically realistic, network topologies, as well as develop new tools and measures for the quantification of oscillatory dynamics in such networks. Indeed, the ability for this research to analyze the role of cellular properties in dictating network dynamics was facilitated by the choice to directly analyze the large scale spiking neural networks rather than reduce them.

Finally, the multitude of interneurons in the brain begs a more fundamental neuroscientific question: what role does this diversity serve? My research provides a potential explanation in the different types of synchronous oscillatory dynamics brought about by changing inhibitory cell properties. Indeed, for the brain to be responsible for such a vast range of critical functions necessary for human survival and flourishing, neural networks much be able to achieve a corresponding range of differentiable dynamics. Given the results of the research presented in this dissertation, it is possible that intereneuronal diversity serves as an impetus for diverse oscillatory dynamics that could be responsible for a variety of brain functions and behaviors.

5.2 Future Directions

There are a variety of future directions this research could take, some of which I plan to pursue in post-doctoral studies. Perhaps the most straightforward of these is expanding the type of analysis presented in this dissertation to the study of other rhythms besides gamma. Some results presented here approach the theta frequency band, begging the question of whether the networks studied in this research could

be made to oscillate with a theta frequency. Such research, when viewed alongside some of the papers cited in this dissertation that look at oscillations in non-gamma frequency bands (particularly work by Nancy Kopell), could provide further insights into whether oscillations of different frequencies can be achieved by similar networks, or whether the mechanisms underlying these different oscillations are so distinct that network-level changes are required to change the freuqency band of the oscillatory activity.

A more biologically-motivated extension of this research is the study of epilepsy, which is discussed briefly in Section 1.2.3. A more detailed analysis of the different mechanisms underlying "noisy" oscillations, which are more indicative of the rhythms observed in the brain, versus oscillations containing complete neural synchrony, which occur primarily during seizures, might provide insights into the development of epileptic events. Moreover, computational analysis of neural networks known to produce epileptic seizures, utilizing the techniques developed in this dissertation, could provide insights into ways in which seizure dynamics might be disrupted.

BIBLIOGRAPHY

BIBLIOGRAPHY

[1] Abbott, L.F.: Lapicques introduction of the integrate-and-fire model neuron (1907). Brain research bulletin **50**(5), 303–304 (1999)

[2] Achuthan, S., Canavier, C.C.: Phase-resetting curves determine synchronization, phase locking, and clustering in networks of neural oscillators. J Neurosci **29**(16), 5218–5233 (2009)

[3] Ascoli, G.A., Atkeson, J.C.: Incorporating anatomically realistic cellular-level connectivity in neural network models of the rat hippocampus. Biosystems **79**, 173–181 (2005)

[4] Aton, S.J., Broussard, C., Dumoulin, M., Seibt, J., Watson, A., Coleman, T., Frank, M.G.: Visual experience and subsequent sleep induce sequential plastic changes in putative inhibitory and excitatory cortical neurons. PNAS **110**(8), 3101–3106 (2013)

[5] Bargmann, C.I., Marder, E.: From the connectome to brain function. Nature Methods **10**, 483490 (2013)

[6] Barnett, M.W., Larkman, P.M.: The action potential. Practical Neurology **7**(3), 192–197 (2007). URL http://pn.bmj.com/content/7/3/192

[7] Barthó, P., Hirase, H., Monconduit, L., Zugaro, M., Harris, K.D., Buzsáki, G.: Characterization of neocortical principal cells and interneurons by network interactions and extracellular features. Journal of neurophysiology **92**(1), 600–608 (2004)

[8] Bartos, M., Vida, I., Frotscher, M., Meyer, A., Monyer, H., Geiger, J.R.P., Jonas, P.: Fast synaptic inhibition promotes synchronized gamma oscillations in hippocampal interneuron networks. PNAS **99**(20), 13,222–13,227 (2002)

[9] Bartos, M., Vida, I., Jonas, P.: Synaptic mechanisms of synchronized gamma oscillations in inhibitory interneuron networks. Nature Reviews Neuroscience **8**, 45–56 (2007)

[10] Beierlein, M., Gibson, J.R., Connors, B.W.: A network of electrically coupled interneurons drives synchronized inhibition in neocortex. Nature neuroscience **3**(9), 904–910 (2000)

[11] Beierlein, M., Gibson, J.R., Connors, B.W.: Two dynamically distinct inhibitory networks in layer 4 of the neocortex. Journal of neurophysiology **90**(5), 2987–3000 (2003)

[12] Best, J., Park, C., Terman, D., Wilson, C.: Transitions between irregular and rhythmic firing patterns in excitatory-inhibitory neuronal networks. Journal of computational neuroscience **23**(2), 217–235 (2007)

[13] Bharath, R., Sinha, S., Panda, R., Raghavendra, K., George, L., Chaitanya, G., Gupta, A., Satishchandra, P.: Seizure frequency can alter brain connectivity: evidence from resting-state fmri. American Journal of Neuroradiology **36**(10), 1890–1898 (2015)

[14] Börgers, C., Franzesi, G.T., LeBeau, F.E., Boyden, E.S., Kopell, N.J.: Minimal size of cell assemblies coordinated by gamma oscillations. PLoS Comput Biol **8**(2), e1002,362 (2012)

[15] Börgers, C., Kopell, N.: Synchronization in networks of excitatory and inhibitory neurons with sparse, random connectivity. Neural computation **15**(3), 509–538 (2003)

[16] Börgers, C., Kopell, N.: Effects of noisy drive on rhythms in networks of excitatory and inhibitory neurons. Neural computation **17**(3), 557–608 (2005)

[17] Börgers, C., Krupa, M., Gielen, S.: The response of a classical hodgkin–huxley neuron to an inhibitory input pulse. Journal of computational neuroscience **28**(3), 509–526 (2010)

[18] Borgers, C., Walker, B.: Toggling between gamma-frequency activity and suppression of cell assemblies. Frontiers in computational neuroscience **7**, 33 (2013)

[19] Bosman, C.A., Schoffelen, J.M., Brunet, N., Oostenveld, R., Bastos, A.M., Womelsdorf, T., Rubehn, B., Stieglitz, T., Weerd, P.D., Fries, P.: Attentional stimulus selection through selective synchronization between monkey visual areas. Neuron **75**, 875–888 (2012)

[20] Brea, J.N., Kay, L.M., Kopell, N.J.: Biophysical model for gamma rhythms in the olfactory bulb via subthreshold oscillations. Proceedings of the National Academy of Sciences **106**(51), 21,954–21,959 (2009)

[21] Brown, E., Moehlis, J., Holmes, P.: On the phase reduction and response dynamics of neural oscillator populations. Neural computation **16**(4), 673–715 (2004)

[22] Brunel, N., Hansel, D.: How noise affects the synchronization properties of recurrent networks of inhibitory neurons. Neural Computation **18**, 1066–1110 (2006)

[23] Buhl, E.H., Halasy, K., Somogyi, P.: Diverse sources of hippocampal unitary inhibitory postsynaptic potentials and the number of synaptic release sites. Nature **368**, 28 (1994)

[24] Bury, L.A., Sabo, S.L.: How its made: the synapse. Molecular interventions **10**(5), 282 (2010)

[25] Buzsáki, G., Wang, X.J.: Mechanisms of gamma oscillations. Annual review of neuroscience **35**, 203–225 (2012)

[26] Canavier, C.C., Wang, S., Chandrasekaran, L.: Effects of phase response curve skew on synchronization with and without conduction delays. Frontiers in Neural Circuits **7**(194), 1–18 (2013)

[27] Cannon, J., McCarthy M.M.and Lee, S., Lee, J., Borgers, C., Whittington, M., Kopell, N.: Neurosystems: brain rhythms and cognitive processing. Eur J Neurosci **39**(5), 705–719 (2014)

[28] Castro-Alamancos, M.A., Rigas, P., Tawara-Hirata, Y.: Resonance (10 hz) of excitatory networks in motor cortex: effects of voltage-dependent ion channel blockers. The Journal of physiology **578**(1), 173–191 (2007)

[29] Chow, C.C., White, J.A., Ritt, J., Kopell, N.: Frequency control in synchronized networks of inhibitory neurons. The Journal of Computational Neuroscience **5**, 407–420 (1998)

[30] Couto, J., Linaro, D., Schutter, E.D., Giugliano, M.: On the firing rate dependency of the phase response curve of rat purkinje neurons in vitro. PLoS Computational Biology **11**(3), 1–23 (2015)

[31] Cui, J., Canavier, C.C., Butera, R.J.: Functional phase response curves: A method for understanding synchronization of adapting neurons. Journal of Neurophysiology **102**, 387–398 (2009)

[32] Cutsuridis, V., Cobb, S., Graham, P.: Encoding and retrieval in a model of the hippocampal ca1 microcircuit. HIPPOCAMPUS **20**, 423–446 (2010)

[33] Cutsuridis, V., Hasselmo, M.: Gabaergic contributions to gating, timing, and phase precession of hippocampal neuronal activity during theta oscillations. HIPPOCAMPUS **22**, 1597–621 (2012)

[34] Deco, G., Thiele, A.: Cholinergic control of cortical network interactions enables feedback-mediated attentional modulation. European Journal of Neuroscience **34**(1), 146–157 (2011)

[35] DeFelipe, J.: Sesquicentenary of the birthday of santiago ramón y cajal, the father of modern neuroscience. Trends in neurosciences **25**(9), 481–484 (2002)

[36] Desimone, R., Duncan, J.: Neural mechanisms of selective visual attention. Annual Reviews Neuroscience **18**, 193–222 (1995)

[37] Dipoppa, M., Krupa, M., Torcini, A., Gutkin, B.S.: Splay states in finite pulse-coupled networks of excitable neurons. SIAM Journal of Applied Dynamical Systems **11**(3), 864–894 (2012)

[38] Ermentrout, B., Pascal, M., Gutkin, B.: The effects of spike frequency adaptation and negative feedback on the synchronization of neural oscillators. Neural Computation **13**, 1285–1310 (2001)

[39] Ermentrout, B., Wechselberger, M.: Canards, clusters, and synchronization in a weakly coupled interneuron model. SIAM Journal of Applied Dynamical Systems **8**(1), 253–278 (2009)

[40] Ermentrout, G.B.: Type i membranes, phase resetting curves, and synchrony. Neural Computation **8**(5), 979–1001 (1996)

[41] Ermentrout, G.B., Glass, L., Oldman, B.E.: The shape of phase-resetting curves in oscillators with a saddle node on an invariant circle bifurcation. Neural Computation **24**, 3111–3125 (2012)

[42] Ermentrout, G.B., Kopell, N.: Fine structure of neural spiking and synchronization in the presence of conduction delays. Proceedings of the National Academy of Sciences **95**(3), 1259–1264 (1998)

[43] Ermentrout, G.B., Terman, D.H.: Mathematical Foundations of Neuroscience. Springer (2010)

[44] Ferguson, K.A., Huh, C.Y.L., Amilhon, B., Williams, S., Skinner, F.K.: Experimentally constrained ca1 fast-firing parvalbumin-positive interneuron network models exhibit sharp transitions into coherent high frequency rhthyms. Frontiers in Computational Neuroscience **7** (2013)

[45] Fink, C.G., Booth, V., Zochowski, M.: Cellularly-driven differences in network synchronization propensity are differentially modulated by firing frequency. PLoS Computational Biology **7**(5) (2011)

[46] Fries, P.: A mechanism for cognitive dynamics: neuronal communication through neuronal coherence. TRENDS in Cognitive Sciences **9**(10), 474–480 (2005)

[47] Gibson, J.R., Beierlein, M., Connors, B.W.: Two networks of electrically coupled inhibitory neurons in neocortex. Nature **402**(6757), 75–79 (1999)

[48] Goel, P., Ermentrout, B.: Synchrony, stability, and firing patterns in pulse-coupled oscillators. Physica D **163**, 191–216 (2002)

[49] Golomb, D., Rinzel, J.: Dynamics of globally coupled inhibitory neurons with heterogeneity. Phys. Rev. E **48**, 4810–1814 (1993)

[50] Golomb, D., Rinzel, J.: Clustering in globally coupled inhibitory neurons. Physica D **72**, 259–282 (1994)

[51] Gonchar, Y., Burkhalter, A.: Three distinct families of gabaergic neurons in rat visual cortex. Cerebral Cortex **7**(4), 347–358 (1997)

[52] Hansel, D., Mato, G., Meunier, C.: Synchrony in excitatory neural networks. Neural computation **7**(2), 307–337 (1995)

[53] Hasselmo, M., Giocomo, L.: Cholinergic modulation of cortical function. Journal of Molecular Neuroscience **30**, 133–135 (2006)

[54] Hasselmo, M.E., Sarter, M.: Modes and models of forebrain cholinergic neuromodulation of cognition. Neuropsychopharmacology **36**(1), 52–73 (2011)

[55] Hodgkin, A.L.: The local electric changes associated with repetitive action in a non-medullated axon. Journal of Physiology **107**, 165–181 (1948)

[56] Hodgkin, A.L., Huxley, A.F.: Action potentials recorded from inside a nerve fibre. Nature **144**(3651), 710–711 (1939)

[57] Hodgkin, A.L., Huxley, A.F.: A quantitative description of membrane current and its application to conduction and excitation in nerve. Journal of Physiology **117**, 500–544 (1952)

[58] Izhikevich, E.M.: Simple model of spiking neurons. IEEE Transactions on neural networks **14**(6), 1569–1572 (2003)

[59] Karson, M.A., Tang, A.H., Milner, T.A., Alger, B.E.: Synaptic cross talk between perisomatic-targeting interneuron classes expressing cholecystokinin and parvalbumin in hippocampus. The Journal of Neuroscience **29**(13), 4140–4154 (2009)

[60] Kilpatrick, Z.P., Ermentrout, B.: Sparse gamma rhythms arising through clustering in adapting neuronal networks. PLoS Computational Biology **7**(11), 1–17 (2011)

[61] Klausberger, T., Magill, P.J., Márton, L.F., Roberts, J.D.B., Cobden, P.M., Buzsáki, G., Somogyi, P.: Brain-state-and cell-type-specific firing of hippocampal interneurons in vivo. Nature **421**(6925), 844–848 (2003)

[62] Klausberger, T., Somogyi, P.: Neuronal diversity and temporal dynamics: the unity of hippocampal circuit operations. Science **321**(5885), 53–57 (2008)

[63] Kopell, N., Börgers, C., Pervouchine, D., Malerba, P., Tort, A.: Gamma and theta rhythms in biophysical models of hippocampal circuits. In: Hippocampal Microcircuits, pp. 423–457. Springer (2010)

[64] Kopell, N., Ermentrout, G.B., Whittington, M.A., Traub, R.D.: Gamma rhythms and beta rhythms have different synchronization properties. PNAS **97**(4), 1867–1872 (2000)

[65] Kriener, B.: How synaptic weights determine stability of synchrony in networks of pulse-coupled excitatory and inhibitory oscillators. Chaos: An Interdisciplinary Journal of Nonlinear Science **22**(3), 033,143 (2012)

[66] Krupa, M., Gielen, S., Gutkin, B.: Adaptation and shunting inhibition leads to pyramidal/interneuron gamma with sparse firing of pyramidal cells. Journal of computational neuroscience **37**(2), 357–376 (2014)

[67] Ladenbauer, J., Augustin, M., Shiau, L., Obermayer, K.: Impact of adaptation currents on synchronization of coupled exponential integrate-and-fire neurons. PLoS Computational Biology **8**(4), 1–19 (2012)

[68] Larsen, W.: Biological implications of gap junction structure, distribution and composition: a review. Tissue and Cell **15**(5), 645–671 (1983)

[69] Lawrence, J., Saraga, F., Churchill, J., Startling, J., Travis, K., Skinner, F., McBain, C.: Somatodendritic kv7/kcnq/m channels control interspike interval in hippocampal interneurons. The Journal of Neuroscience **26**(47), 12,325–12,338 (2006)

[70] Luck, S.J., Chelazzi, L., Hillyard, S.A., Desimone, R.: Neural mechanisms of spatial selective attention in areas v1, v2, and v4 of macaque visual cortex. Annual Reviews Neuroscience **77**, 24–42 (1997)

[71] Mancilla, J.G., Lewis, T.J., Pinto, D.J., Rinzel, J., Connors, B.W.: Synchronization of electrically coupled pairs of inhibitory interneurons in neocortex. The Journal of Neuroscience **27**(8), 2058–2073 (2007)

[72] Marder, E.: Neuromodulation of neuronal circuits: Back to the future. Neuron **76**(1), 1–11 (2012)

[73] Markram, H., Toledo-Rodriguez, M., Wang, Y., Gupta, A., glad Silberberg, Wu, C.: Interneurons of the neocortical inhibitory system. Natural Reviews Neuroscience **5**, 793–807 (2004)

[74] Mejias, J., Longtin, A.: Optimal heterogeneity for coding in spiking neural networks. Physical Review Letters **108**(22), 228,102 (2012)

[75] Mejias, J.F., Longtin, A.: Differential effects of excitatory and inhibitory heterogeneity on the gain and asynchronous state of sparse cortical networks. Frontiers in computational neuroscience **8**, 107 (2014)

[76] Mody, I., Pearce, R.A.: Diversity of inhibitory neurotransmission through gaba a receptors. Trends in neurosciences **27**(9), 569–575 (2004)

[77] Moon, S.J., Cook, K.A., Rajendran, K., Kevrekidis, I.G., Cisternas, J., Laing, C.R.: Coarse-grained clustering dynamics of heterogeneously coupled neurons. Journal of Mathematical Neuroscience **5**(2), 1–20 (2015)

[78] Muller, J.F., Mascagni, F., McDonald, A.J.: Pyramidal cells of the rat basolateral amygdala: synaptology and innervation by parvalbumin-immunoreactive interneurons. Journal of Comparative Neurology **494**(4), 635–650 (2006)

[79] Olufsen, M.S., Whittington, M.A., Camperi, M., Kopell, N.: New roles for the gamma rhythm: population tuning and preprocessing for the beta rhythm. Journal of computational neuroscience **14**(1), 33–54 (2003)

[80] Oprisan, S.A., Prinz, A.A., Canavier, C.: Phase resetting and phase locking in hybrid circuits of one model and one biological neuron. Biophysical Journal **87**, 2283–2298 (2004)

[81] Parent, J.M., Timothy, W.Y., Leibowitz, R.T., Geschwind, D.H., Sloviter, R.S., Lowenstein, D.H.: Dentate granule cell neurogenesis is increased by seizures and contributes to aberrant network reorganization in the adult rat hippocampus. Journal of Neuroscience **17**(10), 3727–3738 (1997)

[82] Perrenoud, Q., Rossier, J., Geoffrey, H., Vitalis, T., Gallopin, T.: Diversity of gabaergic interneurons in layer via and vib of mouse barrel cortex. Cerebral Cortex **23**, 423–441 (2013)

[83] Povysheva, N.V., Zaitsev, A.V., Rotaru, D.C., Gonzalez-Burgos, G., Lewis, D.A., Krimer, L.S.: Parvalbumin-positive basket interneurons in monkey and rat prefrontal cortex. Journal of neurophysiology **100**(4), 2348–2360 (2008)

[84] Reynolds, J.H., Chelazzi, L., Desimone, R.: Competitive mechanisms subserve attention in macaque areas v2 and v4. The Journal of Neuroscience **19**(5), 1736–1753 (1999)

[85] Rich, S., Booth, V., Zochowski, M.: Intrinsic cellular properties and connectivity density determine variable clustering patterns in randomly connected inhibitory neural networks. Frontiers in Neural Circuits **10**, 82 (2016)

[86] Rich, S., Zochowski, M., Booth, V.: Dichotomous dynamics in ei networks with strongly and weakly intra-connected inhibitory neurons. Frontiers in Neural Circuits **11** (2017)

[87] Rich, S., Zochowski, M., Booth, V.: Effects of neuromodulation on excitatory–inhibitory neural network dynamics depend on network connectivity structure. Journal of Nonlinear Science pp. 1–24 (2018)

[88] del Rio, C.A.C., Lawrence, J.J., Erdelyi, F., Szabo, G., Mccain, C.J.: Cholinergic modulation amplifies the intrinsic oscillatory properties of ca1 hippocampal cholecystokinin-positive interneurons. The Journal of Physiology **589**(3), 609–627 (2011)

[89] del Rio, C.A.C., McBain, C.J., Pelkey, K.A.: An update on cholinergic regulation of cholecystokinin-expressing basket cells. The Journal of Physiology **590**(4), 695–702 (2012)

[90] Roach, J.P., Ben-Jacob, E., Sander, L.M., Zochowski, M.R.: Formation and dynamics of waves in a cortical model of cholinergic modulation. PLoS computational biology **11**(8), e1004,449 (2015)

[91] Ruivo, L.M.T.G., Mellor, J.R.: Cholinergic modulation of hippocampal network function. Frontiers in Synaptic Neuroscience **5** (2013)

[92] Saraga, F., Wu, C., Zhang, L., Skinner, F.: Active dendrites and spike propagation in multi compartment models of oriens-lacunosum/moleculare hippocampal interneurons. The Journal of Physiology **552**, 673–689 (2003)

[93] Sarter, M., Hasselmo, M.E., Bruno, J.P., Givens, B.: Unraveling the attentional functions of cortical cholinergic inputs: interactions between signal-driven and cognitive modulation of signal detection. Brain Research Reviews **48**(1), 98–111 (2005)

[94] Schemer, M.A., Lewis, T.J.: The Theory of Weakly Coupled Oscillators, vol. 6. Springer (2012)

[95] Schultheiss, N., Prinz, A., Butera, R.J. (eds.): Phase Response Curves in Neuroscience: Theory, Experiment and Analysis. Springer Series in Computational Neuroscience. Springer-Verlag (2014)

[96] Somogyi, P., Klausberger, T.: Defined types of cortical interneurone structure space and spike timing in the hippocampus. The Journal of physiology **562**(1), 9–26 (2005)

[97] Splettstoesser, T.: Synapse schematic. URL https://www.scistyle.com/

[98] Stiefel, K.M., Gutkin, B.S., Sejnowski, T.J.: Cholinergic neuromodulation changes phase response curve shape and type in cortical pyramidal neurons. PLoS ONE **3**(12) (2008)

[99] Stiefel, K.M., Gutkin, B.S., Sejnowski, T.J.: The effects of cholinergic neuromodulation on neuronal phase-response curves of modeled cortical neurons. Journal of computational neuroscience **26**(2), 289–301 (2009)

[100] Talathi, S.S., Hwang, D.U., Carney, P.R., Ditto, W.L.: Synchrony with shunting inhibition in a feedforward inhibitory network. Journal of Computational Neuroscience **28**, 305–321 (2010)

[101] Talathi, S.S., Hwang, D.U., Ditto, W.L.: Spike timing dependent plasticity promotes synchrony of inhibitory networks in the presence of heterogeneity. Journal of Computational Neuroscience **25**, 263–281 (2008)

[102] Talathi, S.S., Hwang, D.U., Militias, A., Carney, P.R., Ditto, W.L.: Predicting synchrony in heterogeneous pulse coupled oscillators. Phys. Rev. E **80** (2009)

[103] Tateno, T., Harsch, A., Robinson, H.: Threshold firing frequency-current relationships of neurons in rat somatosensory cortes: Type 1 and type 2 dynamics. J. Neurophysiology **92**, 2283–2294 (2004)

[104] Tateno, T., Robinson, H.P.C.: Phase resetting curves and oscillatory stability in interneurons of rat somatosensory cortex. Biophysical Journal **92**, 683–695 (2007)

[105] Terman, D., Kopell, N., Bose, A.: Dynamics of two mutually coupled slow inhibitory neurons. Physica D **117**, 241–275 (1997)

[106] Tiesinga, P., Sejnowski, T.J.: Cortical enlightenment: Are attentional gamma oscillations driven by ing or ping? Neuron **63**, 727–732 (2009)

[107] Tikidji-Hamburyan, R.A., Martnez, J.J., White, J.A., Canavier, C.C.: Resonant interneurons can increase robustness of gamma oscillations. Journal of Neuroscience **35**(47), 15,682–15,695 (2015)

[108] Traub, R.D., Jefferys, J.G., Whittington, M.A.: Simulation of gamma rhythms in networks of interneurons and pyramidal cells. Journal of computational neuroscience **4**(2), 141–150 (1997)

[109] Traub, R.D., Spruston, N., Soltesz, I., Kenneth, A., Whittington, M.A., Jeffreys, J.G.R.: Gamma-frequency oscillations: a neuronal population phenomenon, regulated by synaptic and intrinsic cellular processes, and inducing synaptic plasticity. Progress in Neurobiology **55**, 563–575 (1998)

[110] Viriyopase, A., Memmesheimer, R.M., Gielen, S.: Cooperation and competition of gamma oscillation mechanisms. Journal of Neurophysiology (2016)

[111] van Vreeswijk, C., Hansel, D.: Patterns of synchrony in neural networks with spike adaptation. Neural Computation **13**, 959–992 (2001)

[112] Vreeswijk, C.V., Abbott, L.F., Ermentrout, G.B.: When inhibition not excitation synchronizes neural firing. The Journal of Computational Neuroscience **1**, 313–321 (1994)

[113] Wang, S.J., Hilgetag, C., Zhou, C.: Sustained activity in hierarchical modular neural networks: self-organized criticality and oscillations. Frontiers in computational neuroscience **5**, 30 (2011)

[114] Wang, X.J.: Neurophysiological and computational principles of cortical rhythms in cognition. Physiological Review **90**, 1195–1268 (2010)

[115] Wang, X.J., Buzsaki, G.: Gamma oscillation by synaptic inhibition in a hippocampal interneuronal network model. The Journal of Neuroscience **16**(20), 6402–6413 (1996)

[116] Ward, L.M.: Synchronous neural oscillations and cognitive processes. Trends in cognitive sciences **7**(12), 553–559 (2003)

[117] Wendling, F., Benquet, P., Bartolomei, F., Jirsa, V.: Computational models of epileptiform activity. Journal of neuroscience methods **260**, 233–251 (2016)

[118] White, J.A., Chow, C.C., Rit, J., Soto-Treviño, C., Kopell, N.: Synchronization and oscillatory dynamics in heterogeneous, mutually inhibited neurons. Journal of computational neuroscience **5**(1), 5–16 (1998)

[119] Whittington, M., Traub, R.D., Kopell, N., Ermentrout, B., Buhl, E.: Inhibition-based rhythms: experimental and mathematical observations on network dynamics. International Journal of Psychophysiology **38**, 315–336 (2000)

[120] Whittington, M.A., Traub, R.D.: Interneuron diversity series: inhibitory interneurons and network oscillations in vitro. Trends in neurosciences **26**(12), 676–682 (2003)

[121] Whittington, M.A., Traub, R.D., Jefferys, J.G.: Synchronized oscillations in interneuron networks driven by metabotropic glutamate receptor activation. Nature **373**(6515), 612 (1995)

[122] Xie, J., Wang, Z., Fang, J.: Feedback-dependence and robustness of gamma oscillations in networks with excitatory and inhibitory neurons. Procedia Engineering **15**, 3103–3108 (2011)

[123] Zahid, T., Skinner, F.K.: Predicting synchronous and asynchronous network groupings of hippocampal interneurons coupled with dendritic gap junctions. Brain Research **1262**, 115–129 (2009)

[124] Zhong, G., Shevtsova, N.A., Rybak, I.A., Harris-Warwick, R.M.: Neuronal activity in the isolated mouse spinal cord during spontaneous deletions in fictive locomotion: insights into locomotor central pattern generator organization. J. Physiology **590**(19), 4735–4759 (2012)